PATTERNING VIA OPTICAL SATURABLE TRANSITIONS

by

Precious Cantú

A dissertation submitted to the faculty of
The University of Utah
in partial fulfillment of the requirements for the degree of

Doctor of Philosophy

Department of Electrical and Computer Engineering

The University of Utah

August 2015

The University of Utah Graduate School

STATEMENT OF DISSERTATION APPROVAL

The dissertation of **Precious Cantú**

has been approved by the following supervisory committee members:

Rajesh Menon	, Chair	**06/05/2015** Date Approved
Cynthia M. Furse	, Member	**06/05/2015** Date Approved
Florian Solzbacher	, Member	**06/18/2015** Date Approved
Henry S. White	, Member	**06/05/2015** Date Approved
Bruce K. Gale	, Member	**06/18/2015** Date Approved
Henry I. Smith	, Member	**06/05/2015** Date Approved

and by **Gianluca Lazzi** , Chair/Dean of

the Department/College/School of **Electrical and Computer Engineering**

and by David B. Kieda, Dean of The Graduate School.

ABSTRACT

For the past 40 years, optical lithography has been the patterning workhorse for the semiconductor industry. However, as integrated circuits have become more and more complex, and as device geometries shrink, more innovative methods are required to meet these needs. In the far-field, the smallest feature that can be generated with light is limited to approximately half the wavelength. This so-called far-field diffraction limit or the Abbé limit (after Prof. Ernst Abbé who first recognized this) effectively prevents the use of long-wavelength photons (>300nm) from patterning nanostructures (<100nm). Even with a 193nm laser source and extremely complicated processing, patterns below $\sim$ 20nm are incredibly challenging to create. Sources with even shorter wavelengths can potentially be used. However, these tend to be much more expensive and of much lower brightness, which in turn limits their patterning speed. Multi-photon reactions have been proposed to overcome the diffraction limit. However, these require very large intensities for modest gain in resolution. Moreover, the large intensities make it difficult to parallelize, thus limiting the patterning speed. In this dissertation, a novel nanopatterning technique using wavelength-selective small molecules that undergo single-photon reactions, enabling rapid top-down nanopatterning over large areas at low-light intensities, thereby allowing for the circumvention of the far-field diffraction barrier, is developed and experimentally verified. This approach, which I refer to as Patterning via Optical Saturable Transitions (POST) has the potential for massive parallelism, enabling the creation of nanostructures and devices at a speed far surpassing what is currently possible with conventional optical lithographic techniques. The fundamental understanding of this technique goes beyond optical lithography in the semiconductor industry and is applicable to any area that requires the rapid patterning of large-area two- or three-dimensional complex geometries. At a basic level, this research intertwines the fields of electrochemistry, material science, electrical engineering, optics, physics, and mechanical engineering with the goal of developing a novel super-resolution lithographic technique.

To my Bukes

"Strive for excellence, encourage communication across borders, and ignore the political boundaries that otherwise separate us"

– Jesse Owens

CONTENTS

ACKNOWLEDGMENTS

First and foremost, I would like to express my special appreciation and thanks to my advisor, Dr. Rajesh Menon; you have been a tremendous mentor for me. I would like to thank you for encouraging my research and for allowing me to grow as a research scientist. Your advice on both research as well as on my career have been priceless. I would also like to thank my committee members, Dr. Cynthia Furse, Dr. Hank Smith, Dr. Henry White, Dr. Florian Scholzbacher, and Dr. Bruce Gale, for serving as my committee members. I also want to thank you for letting my defense be an enjoyable moment, and for your brilliant comments and suggestions; thanks to you. I would also like to express my gratitude to my collaborators on this work at Politecnico di Milano, PoliMi, Istituto Italiano di Tecnologia, Dr. Rossella Castagna and Dr. Chiara Bertarelli, and at the University of Wisconsin-Madison, Dr. Trisha L. Andrew and Benjamin Pollock, who have all been instrumental in the success of this work and for the synthesis and characterization of the diarylethene photochromic molecule, enabling me to demonstrate the feasibility of POST.

I am grateful to Apratim Majumder and Farhana Masid and my labmates in the Menon group for making my graduate student life more bearable and, often, entertaining.

I also want to thank the National Science Foundation Graduate Research Fellowship Program (NSF GRFP) for their financial support under Grant No. 0750758. I would also like to thank the Nano Institute of Utah at the University of Utah for their financial support granted through the Nanotechnology Training Program. Finally I would like to thank the More Graduate Education at Mountain States Alliance Fellowship at the University of Arizona for their financial support.

Furthermore, I would also like to acknowledge with much appreciation the crucial role of the staff of the University of Utah Nanofab, the Mechanical Engineering Student Machine Shop, the Chemistry Mechanical Shop, and the Kurt J. Lesker Company who have been instrumental in the successful completion of this work.

Last but not least, I would like to thank my family and friends for their understanding and encouragement throughout these past years. It would be impossible for me to successfully finish this dissertation without their tremendous support.

CHAPTER 1

INTRODUCTION

1.1 Motivation

The pulse of the semiconductor industry for the past 40 years has been governed by Moore's law. Moore's law is an observation made by Gordon Moore, co-founder of the Intel Corp., in 1965, in which he predicted that the number of transistors that could fit on a microchip would double every two years, Figure 1.1. So essentially every two years computers would become twice as powerful. For the past 40 years, this has been fairly accurate, but for the past 10 years, we have fallen behind this exponential growth that Moore predicted. The current microchips have about 1 billion transistors, but if we were keeping up with Moore's law we would be up to 4-5 billion transistors by today. To address this decline in exponential growth, new advancements in lithography must be made to pattern at scales from micrometers down to nanometers. However, this persistent growth in computing power has led to increase cost and complexity of the techniques used to pattern at these scales.

This dissertation describes and demonstrates an alternative optical lithographic technique that achieves deep sub-wavelength resolution using novel photo-switchable molecules. This approach has the potential to enable optical nanopatterning (<10nm) over large areas (hundreds of cm^2).

1.2 Optical Projection Lithography

The semiconductor industry applies pattern replication via optical-projection lithography, or OPL, to create nanostructures that form the basis of integrated circuits, which in turn drive all of modern electronics, Figure 1.2. OPL uses a photomask, Figure 1.3, which is a glass substrate that contains a scaled-up version of the desired pattern. This pattern is imaged with 4X demagnification using a complex optical system onto a silicon wafer. The image is recorded in a photoresist that coats the wafer surface. The wafer is scanned at high speed and this image is reproduced at staggered locations (referred to as fields or dies) on

the wafer. Typical silicon wafers in manufacturing are 300mm in diameter, while the field size is $\sim$ 32mm X 24mm. The field is limited by the flatness of the surface of the wafer. For accurate lithography, this surface has to be flat to a small fraction of the depth-of-focus of the imaging system, typically a few hundred nanometers. OPL is ubiquitous in semiconductor manufacturing primarily due to its high speed. It is not unheard of for OPL tools to print two hundred 300mm-wafers per hour, i.e., one 300mm-wafer is printed in $\sim$ 18 seconds! Such tools are among the most complex manufacturing machines ever built by humans and can cost in excess of $40M each, Figure 1.4.

Incidentally, each photomask has to be patterned via a pattern-generation process. Suffice it to say, the photomask can take several weeks if not months to generate, and can itself cost in excess of $50K. Up to 30 different photomasks are typically required to create a single integrated circuit device. One can see that the cost of manufacturing at the nanoscale adds up very quickly. It is difficult to justify these costs unless they are amortized over a large number of products (as is the case for memory chips and microprocessors). Unfortunately, in almost all growing industries the product volumes do not exist to justify these manufacturing techniques. In addition, since the pattern on the photomask is fixed, OPL is extremely inflexible and is not easily amenable to experimentation. For instance, if one wants to change the geometry to study potential improvement in device performance, a new photomask that could cost over $50K would have to be ordered. Finally, OPL is highly optimized for rectilinear structures. It is not suitable for printing more complex geometries such as those employed in Figure 1.5. The pattern on the photomask is generated primarily via scanning-electron beam lithography (SEBL). SEBL employs a tightly focused beam of electrons that are then scanned over an electron-sensitive resist that coats the substrate, Figure 1.6. At high energies (over 30keV typically), the electrons can be focused to spots of less than 10nm full-width-at-half-maximum (FWHM). Thereby high-resolution patterns can be generated, Figure 1.7. The main drawbacks of SEBL are: (1) it is agonizingly slow due to its inherent serial nature, (2) pattern-placement and overlay accuracies are significantly worse than the resolution, since electrons are easily affected by stray electromagnetic and electrostatic fields as well as temperature and other environmental variations, Figure 1.8, and (3) it requires ultra-high vacuum and high-voltage electronics as well as low noise amplifiers, all of which add to their cost and complexity. Other pattern-generation technologies based on charged particles such as ion beams share these same disadvantages.

Photons, on the contrary, can create patterns extremely fast. However, they suffer from the far-field diffraction limit,[1] and hence, are limited to features that are larger than about

one-half the wavelength, Figure 1.9. Yet, efforts to address this diffraction limit have been largely based on nonlinear processes such as multi-photon absorption.[2–4]

Current photolithography is generally performed with projection printing utilizing ultraviolet (UV) light. In projection printing, light passes through a reticle or mask and is focused on the wafer through a 4:1 reduction lens system (Figure 1.2). The wavelength of light utilized is critical as shorter wavelengths of light allow smaller features to be printed. The direct proportionality of this relationship is described by the minimum resolvable spatial period (Equation 1.1).

$$P_{min} = \frac{\lambda}{2NA} \tag{1.1}$$

Other factors governing the minimum feature resolution are the numerical aperture (NA) of the lens. This relationship has led photolithographers to drive toward the use of ever shorter wavelengths of light and even higher numerical aperture for the production of transistors.

1.3 Alternative Lithographic Approaches

Several techniques such as photo-induced deactivation (RAPID) lithography,[4] Multiphoton Absorption Polymerization,[3] and Two-Photon Continous Flow lithography (TP-CFL)[2] have been proposed to circumvent this far-field diffraction limit. The first two of these suffer from poor image contrast and require high light intensities, which limit their potential for parallelizability and high throughput. TP-CFL still suffers from fabrication of large-volume structures with high throughput. The last approach AMOL[5] is the predecessor to the proposed approach of this dissertation, Patterning via Optical Saturable Transitions (POST).[6–10] AMOL utilizes photochromic molecules that can be optically switched between two thermally stable states, one opaque and the other transparent. When a layer of this material is exposed to a focused bright spot at λ_1 (the wavelength that converts from the opaque to the transparent form) and simultaneously to a focused node at λ_2 (the wavelength that reverses the transformation), the ensuing photochemical equilibrium results in a sub-wavelength transparent region in the vicinity of the node, Figure 1.10. The focal ring at λ_2 is in direct competition with the round spot at λ_1, and this creates a localized sub-wavelength aperture. Light at λ_1 penetrates through this aperture, forming a nanoscale probe. The lateral size of this probe is not limited by diffraction, but by material parameters and the ratio of the intensities at the two wavelengths. In other words, optical near-fields

are generated from afar. However, AMOL is limited to surface (2-D) patterning and in its current implementation, also suffers from the requirement of high light intensities.[5]

1.4 Dissertation Outline

A fundamental problem addressed in this dissertation is the demonstration of decisively circumventing the diffraction barrier in optical nanopatterning at low light intensities, something that was considered impossible only a few years ago. The innovativeness of this idea is that it is aimed at developing a novel, scalable, cost-effective super-resolution photolithography technique for nanofabrication, by demonstrating a new scaling law.

In this dissertation, the concept of patterning via optical saturable transitions (POST) is described, and experimentally verified. In Chapter 1, the motivation of this dissertation is alluded, the current industry optical lithographic technique and alternative lithographic approaches are discussed and summarized. In Chapter 2, the principle of a super-resolution microscopy technique, Stimulated Emission Depletion (STED), which is the analogue of AMOL and POST, is described. Absorbance Modulation Optical Lithography (AMOL) is described in further detail. The photochemistry of the organic photochrome, BTE, used in both AMOL and POST is described as well as the advantages of the POST technique. In Chapter 3, the principle of interference lithography is explained and the types of laser interferometers used in this dissertation are discussed. In Chapter 4, the design and fabrication of a custom high vacuum thermal evaporator which is employed for the preparation of the thin-films in my studies is illustrated. The chapter includes the details of the preparation of the samples and also the characterization of the thin film samples under investigation. In Chapter 5, the electrochemical *locking* step is discussed and the experimental setup is illustrated along with the UV-Vis spectrophotometer used for the optical characterization. In Chapter 6, we characterized a photochromic molecule, compound **1**, as a resist material for optical nanopatterning. We have shown that the molecule can be used as both a negative-tone or positive-tone resist with the appropriate choice of developer. In Chapter 7, we introduce a new *locking* step for POST, which I call selective dissolution of one photoisomer. In Chapter 8, a review and simple simulation model for POST is presented. In Chapter 9, a detailed protocol for POST fabrication and characterization is presented and described. And finally in Chapter 10, A new nanopatterning technique is introduced and discussed that exploits the extreme precision that is now available in mechanical translation, which I call NanoResolution via NanoTranslation (NRNT).

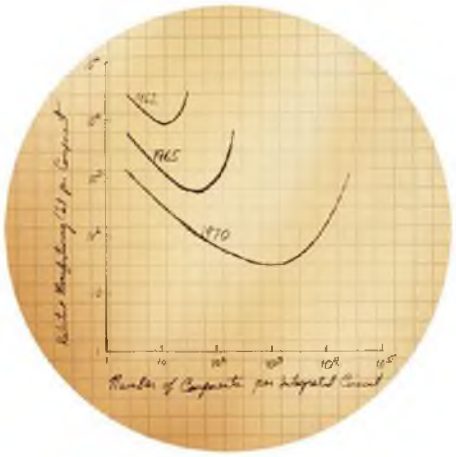

Figure 1.1: Cost vs. time sketch from Moore's 1964 notebook. [Image courtesy of Computer History Museum].

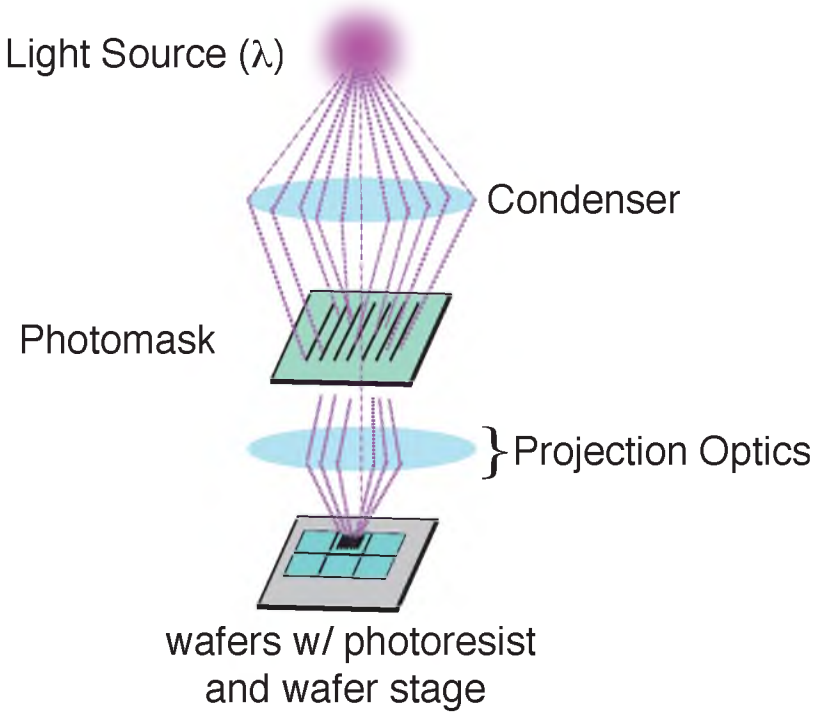

Figure 1.2: Optical projection lithography system.

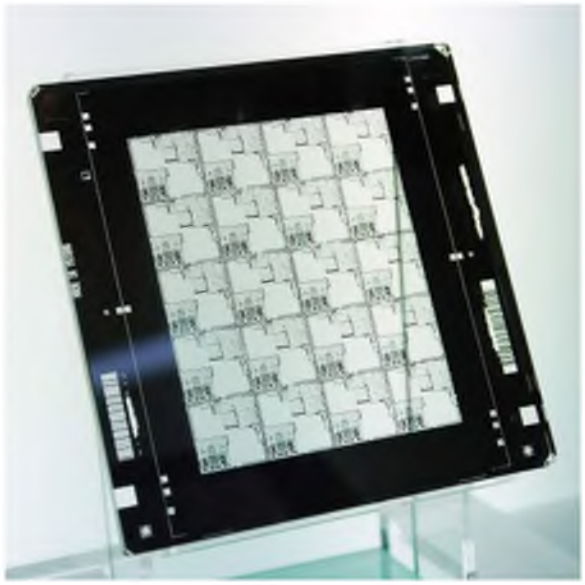

Figure 1.3: Semiconductor Photomask. [Image attributed to Pellden under the Creative Commons Attribution-Share Alike 3.0 Unported License.]

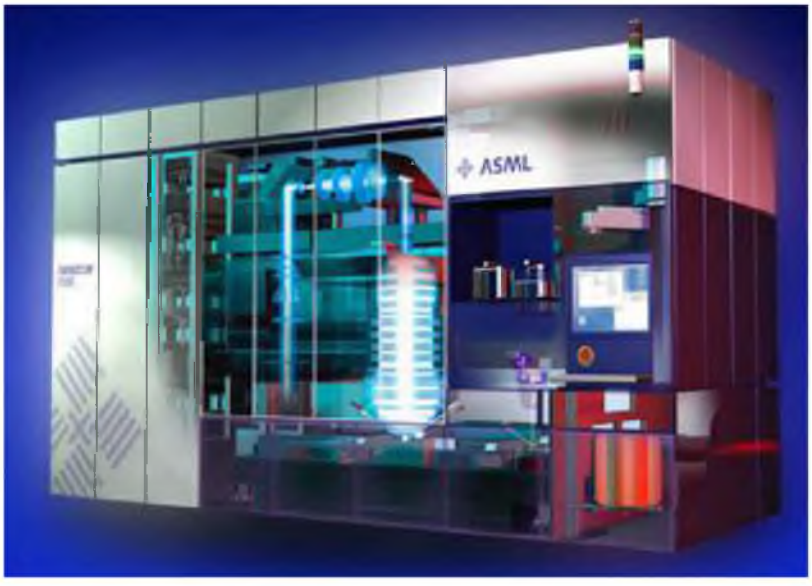

Figure 1.4: Industry OPL system for chip production. The bright area in the center of the machine represents the optical projection lense. [Image courtesy of ASML]

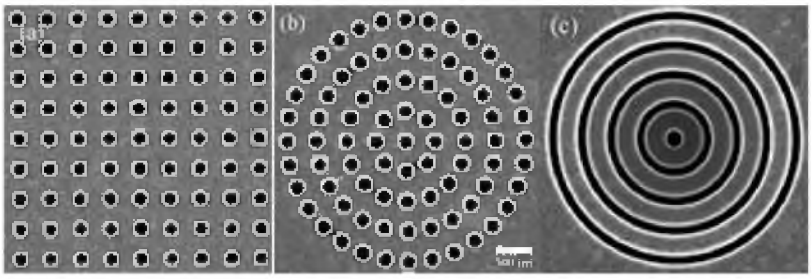

Figure 1.5: Complex geometries fabricated by focused ion beam. [Image courtesy of Olivier Martin, EPFL]

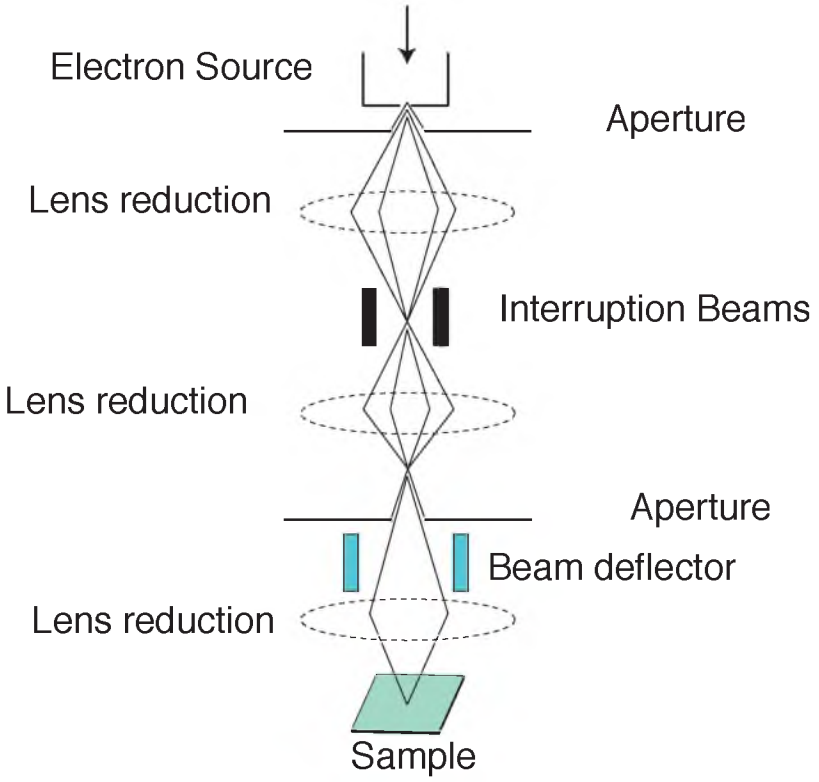

Figure 1.6: Scanning Electron Beam Lithography system

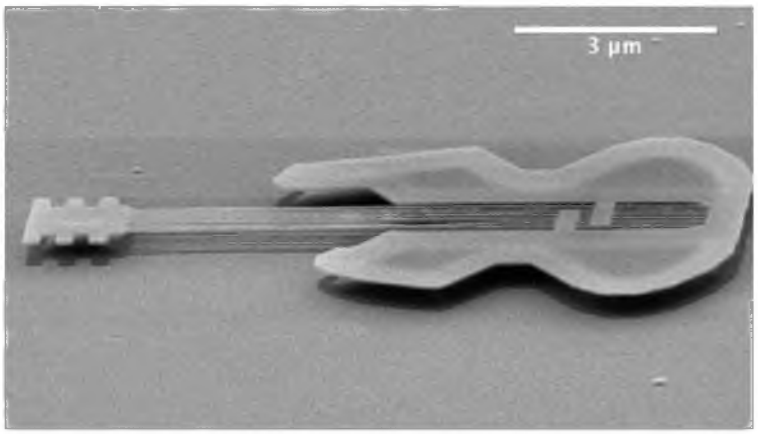

(a)

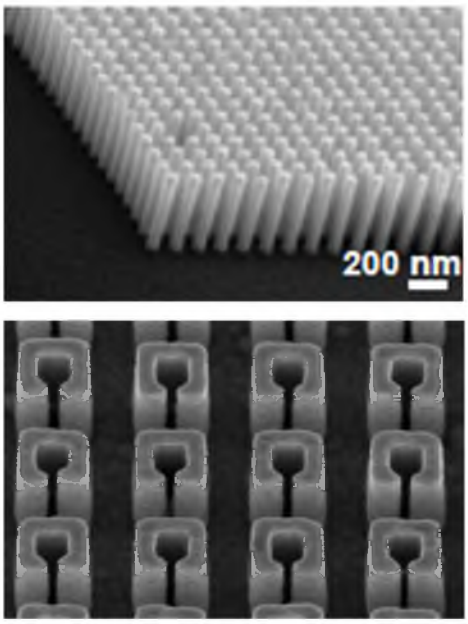

(b)

Figure 1.7: SEBL images. (a) Nano guitar. [Image credit to D. Carr & H. Craighead]. (b)Fabricated split-ring resonators (SRRs) - plasmonic nanostructures. [Image courtesy of Yasin Ekinci, Paul Scherrer Institute].

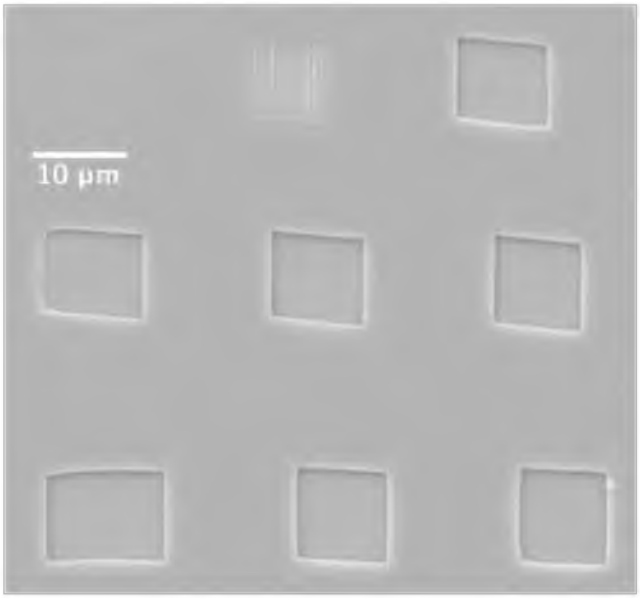

(a)

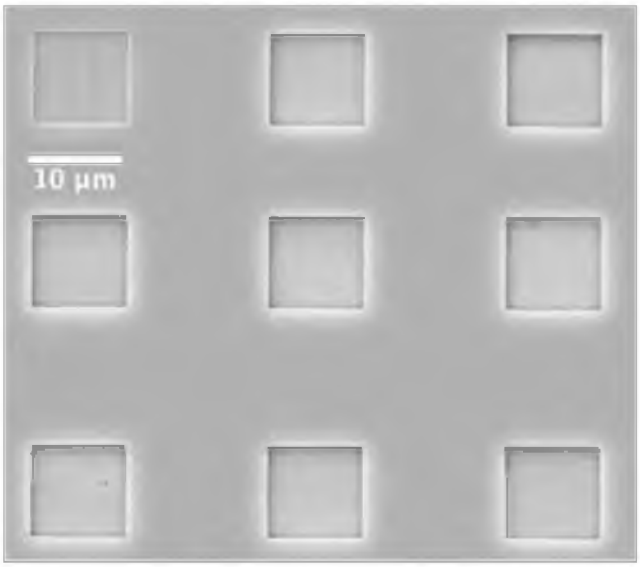

(b)

Figure 1.8: Localized charging of GaN substrate. (a) Less conductive GaN substrate 10μm square box in the upper left has the lowest dose and the lower right box has the highest dose. (b) Identical pattern as in (a), now with $\sim$ 10nm of conductive layer of aluminum evaporated on top of resist. [Reprinted with permission from JC Nabity Lithography systems, jcnabity.com].

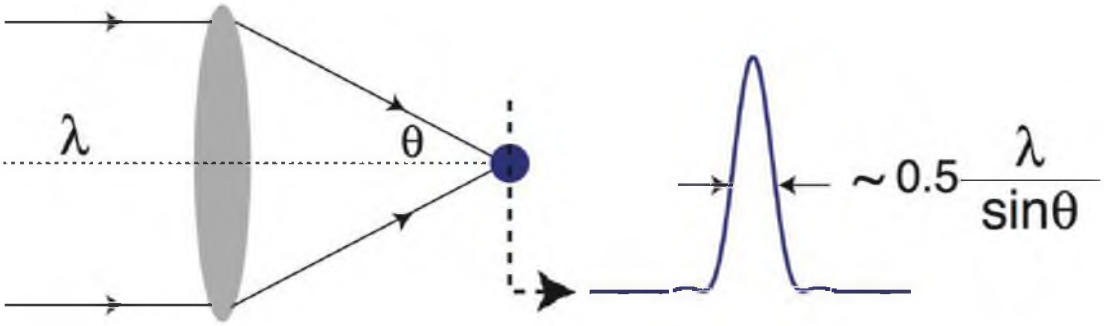

Figure 1.9: Ernst Abbé diffraction limit

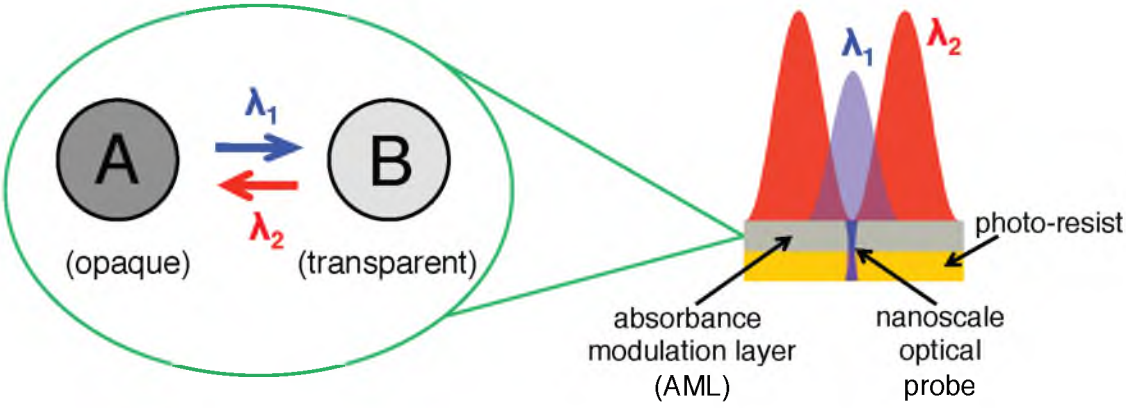

Figure 1.10: Absorbance Modulation Optical Lithography (AMOL)

1.5 References

[1] E. Abbe. Beitrge zur theorie des mikroskops und der mikroskopischen wahrnehmung. *Arch. mikrosk. Anat. Entwichlungsmech*, 9:413–468, 1873.

[2] S. C. Laza, M. Polo, A. A. R. Neves et al. Two-photon continuous flow lithography. *Advanced Materials*, 24(10):1304–1308, 2012.

[3] L. Li and J. T. Fourkas. Multiphoton polymerization. *Materials Today*, 10(6):30–37, 2007.

[4] L. Li, R. R. Gattass, E. Gershgoren et al. Achieving $\lambda/20$ resolution by one-color initiation and deactivation of polymerization. *Science*, 324(5929):910–913, 2009.

[5] T. L. Andrew, H.-Y. Tsai and R. Menon. Confining light to deep subwavelength dimensions to enable optical nanopatterning. *Science*, 324(5929):917–921, 2009.

[6] N. Brimhall, T. L. Andrew, R. V. Manthena et al. Breaking the far-field diffraction limit in optical nanopatterning via repeated photochemical and electrochemical transitions in photochromic molecules. *Physical Review Letters*, 107:205501, 2011.

[7] P. Cantu, N. Brimhall, T. L. Andrew et al. Subwavelength nanopatterning of photochromic diarylethene films. *Applied Physics Letters*, 100(18):183103, 2012.

[8] P. Cantu, T. L. Andrew and R. Menon. Nanopatterning of diarylethene films via selective dissolution of one photoisomer. *Applied Physics Letters*, 103(17):173112, 2013.

[9] P. Cantu, T. L. Andrew and R. Menon. Patterning via optical-saturable transformations: A review and simple simulation model. *Applied Physics Letters*, 105(19):193105, 2014.

[10] P. Cantu, T. L. Andrew and R. Menon. Patterning via optical saturable transitions - fabrication and characterization. *Journal of Visual Experiements*, 94:e52449, 2014.

CHAPTER 2

BACKGROUND

2.1 Stimulated Emmission Depletion (STED) Microscopy

In the early 1990s, the German physicist and most recently, 2014 Nobel Prize winner in Chemistry, Stefan W. Hell, developed the super-resolution microscopy technique, stimulated emission depletion (STED). Fluorescence microscopy is the most widely used imaging modality in biological research as cellular environments are crowded, highly packed environments, so for the ability to see the interactions between molecules and cells, one would need a resolution at the cellular scale; this is where STED microscopy comes in. The resolution of a light microscope is fundamentally limited by diffraction to about 200nm.[1] So if you have two features that are residing at a closer distance than 200nm (1/2 the wavelength of light), as is the case in biological environments, then it is not possible to distinguish the two. Two features of the same kind, in order to be separated by the a light microscope, have to be further away from each other, by more than the distance, d, given by the wavelength of light, λ, divided by twice the numerical aperture of the objective lens. And this value amounts to at least 200nm. This is why for over a century, biologists thought that it would be impossible to see single molecules with a light microscope.

However, in recent years, STED microscopy has made dramatic resolution progress. This technique has demonstrated measured point-spread functions of 5.8nm in width.[2] In a typical STED microscope, the phenomenon works by the nonlinear, spatially modulated de-excitation of fluorophores to quench fluorescence of the fluorophores to areas or volumes smaller than the diffraction limit. A collimated excitation beam is focused to a point by an objective lens to achieve an approximately Gaussian, diffraction-limited point-spread-function (PSF) in the sample plane. A red-shifted in wavelength, STED beam, is modified with a phase plate to create a donut–shaped spot with a null in the center and is then combined with the excitation beam to create two collinear beams. This STED beam causes the fluorophores on the periphery of the beam to quench. As the intensity of the STED beam is increased relative to the excitation beam, the spot size

at the focus is squeezed down to an area or volume much smaller than the diffraction limit, Figure 2.1. Hell suggested that one could take this idea and apply it to optical lithography.[3,4] The major differences between the concept of STED in microscopy and its use in lithography is the use of photochromes instead of fluorophores and the need for a *locking* mechanism. Previously, our group has applied the basic STED concept in reverse, to achieve super-resolved features in conventional photoresist. This technique, which we call Absorbance Modulation Optical Lithography,[5] is, however, limited to surface (2-D) patterning in its current implementation and suffers from the requirement of high light intensities. To overcome these disadvantages of AMOL, we have invented a new method of nanoscale fabrication that addresses the limitations of AMOL. This method, which we call Patterning via Optical Saturable Transitions (POST),[6–10] uses specific combinations of chemical species that enable nanopatterning, which makes use of spectrally selective reversible and irreversible transitions enabled by chemistry. So we are able to circumvent the diffraction barrier in optical lithography by exploiting chemistry rather than wavelength.

2.2 Diarylethene Photochromic Molecule

In the late 19th century, organic photochromes where first observed.[11] Photochromism can be defined as a reversible photo-induced transformation between two isomeric states. Among the many photochromic molecules, a diarylethene derivative serves as the candidate photochrome in this dissertation. It is appealing due to its resistance to photo-fatigue, thermal irreversibility, and its high photo-reactivity. As shown in Scheme 2.1, the candidate diarylethene derivative, 1,2-bis(5,5-dimethyl-2,2-bithiophen-yl) perfluorocyclopent-1-ene, known colloquially as BTE, has two isomeric states, the closed-ring isomer, **1c**, and the open-ring isomer, **1o**. Irradiation of **1o** with UV light (λ_1) results in a photoisomerisation that transitions to **1c**. The reverse reaction is done by irradiation of **1c** with longer wavelength visible light (λ_2).

In an optical lithographic scheme it is most desirable to have high selectivity between each form of the isomers, meaning the UV-Vis absorption spectra of the photochrome should have as large as possible separation bands. Figure 2.2 (a,b) shows the absorption spectra of the thin-film BTE and BTE in hexane solution. The absorption peak of the open-ring isomer, **1o**, is at 325nm. The closed-ring isomer, **1c**, has the peak absorption at 633nm.

2.3 Patterning via Optical Saturable Transitions (POST)

The objective of this dissertation is to develop a novel nanopatterning technique using wavelength-selective small molecules that undergo single-photon reactions, enabling rapid

top-down nanopatterning over large areas at low light intensities, thereby allowing for the circumvention of the far-field diffraction barrier. This alternative optical lithographic approach exploits unique combinations of spectrally selective reversible and irreversible photochemical transitions to achieve deep subwavelength resolution with potential extension to 3-dimensions. The idea is to record the nanoscale pattern in an ultra-thin or monolayer film comprised of photochromic molecules. For simplicity, an **A, B, C** scheme is used to explain the technique, as indicated by Figure 2.3. These molecules undergo photoswitching between two isomeric forms, **A** and **B**. When isomer **A** absorbs a photon of wavelength λ_1, it turns into isomer **B**. When **B** absorbs photon of wavelength λ_2, it turns back to **A**. In addition, we engineer the molecules such that **B** can be selectively converted in an irreversible manner to form **C** via a *locking* step. This can be achieved in several ways, including using a photochemical reaction, electrochemical oxidation, chemical oxidation, or isomer-selective dissolution.

The sequence of steps that allows for sub–diffraction-limited patterning is further illustrated in Figure 2.4 in one-dimension for simplicity. In this example, I begin in step 1 with a substrate that is coated with the material all in form **B**. In step 2, this film is exposed to a standing wave at λ_2, which results in interspersed regions of **B** and **A**. In step 3, the substrate is moved relative to the illumination by Δ_1 and the exposure is repeated. The binary (highly nonlinear) nature of the switching process ensures that sub–diffraction-limited regions of **B** interspersed in **A** are formed. The width of the **B** region is approximately given by $P/2 - \Delta_1$ in this example, where **P** is the period of the standing wave. In step 4, the *locking* mechanism is invoked to convert all **B** regions irreversibly to **C**. In step 5, a uniform exposure to λ_1 converts all material (except those that are locked into **C**) back into form **B**. In step 6, the sample is displaced relative to the illumination so as to convert regions surrounding **C** back to **A**. In step 7, the sample is displaced relative to the illumination by Δ_2 and the exposure is repeated. Note that as a result, a small region of **B** is placed next to the first **C** region with a spacing that is determined primarily by the difference between the displacements Δ_1 and Δ_2. Since mechanical displacement can be far more accurate and precise compared to the diffraction limit, sub-diffraction-limited patterning is achieved. In step 8, regions in **B** are locked to **C**. The steps 6-8 are repeated until the desired pattern geometry is achieved. Finally, the regions in **C** could be dissolved away, resulting in topographical patterns.

2.4 The *Locking* Step

In conventional lithography, an image is permanently impressed into a recording medium, typically photoresist. In the technique to be described here, an image is recorded into a recording medium, a photochrome, but it is not permanent as the image can be *erased*. To make the image permanent, a *locking* step is necessary. One of the main challenges of this technique is the mechanism for *locking*. I have experimentally demonstrated two methods to achieve this. The first approach is based upon electrochemical oxidation of the closed-ring isomer, **1c**, of BTE, Figure 2.5. The alternative approach to electrochemical *locking* is by simply dissolving away one of the isomers selectively. Empirically, I discovered that ethylene glycol is able to selectively dissolve the closed-ring isomer, **1c**, at a much faster rate as compared to the open-ring isomer, **1o**. As illustrated in Figure 2.6, we can then simply dissolve away **1c** to *lock* the pattern in place. My experiments suggest a dissolution selectivity of greater than 20:1, Figure 2.7. I also performed careful Density Functional Theory (DFT) simulations to prove that the selective solubility can be explained by the increased dipole moment of **1c** compared to **1o**, Figure 2.8.

The closed-ring isomer, **1c**, has an extended conjugation of its π-electron cloud, which allows for **1c** to have a lower oxidation potential than the open-ring isomer.[12] Therefore, my *locking* mechanisms rely on the selective oxidation or dissolution of the closed-ring isomer.

2.4.1 Electrochemical Oxidation

The electrochemical oxidation *locking* step is achieved by electrochemically oxidizing the closed-ring isomer, **1c**, into a stable cation. This product cation is preferentially soluble in a polar solvent compared to the unoxidized isomers. Therefore, it allows us to convert the *locked* regions into topographic nanoscale patterns after all the exposures are completed. This idea is illustrated in Figure 2.5.

The BTE molecules were deposited via Low Temperature thermal Evaporation (LTE) in a custom-made vacuum chamber with background pressure of $\sim$1 x 10^{-7} Torr. For electrochemical oxidation of the molecule, all films were deposited on platinum (Pt)-coated silicon substrates, which were obtained by immersion in diluted hydrofluoric acid ($HF:H_2O$ = 1:50) to etch away the native oxide layer. Upon irradiation with short-wavelength UV, the open-ring isomer, **1o**, converts to the closed-ring form, **1c**. A subsequent illumination with a node at λ_2= 633 nm converts the molecules back to the open-ring form, **1o**, except in the near-vicinity of the node. By optically saturating this transition, only a small group of molecules near the node remain in the closed-form, **1c**. Then, selective electrochemical oxidation of the closed-ring form into a stable radical cation completes the patterning.

This is done by applying an oxidation potential of ~0.5V, Figure 2.9. Finally, the sample is developed in a mixture of 95 wt(%) ethylene glycol and 5 wt(%) isopropanol, which dissolves away the cations. Most of the unoxidized BTE remains. Repeating the three patterning steps with subsequent displacement of the sample relative to the optics allows two features to be patterned with a pitch much smaller than allowed by the far-field diffraction limit. Also, as the two photoisomer states are thermally stable, high resolution at low light intensities is achievable.

2.4.2 Selective Dissolution

An alternative approach to the electrochemical *locking* mechanism, that I discovered accidentally in the lab which I investigated further, is based on selective dissolution of one photoisomer. The idea is based upon the selective dissolution of one of the isomers of the BTE, in this case the closed-ring isomer, **1c**. This has the advantage of not requiring a conductive Pt layer, which might be problematic in some devices. Also, it combines the two steps of *locking* and development into a single dissolution step. The idea is illustrated in Figure 2.6.

This electrode-free technique as a highly selective *locking* step bypasses the electrochemical oxidation by exploiting the difference in solubility between the two thermally stable photoisomer states of the molecule, Figure 2.7. In the POST selective dissolution process, a thin film, BTE, is again thermally evaporated onto a substrate (i.e. silicon wafer). Upon uniform irradiation with short-wavelength UV, λ_1, the open-ring isomer, **1o**, converts to the closed-ring form, **1c**. A subsequent illumination with a node, λ_2, at 633nm converts the molecules back to the open-ring form, **1o**, except in the near-vicinity of the node. By optically saturating this transition, the molecules in the closed-ring form, **1c**, remain in a region that is far smaller than the far-field diffraction limit. It is at this stage that the solubility difference *locking* step is applied by developing the sample in a polar solvent (100 wt(%) ethylene glycol). This highly selective solubility *locking* step opens the door to an inexpensive, scalable nanopatterning technique.

2.5 Advantages of POST

POST enjoys 4 major advantages: 1) Resolution is determined predominantly by the quality of the node at λ_2 and sub-10nm nanostructures are feasible with near-UV and visible light. In other words, the far-field diffraction limit is broken. 2) A node can possess a large optical depth-of-focus which increases process latitude and yield.[13–23] 3) Only low intensities are required. This allows for massive parallelism and fast patterning. 4) Scalability to

large areas would require massive parallelism and compatibility with inexpensive replication technologies such as imprint or roll-to-roll lithography.[24,25]

POST also has the potential to create sub-diffraction-limited patterns in the photoresist layer without the use of a mask, alleviating the need to design and manufacture a mask, removing the need to consider the contamination of the mask. These advantages provide a useful technique to access the non-diffraction-limited near-field using far-field optics, providing an opportunity to improve resolving capability. Secondly, the maskless nature of POST allows for quick prototyping of circuit designs as making a mask is often a considerable expense and may also allow for inexpensive surface patterning. However, in order to be able to make use of these advantages, further understanding is needed of the POST process. One particular focus is the resolution limits and process latitudes of a POST system and how these can be improved or affected by system adjustments.

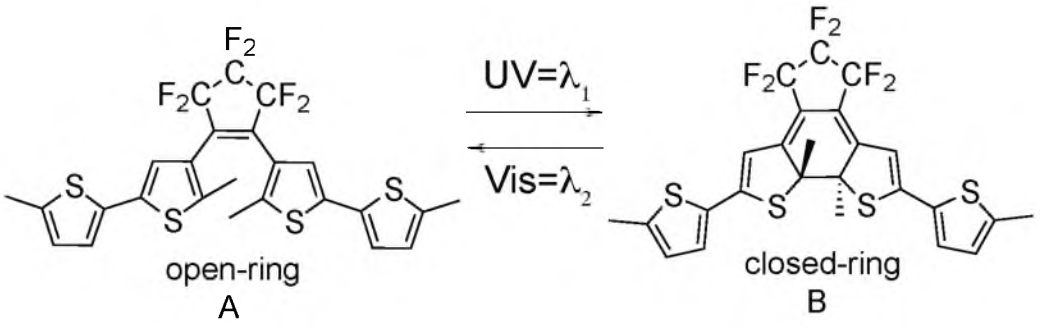

Scheme 2.1: Structures of the open- and closed-ring isomers of compound **1**.

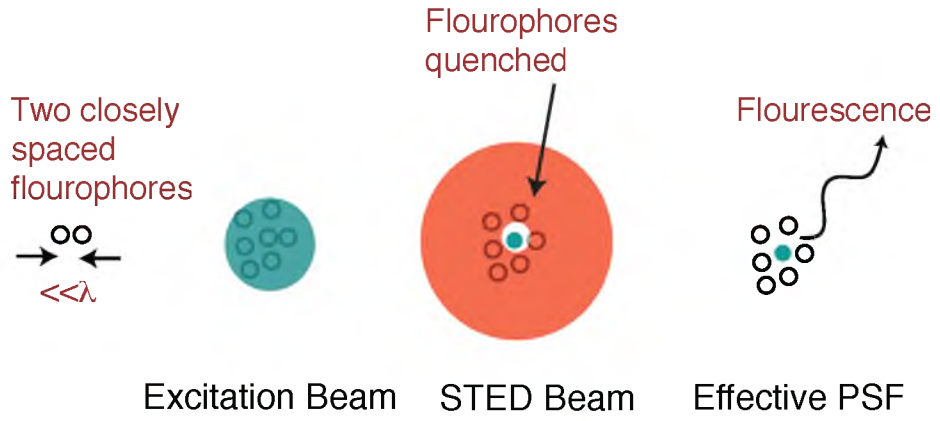

Figure 2.1: Representation of how the effective point spread function is formed by the overlap of the standard PSF and the depletion PSF.

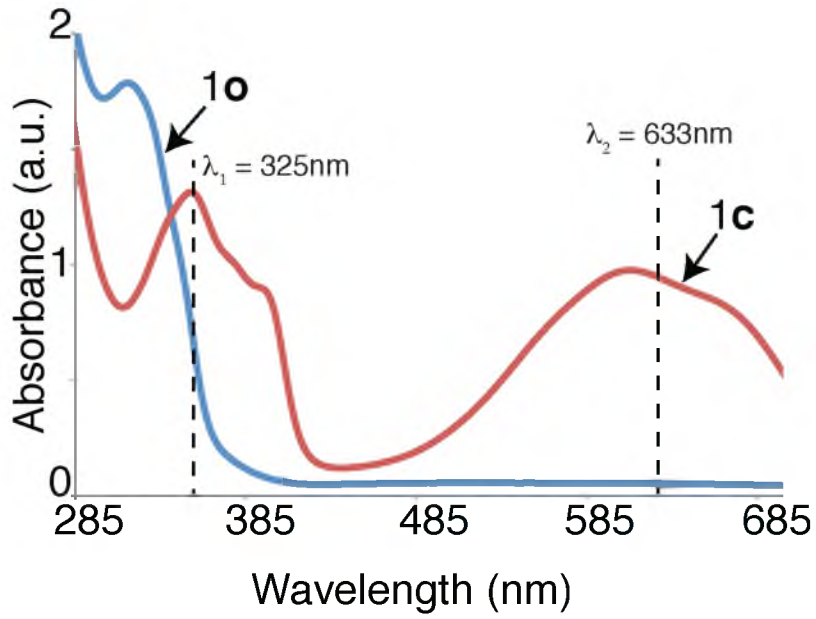

(a)

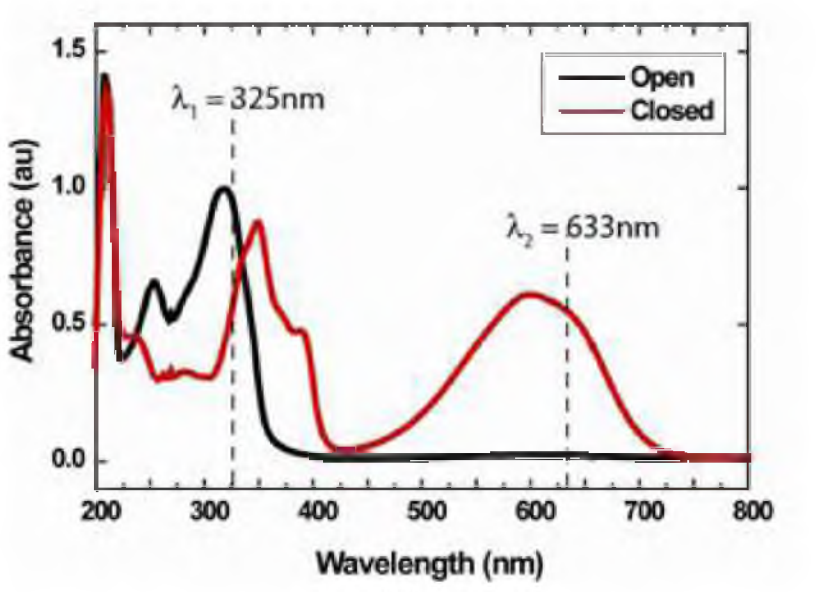

(b)

Figure 2.2: Absorbance spectra of compound **1** in the open and closed forms. (a) Thin-film form. (b) In hexane solution.

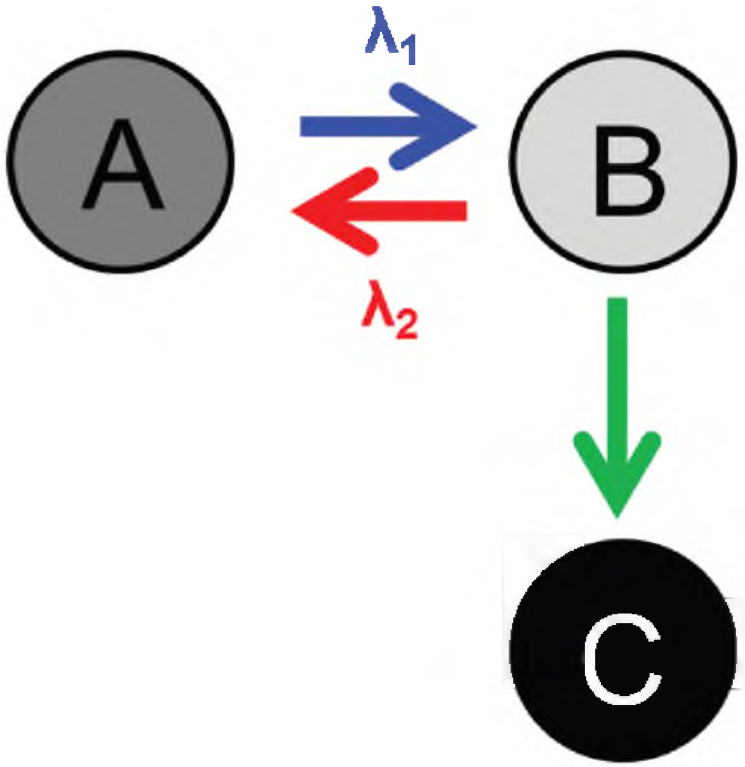

Figure 2.3: **A, B, C** scheme of BTE state transitions.

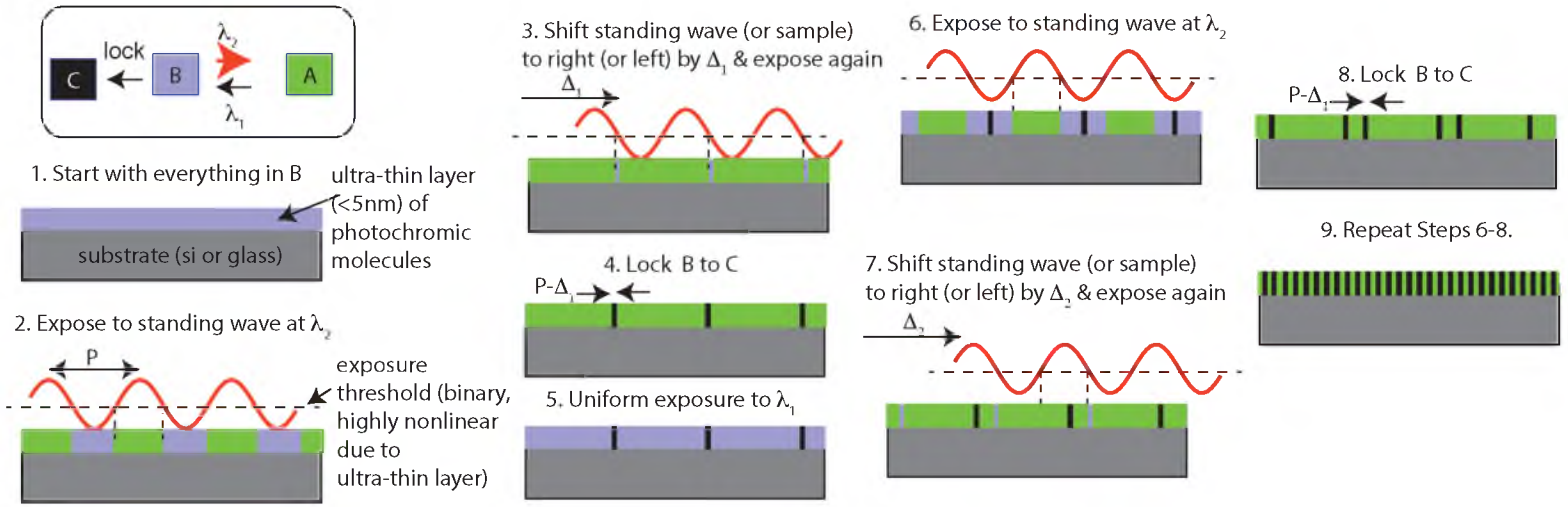

Figure 2.4: POST sequence of steps.

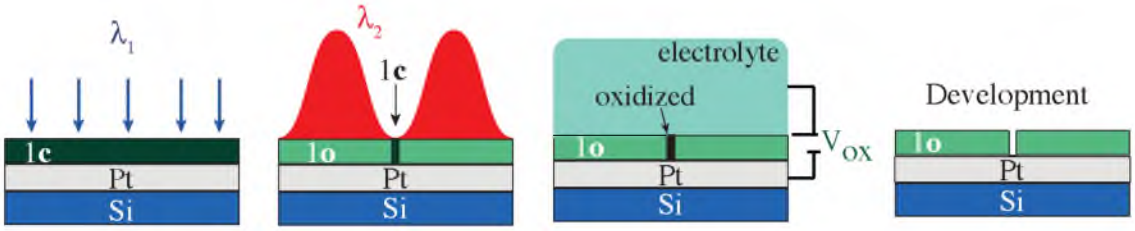

Figure 2.5: Electrochemical oxidation *locking* step.

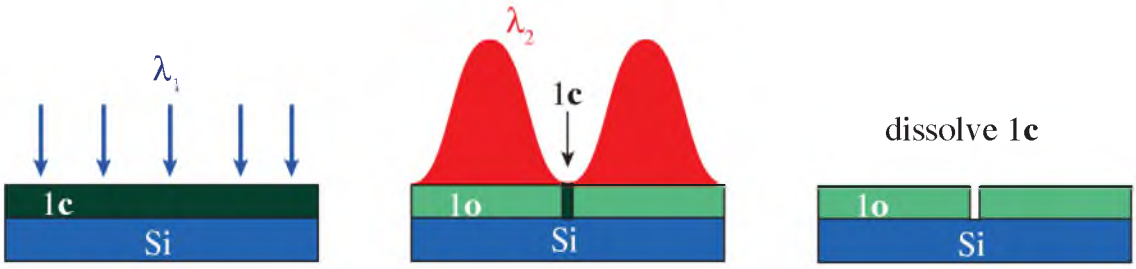

Figure 2.6: Selective dissolution *locking* step.

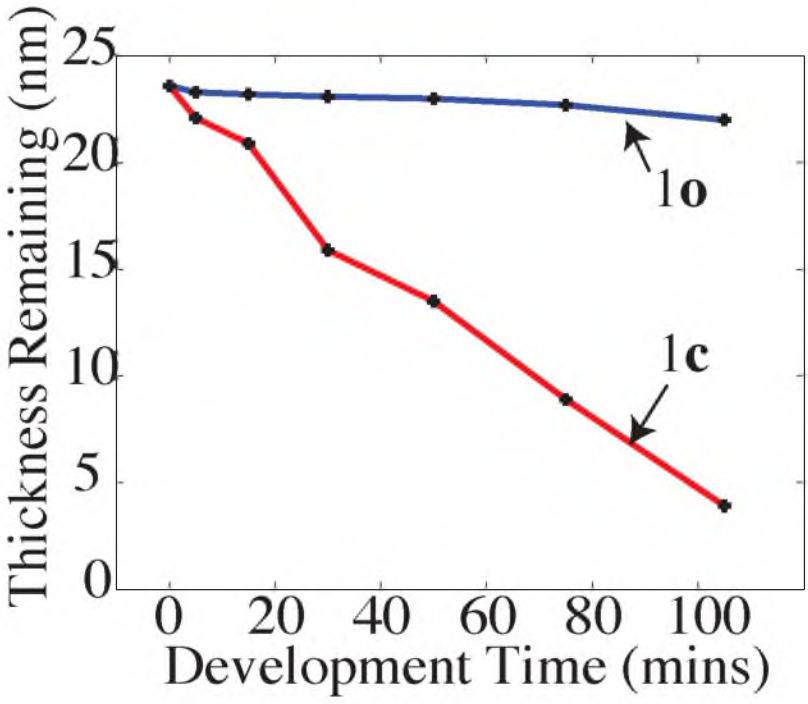

Figure 2.7: Macro-scale solubility of **1c** and **1o** in 100 wt(%) ethylene glycol.

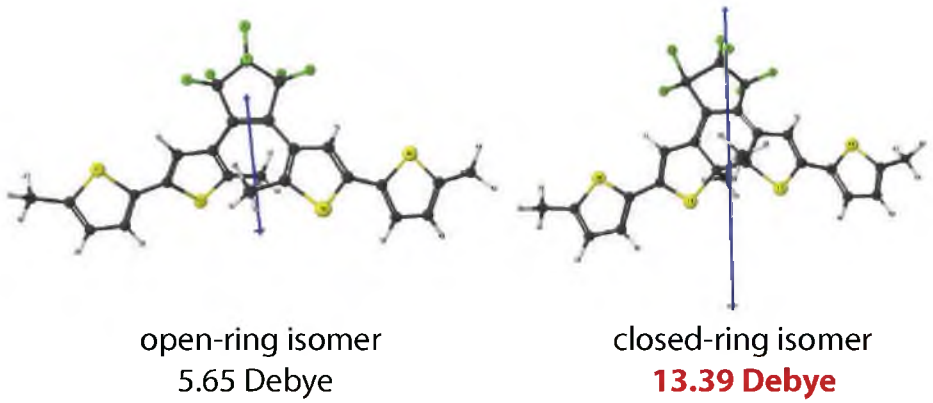

Figure 2.8: Density functional theory (DFT) calculations of open- and closed-ring isomer.

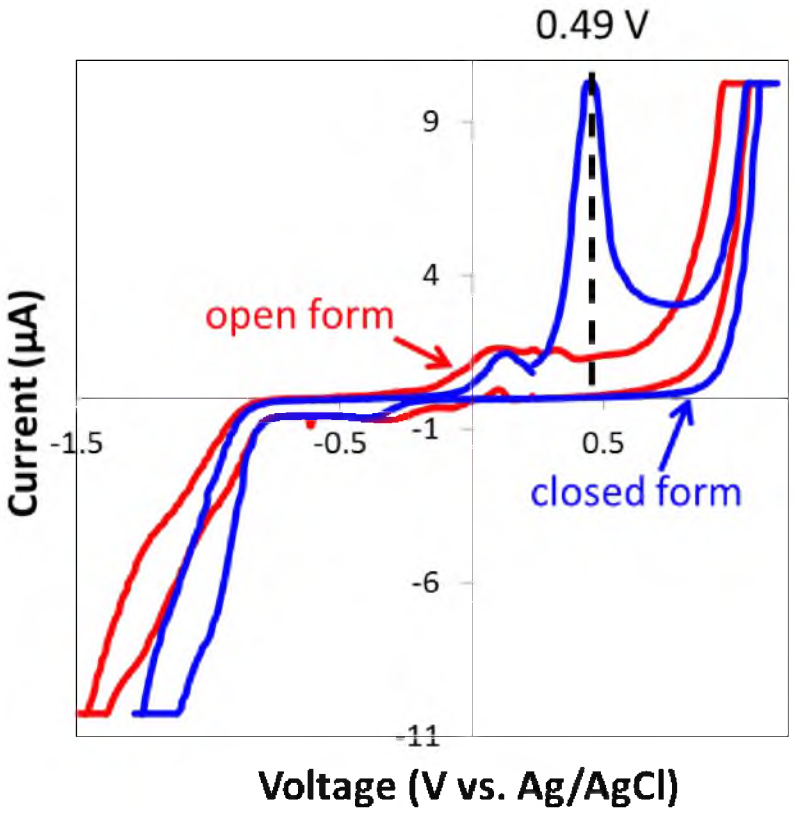

Figure 2.9: Cyclic voltammetry (CV) of thin-film BTE.

2.6 References

[1] E. Abbe. Beitrge zur theorie des mikroskops und der mikroskopischen wahrnehmung. *Arch. mikrosk. Anat. Entwichlungsmech*, 9:413–468, 1873.

[2] S. W. Hell, K. Y. Han, S. E. Irvine et al. STED microscopy reveals crystal colour centres with nanometric resolution. *Nature Photonics*, 3(3):144–147, 2009.

[3] S. Hell, S. Jakobs and L. Kastrup. Imaging and writing at the nanoscale with focused visible light through saturable optical transitions. *Applied Physics A*, 77(7):859–860, 2003.

[4] S. W. Hell. Strategy for far-field optical imaging and writing without diffraction limit. *Physics Letters A*, 326:140 – 145, 2004.

[5] T. L. Andrew, H.-Y. Tsai and R. Menon. Confining light to deep subwavelength dimensions to enable optical nanopatterning. *Science*, 324(5929):917–921, 2009.

[6] N. Brimhall, T. L. Andrew, R. V. Manthena et al. Breaking the far-field diffraction limit in optical nanopatterning via repeated photochemical and electrochemical transitions in photochromic molecules. *Physical Review Letters*, 107:205501, 2011.

[7] P. Cantu, N. Brimhall, T. L. Andrew et al. Subwavelength nanopatterning of photochromic diarylethene films. *Applied Physics Letters*, 100(18):183103, 2012.

[8] P. Cantu, T. L. Andrew and R. Menon. Nanopatterning of diarylethene films via selective dissolution of one photoisomer. *Applied Physics Letters*, 103(17):173112, 2013.

[9] P. Cantu, T. L. Andrew and R. Menon. Patterning via optical-saturable transformations: A review and simple simulation model. *Applied Physics Letters*, 105(19):193105, 2014.

[10] P. Cantu, T. L. Andrew and R. Menon. Patterning via optical saturable transitions - fabrication and characterization. *Journal of Visual Experiements*, 94, 2014.

[11] J. Fritzsche. *Comptes Rendus Acad. Sci.*, 69(1035), 1867.

[12] A. Peters and N. R. Branda. Electrochemically induced ring-closing of photochromic 1,2-dithienylcyclopentenes. *Chemical Communications*, 954–955, 2003.

[13] M. Sakai, S.-i. Ishiuchi, M. Fujii et al. Formation of a doughnut laser beam for super-resolving microscopy using a phase spatial light modulator. *Optical Engineering*, 43(5):1136–1143, 2004.

[14] M. P. MacDonald, L. Paterson, G. Armstrong et al. Laguerre-Gaussian laser modes for biophotonics and micromanipulation. *Proceedings of SPIE*, 5147:48–59, 2003.

[15] A. Vasara, J. Turunen and A. T. Friberg. Realization of general nondiffracting beams with computer-generated holograms. *Journal of the Optical Society of America A*, 6(11):1748–1754, 1989.

[16] C. Paterson and R. Smith. Higher-order Bessel waves produced by axicon-type

computer-generated holograms. *Optics Communications*, 124(1??2):121–130, 1996.

[17] T. Watanabe, M. Fujii, Y. Watanabe et al. Generation of a doughnut-shaped beam using a spiral phase plate. *Review of Scientific Instruments*, 75(12):5131–5135, 2004.

[18] J. A. O. Huguenin, B. C. dos Santos, P. A. M. dos Santos et al. Topological defects in moiré fringes with spiral zone plates. *Journal of the Optical Society of America A*, 20(10):1883–1889, 2003.

[19] H.-Y. Tsai, H. I. Smith and R. Menon. Fabrication of spiral-phase diffractive elements using scanning-electron-beam lithography. *Journal of Vacuum Science & Technology B*, 25(6):2068–2071, 2007.

[20] D. Yelin, B. E. Bouma and G. J. Tearney. Generating an adjustable three-dimensional dark focus. *Optics Letters*, 29(7):661–663, 2004.

[21] R. Ozeri, L. Khaykovich and N. Davidson. Long spin relaxation times in a single-beam blue-detuned optical trap. *Physical Review A*, 59:R1750–R1753, 1999.

[22] J. Arlt and M. J. Padgett. Generation of a beam with a dark focus surrounded by regions of higher intensity: the optical bottle beam. *Optics Letters*, 25(4):191–193, 2000.

[23] D. McGloin, G. Spalding, H. Melville et al. Three-dimensional arrays of optical bottle beams. *Optics Communications*, 225:215–222, 2003.

[24] S. H. Ahn and L. J. Guo. High-speed roll-to-roll nanoimprint lithography on flexible plastic substrates. *Advanced Materials*, 20(11):2044–2049, 2008.

[25] H. Schift. Nanoimprint lithography: An old story in modern times? a review. *Journal of Vacuum Science & Technology B*, 26(2):458–480, 2008.

CHAPTER 3

INTERFERENCE LITHOGRAPHY AND INERT ATMOSPHERE SAMPLE HOLDER

3.1 Principle of Interference

The ability to fabricate uniform nanoscale features is a critical issue as scientific and engineering quests reach the nanometer scale. These nanostructures must also cover a relatively large area to be useful in many applications. Interference lithography (IL) is a technique that can be used to accomplish this while keeping manufacturing costs within an acceptable range.

IL uses interference of light to pattern the underlying substrate. In this dissertation, a photochromic layer by means of multiple exposures and rotations two- and three-dimensional patterns can be obtained. The possible number of periodic patterns obtainable using interference lithography is only limited by the number of exposures and the number of beams in use. Two interference lithographic techniques were used in this dissertation. It is one of the few preferred methods for fabricating large areas of periodic patterns because of lower cost and parallel method of fabrication.

Interference lithography is a method used to obtain periodic patterns over a large area. Two coherent waves interfere to produce a standing wave. This standing wave when observed on a plane perpendicular to the wave propagation consists of alternating fringes of high brightness regions and dark regions. This pattern is made use of in interference lithography by recording it on a recording medium which is in turn used in transferring the pattern on to the substrate below.

The feature sizes realizable using interference lithography are less than what is realizable with the most advanced stepper lithography at mid-ultra violet wavelengths. In addition, the equipment needed for the IL setup is comparatively simpler. The process can be easily improved due to the comparatively less complex components involved. A limitation of IL is that only periodic patterns can be fabricated using the method. Though the periodicity of

the structures in different directions can be varied in certain IL systems, this aspect is also not much of a drawback because for most of the applications, uniform periodic patterns are the desired result.

The important parameter of the interference lithography pattern is the pitch or period of the pattern. It is the distance between two similar consecutive points in the pattern, like the distance between the centers of two consecutive peaks or nulls. The period is dependent on the wavelength of the light and the angle at which the beams are incident on the sample. It is given by:

$$P = \frac{\lambda}{2 \sin \theta} \tag{3.1}$$

where P is the period of the grating, λ is the wavelength of the light being used, and θ is the half angle of incidence of the beam.

3.2 Types of Laser Interferometers

3.2.1 Lloyd's Mirror Interferometer

One of the methods used in these experiments is the Lloyd's mirror interferometer. The major advantages of this system are that the period of the grating can be controlled more easily than other methods and that the period of the grating in each of the individual exposures can be changed easily and independently. One more of the advantages of Lloyd's mirror IL is that only one light beam is used when compared to two beams used in other systems of IL. This is beneficial because there are no problems related to stage movement and beam movement as in other IL systems. The result also depends on the mirror used and any scratches on its surface, or a lower reflectance at the wavelength in use.

The Lloyd's mirror interferometer for this dissertation used a Helium Neon (HeNe) laser and spatial filter with a beam expander. Its optical configuration is illustrated in Figure 3.1. The main aim of the beam expansion is to obtain near uniform light intensity on the substrate. This is useful in obtaining large areas of patterned resist with nearly uniform exposure over the whole area exposed. Half of the beam is reflected from the mirror and the other half illuminates the substrate directly. The overlapping of the beams produces the interference pattern on the substrate.

3.2.2 Mach-Zehnder

A Mach-Zehnder interferometer is a technique in which light is reflected into separate arms, transmitted into different directions, and then recombined upon a substrate to produce interference. Its optical configuration is illustrated in Figure 3.2.

A monochromatic HeNe source transmits light that is directed towards mirrors M1 and M2. The beam then propagates through a shutter and a half-wave plate ($\frac{\lambda}{2}$) to control the power in the arms. A polarized beam splitter is oriented at a 45 ° angle at position PBS to direct the split waves orthogonally towards mirrors M3 and M4. The two waves are then reflected by M3 and M4. In one arm, the beam passes through another half-wave plate ($\frac{\lambda}{2}$) to match the polarization in both arms. The beams are then recombined at the substrate surface. The overlapping beams at the substrate surface produce a periodic interference pattern.

3.3 Custom Inert Atmosphere Sample Holder

We previously solved the long-term storage requirement of the samples by storing them under N_2, directly after the initial evaporation.[1] However, the significant line-edge roughness evident in the gratings, Figure 3.3, is likely due to the formation of oxidized products of **1c** in the presence of air.[1] Improving the uniformity of the patterns requires that the exposure and development process be conducted under an inert atmosphere. To address the exposures done in ambient conditions, samples were exposed by sealing the air-sensitive samples between a quartz slide and an aluminum holder, Figure 3.4. However, this preparation was not well suited for the long exposures, as it suffered from eventual oxidation of the material, because of air leakage.

To address the air leakage, we desired to have a sample holder that provides a rigorous inert gas blanketing of the air-sensitive BTE in closed form, **1c**, and maintain an excellent seal for sufficient time to obtain the appropriate exposure conditions. Additional criteria regarding the holder included: (1) that it be easily assembled within an inert atmosphere glove box; (2) minimize sample displacement errors; and (3) be free of intensity artifacts associated with the holder. We also desired to configure the holder so that it could be easily modified for various optical configurations. Figure 3.5 (a-i) shows the construction/assembly steps and Figure 3.6 (a) shows the Solidworks® 3D rendering of the sample holder. The holder was prepared in three main parts, namely the aluminum base and top, along with the 1/4 wave 633nm V-coat window. The base and top were fabricated from aluminum for easy machining. The base contains an o-ring groove for easy alignment and seal when the top with the window is lowered into place onto the sample base. The two pieces are clamped by 3 fastener screws and a gas-tight seal is achieved. In addition, this holder has a port that extends from the sample cavity to a needle valve, which is used to purge oxygen from the cavity with N_2. There is also an outlet port with a one-way valve to maintain

positive pressure. Figure 3.6 (b) shows the machined sample holder.

To verify that we have eliminated the oxygen from the exposure step, we performed several exposures to see if the line edge roughness had improved. Assuming an incident sinusoidal illumination, we can readily simulate the resulting feature size. In Figure 3.7, this feature size is plotted as a function of the exposure time using the solid blue line. The experimentally measured values are shown using crosses. Using the exposure threshold as the only fitting parameter, we can show that this simple model can accurately explain our experimental results. The smallest experimentally obtained feature size was ~85nm, corresponding to a linewidth of $\sim \lambda/7.4$. More precise control of the exposure time should enable even smaller features. Note that as the exposure time is increased, the simulation indicates that the feature size with respect to the period should be reduced significantly below the far-field diffraction limit. You can clearly see from the SEM images that the line-edge roughness has improved with the use of the inert atmosphere sample holder.

A further step was taken to show more precise control of the exposure time, resulting in smaller features and mitigated line-edge roughness (LER). In Figure 3.8, the LW and exposure time are shown for a series of SEMs, resulting in much improved LER and smaller feature sizes, ~68nm, corresponding to a linewidth of $\sim \lambda/9.3$. I was also able to experimentally show double patterning using the inert atmosphere sample holder, as shown in Figure 3.9. The left image is a Scanning Electron micrograph (SEM) of the resulting pattern. The SEM reveals the smallest spacing between the features. The image on the right is a schematic showing orientation of sample for double-exposure using POST.

By increasing the development times, I was able to experimentally show an increase in contrast as shown in Figure 3.10, where the feature size is plotted as a function of the exposure time. The theoretical model is indicated using the solid blue line. Using the exposure threshold as the only fitting parameter, we can show that this simple model can accurately explain our experimental results. The experimentally measured values are shown using crosses for two different development times, specifically 30 min and 90 min, respectively. The smallest experimentally obtained feature size was ~44nm, corresponding to a linewidth of $\sim \lambda/14.4$.

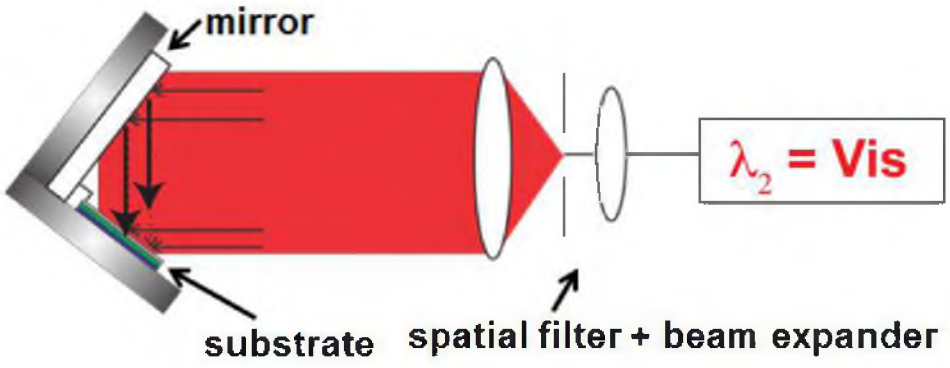

Figure 3.1: Lloyd's mirror setup.

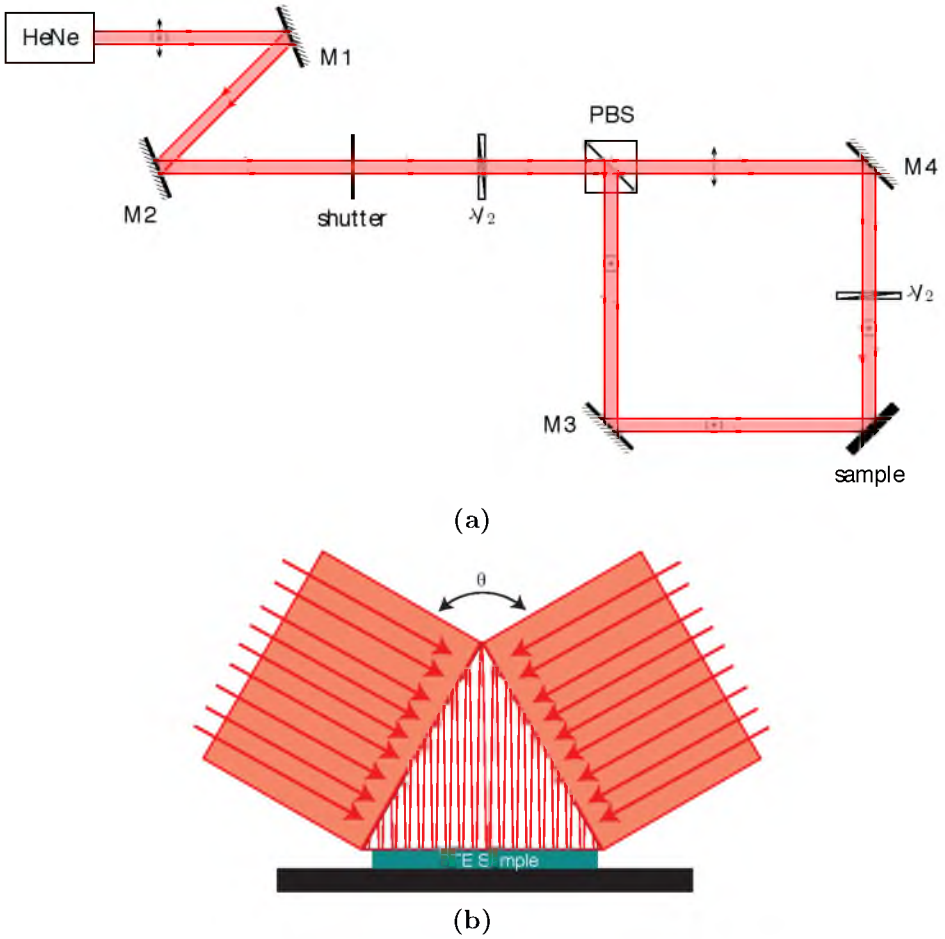

Figure 3.2: Mach-Zehnder setup. (a) Optical setup. (b) Interference pattern generated at sample substrate.

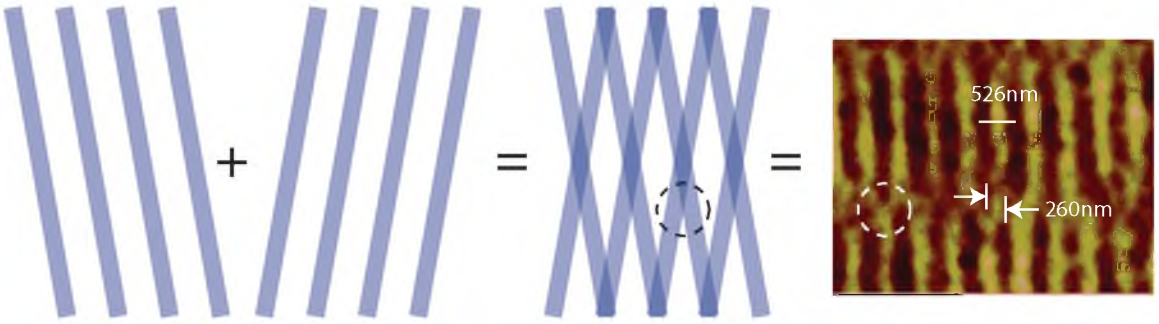

Figure 3.3: Double exposure demonstration. Left: Schematic showing orientation of sample for double-exposure using POST. Right: Atomic-force micrograph of the resulting pattern. The atomic-force micrograph reveals the smallest spacing between the features as ~260 nm, which is approximately half the period of the illuminating standing wave.

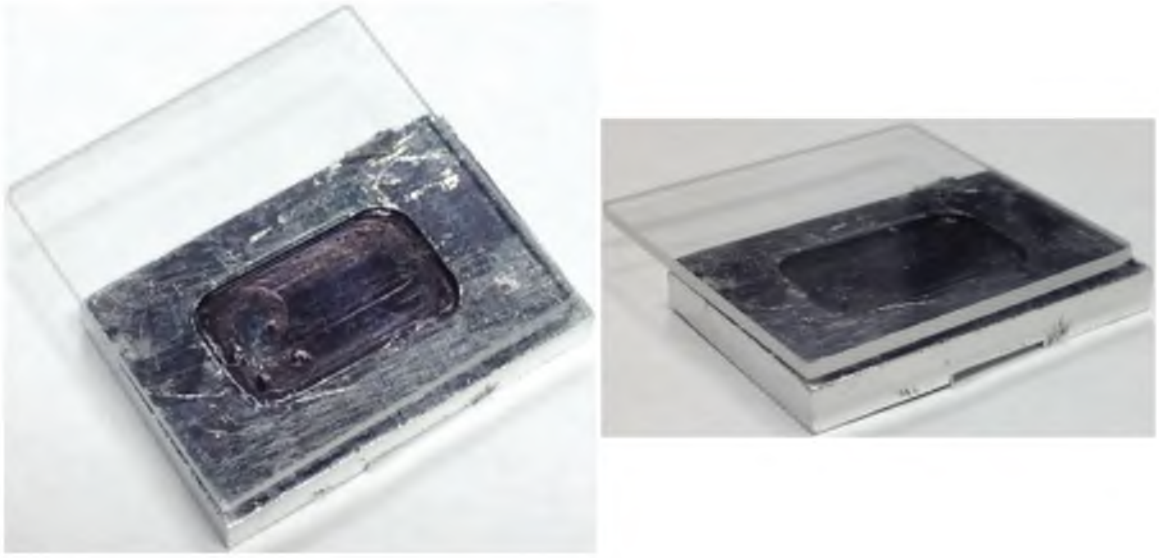

Figure 3.4: Original sample holder with quartz slide.

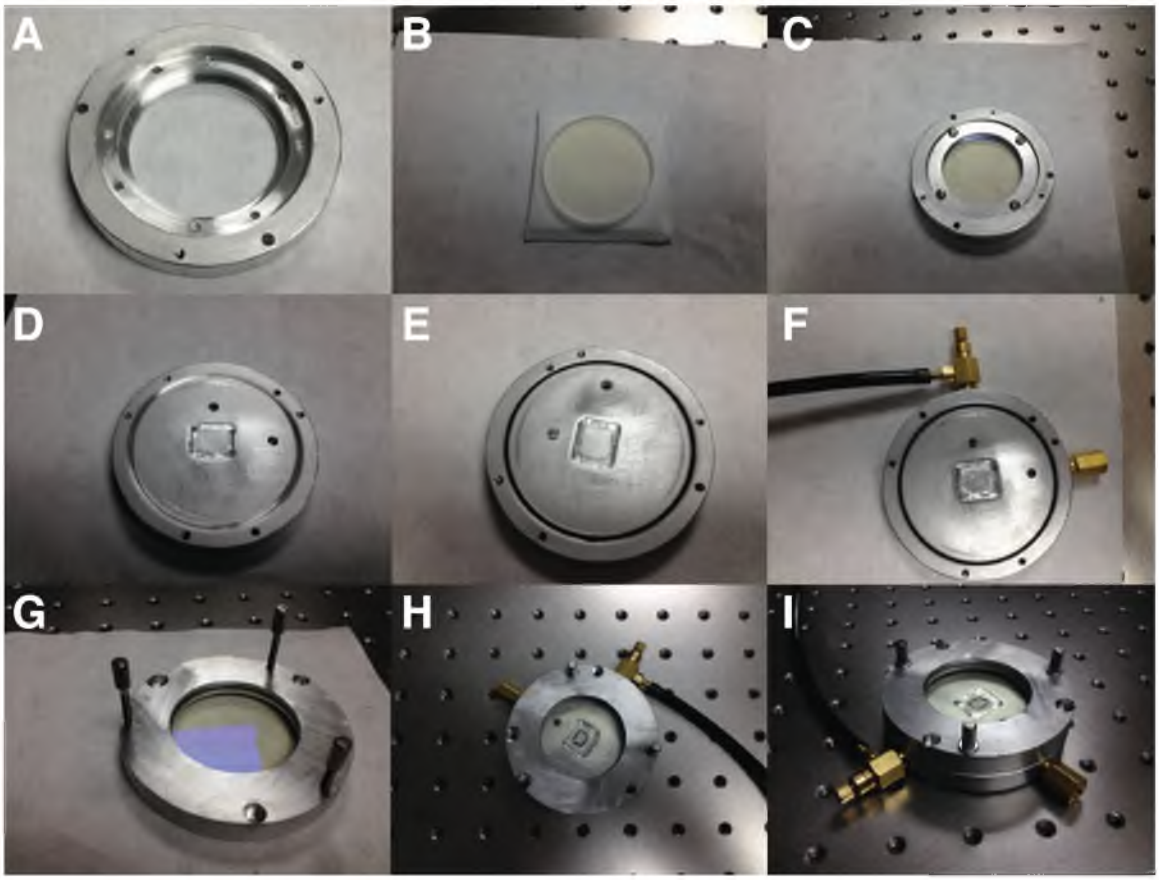

Figure 3.5: Construction/Assembly of custom inert atmosphere sample holder. (a) Pocket for AR coated window. (b) AR coated window. (c) Plate clamp for window. (d) O-ring groove on sample holder base. (e) Installed o-ring. (f) Mini-pneumatic check-valve and needle valve. (g) Three fastening screws. (h) Partially assembled sample holder. (i). Fully assembled custom inert atmosphere sample holder.

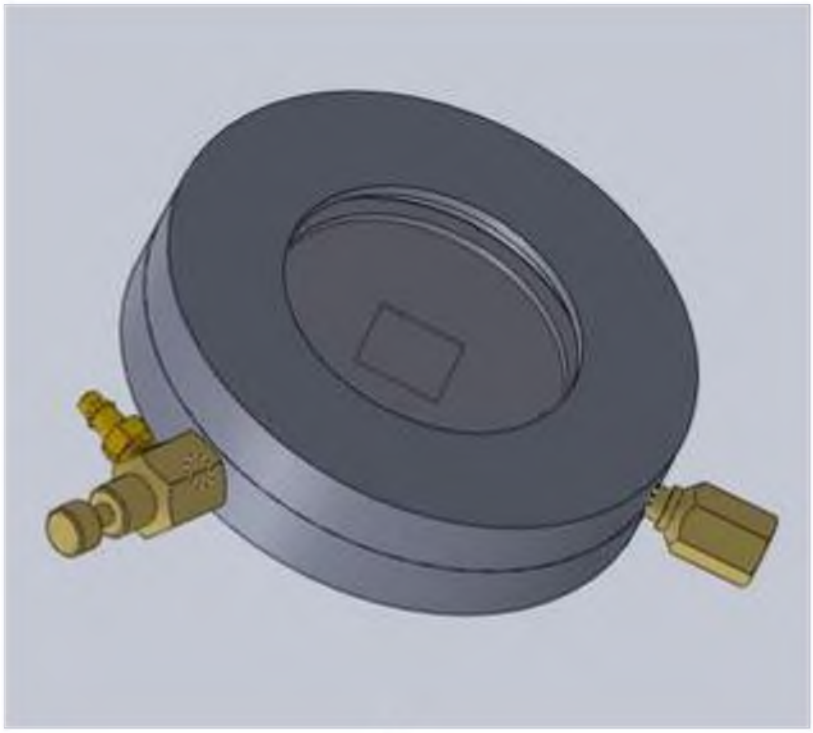

(a)

(b)

Figure 3.6: Inert atmosphere sample holder. (a) Solidworks® 3D rendering. (b) Final machined sample holder.

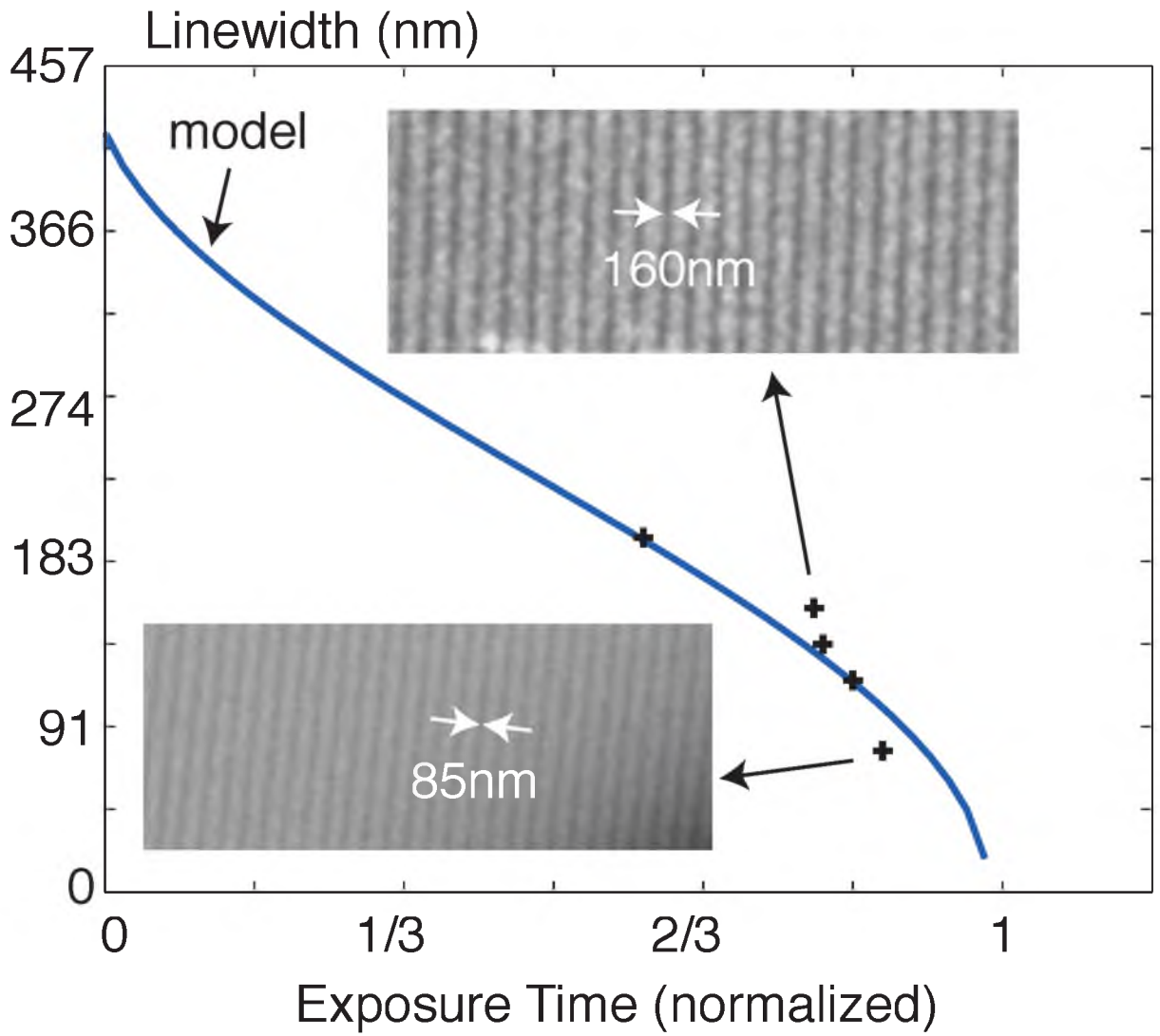

Figure 3.7: Linewidth vs. exposure time for a single development using the inert sample holder. The simulated curve is shown as a solid blue line, while the experimental data are shown using crosses. A sinusoidal illumination with period 457 nm was assumed. Inset: SEM images.

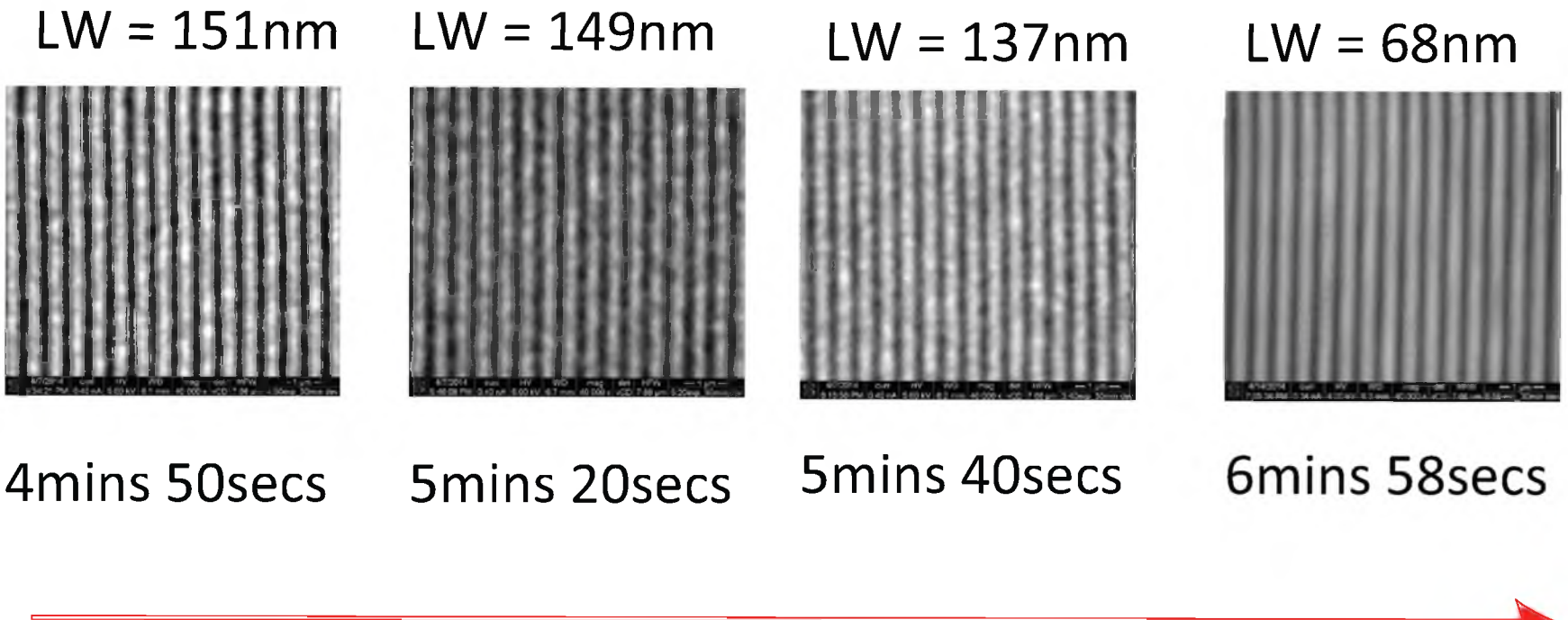

Figure 3.8: Linewidth vs. exposure time for a single development time using the inert sample holder. Period is ~500nm.

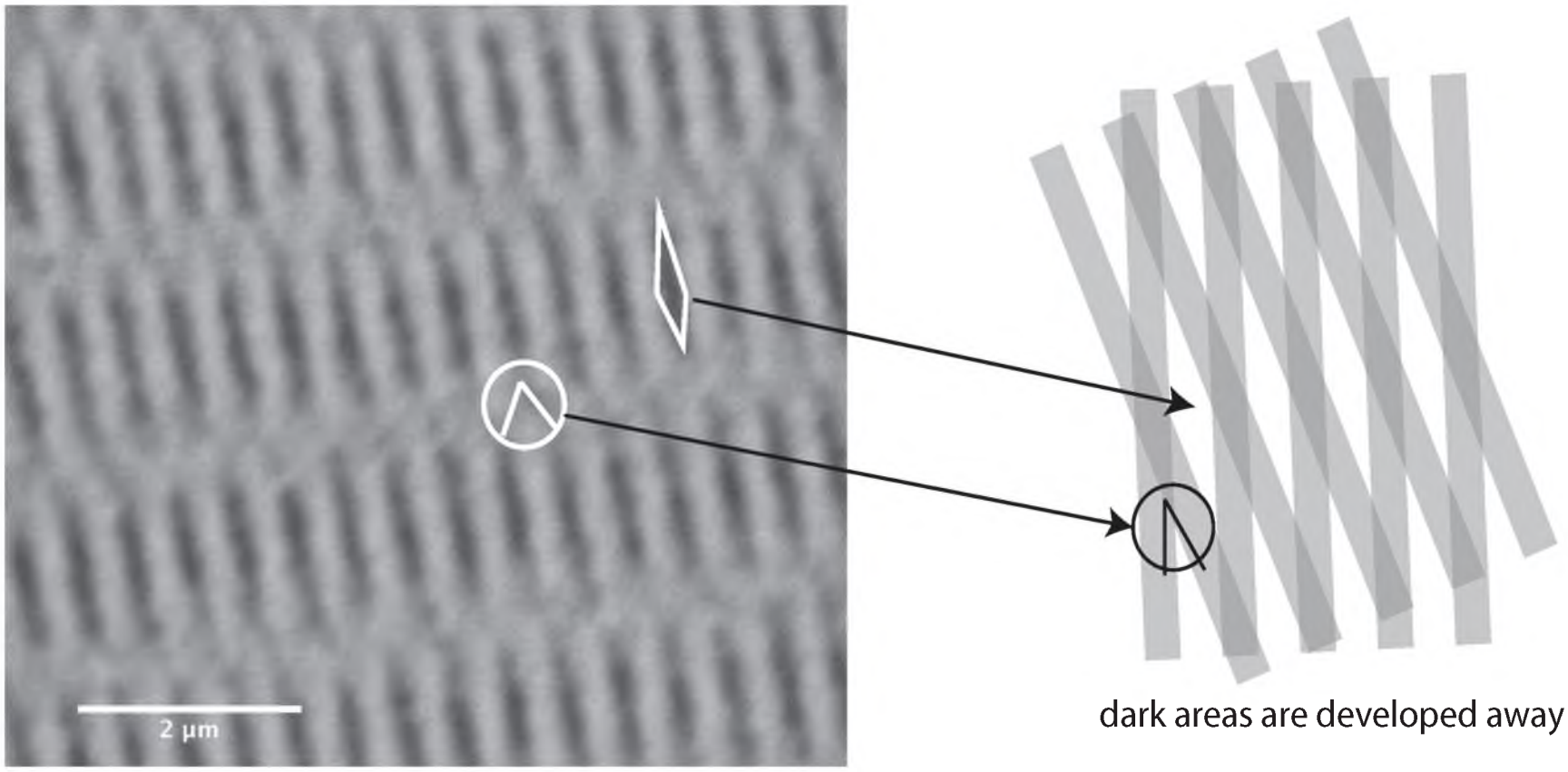

Figure 3.9: Double exposure demonstration. Left: Scanning electron micrograph (SEM) of the resulting pattern. The SEM reveals the smallest spacing between the features. Right: Schematic showing orientation of sample for double exposure using POST.

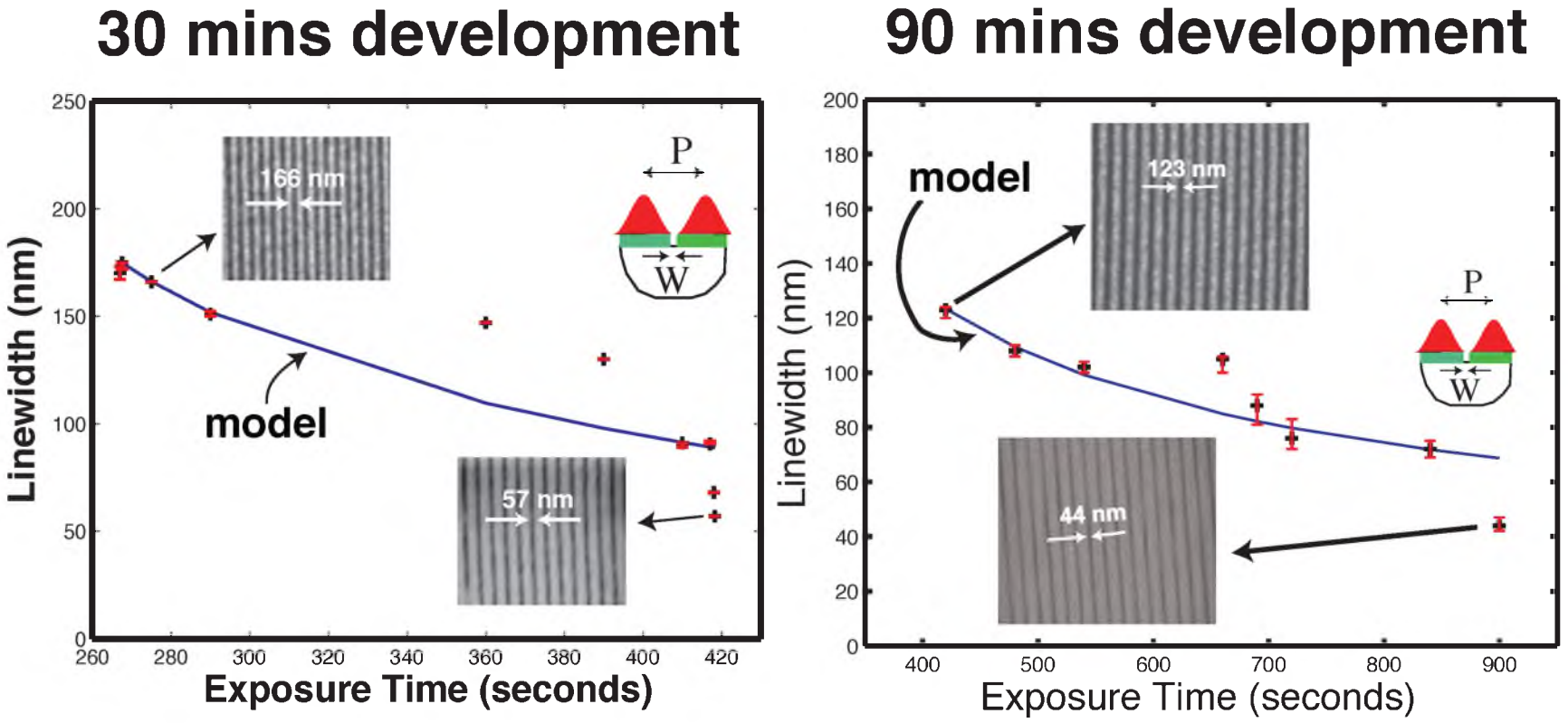

Figure 3.10: Linewidth vs. exposure time for two different development times of 30 min and 90 min, respectively in 100 (wt %) ethelyne glycol using the inert sample holder during exposure. The simulated curve is shown as a solid blue line, while the experimental data are shown using crosses. A sinusoidal illumination with period ~500 nm was assumed. Inset: SEM images.

3.4 References

[1] P. Cantu, N. Brimhall, T. L. Andrew et al. Subwavelength nanopatterning of photochromic diarylethene films. *Applied Physics Letters*, 100(18):183103, 2012.

CHAPTER 4

HIGH VACUUM (HV) SYSTEM

The ability to deposit amorphous thin-films of organic photochromic molecules is essential for both the understanding of fundamental physical phenomena and the application to optical lithography, namely, Patterning via Optical Saturable Transitions (POST). In all cases, a clean, well-characterized interface between the organic photochromic thin-film and the substrate is desirable. Other organic thin-film deposition techniques, such as spin-coating and drop-casting methods, can produce thin-films; however, the morphology is crystalline, which is not compatible with POST. Thermal deposition is the most widely used method for preparation of thin-films. The method is comparatively simple and was adopted for its use in deposition of many organic compounds and metals. The process of film formation by evaporation consists of several physical stages: (1) transformation of the material to be deposited into the gaseous state, (2) transfer of molecules from the evaporation source to the substrate, (3) deposition of these particles on the substrate, (4) rearrangement or modifications of their bindings on the surface of the substrate. The quality and characteristics of the deposit will depend on the rate of deposition, substrate temperature, ambient pressure, etc.

Developing a deposition system capable of making an amorphous homogenous organic thin-film can be quite difficult for several reasons. First, it must have a small throw distance to allow for uniformity of the thin-film. Thin-film properties are sensitive not only to their structures but also to many other parameters including their thickness. Hence, a stringent control of the latter is imperative for reproducible samples. Second, the chamber must be dedicated to only evaporating the organic photochrome in order to prevent contamination. Third, there is a need for a high vacuum deposition pressure of about 1×10^{-6} Torr. Finally, the chamber must have the ability to control the deposition rate of the organic photochrome during deposition. In this chapter, I describe the design, construction, and performance of a high vacuum low temperature organic thin-film evaporator that was easily integrated into the POST technique and also meets all of the above requirements.

4.1 Custom Thermal Evaporator Description

The custom thermal evaporator is described in two parts, which consist of the evaporation chamber and the system components. The system components correspond to the deposition rate controller, the quartz crystal microbalance (QCM) and turbo molecular pump cooling system, and the 10cc charge capacity organic Low Temperature Evaporator (LTE) source power supply, described in detail in section 4.1.1. The complete evaporation system is mounted on a stainless steel custom table with a shelf and housed in our custom class 10 cleanroom facility. The stainless steel table is 4ft.×2ft.×3ft. and has four nonadjusting legs.

4.1.1 Evaporation Chamber Components

Figure 4.1 shows an overview of the custom evaporator system as well as the chamber, turbo molecular pump, deposition rate controller, LTE source power supply, and the roughing pump, Figure 4.1 (a,b,c), respectively. Figure 4.2 (a,b) illustrates a Solidworks® 3D rendering of the system.

The evaporation chamber was designed and fabricated specifically to undertake the work described within this dissertation. The main body of the organic deposition chamber consists of a 304L stainless steel six-way cube with knife-edge 4.5 in. Conflat (CF) flange. A standard 4.5 in. CF flanged 304L stainless steel tee is attached to the six-way cube which holds the sample holder and the quartz crystal (QC) low profile single sensor, as shown in Figure 4.1. The internal volume of the chamber is 94.4 $in.^3$.

The sample holder consists of a custom Fast-Entry Door with 4.5 in. CF flange and dual latch-knobs, as shown in Figure 4.3 and illustrated in Appendix C. The sample holder itself was made adjustable by drilling a hole through the top of the flange and a Swagelok® Ultra-torr vacuum fitting was welded on top and the mounting post from the sample holder is slid through. The Ultra-torr can withstand pressures of 10^{-6} to 10^{-8} torr ranges. In order to monitor the deposition rate, a 5MHz quartz crystal microbalance from Sycon Instruments (Low Profile Sensing Head) was used, Appendix C. The QCM is mounted in such a manner to stay as close as possible to the substrate holder, as shown in Figure 4.4 and illustrated in Appendix C. It is connected to a deposition rate controller from Inficon SQC-310, Figure 4.1 (b). A deposition controller allows rate control of the deposition process using the QCM sensor. The thickness of the thin-film is shown in realtime on the digital readout; this allows for total control of the sample thin-film thickness for repeatability. The QCM is then cooled to a temperature of 30 °C ± 1 °C using an ambient cooling system that contains a dual ×

120mm fan aluminum radiator with 590W of cooling capacity, as shown in Figure 4.1 (a) and illustrated in Appendix C.

Beneath the six-way cube is housed the 10cc charge capacity organic LTE source with custom stainless steel shutter. The LTE source shutter is a custom stainless steel teardrop-shaped plate attached to the manual rod by welding that is housed over the crucible to protect the substrate from evaporation during heating and cooling of the source, Figure 4.5. To measure the pressure inside the chamber, a hot cathode ionization gauge (Bayerd-Alpert) was used. It is housed on the six-way cube with Conflat flanges, Figure 4.1 (a).

4.1.2 Operation

The chamber is pumped by a roughing pump (Varian Triscroll 300 Dry Scroll Pump) in the chaise of the class 10 cleanroom, Figure 4.1 (c), and a turbo molecular pump (Pfeiffers-Balzers TPH-50), Figure 4.1 (a), that allows a pressure of $\sim 10^{-6}$ torr. The roughing pump is capable of reaching a pressure of $\sim 10^{-3}$ torr. Differential pumping is provided by a 50 l/s turbo molecular pump (Pfeiffers-Balzers TPH-50) which is isolated from the chamber by a 4.5 in. stainless steel CF to ISO-63 adapter connected to the six-way cube; it takes the chamber pressure down to high vacuum, $\sim 10^{-6}$ torr.

The LTE source power feedthrough from Kurt J. Lesker Company heats the tungsten basket crucible heater, Figure 4.5 (a), which holds an aluminum oxide (Al_2O_3) crucible, Figure 4.6, from the same company. The LTE source is powered by the power supply and the deposition rate is controlled by the SQC-310 controller, Figure 4.1 (b). A thermocouple monitors the base vacuum pressure of the chamber. The pressure is read out digitally on the vacuum gauge (Varian Multi-Gauge), Figure 4.1 (a).

The calibration of the QCM was checked by also measuring the thickness of the thin-films using a profilometer (Tencor P-10) versus the readout of the SQC-310 controller. The two thicknesses measurements agreed within ± 5 nm.

4.1.3 Helium Leak Testing

To detect the exact position of potential leaks in the system during building, a helium leak detector (Alcatel ASM 180 TD) was used, Figure 4.7. The chamber was evacuated by the turbopump connected in series with the roughing pump of the leak detector and then areas liable to leaks are sprayed with helium. The detector is then able to measure the flow of helium penetrating the leaky part.

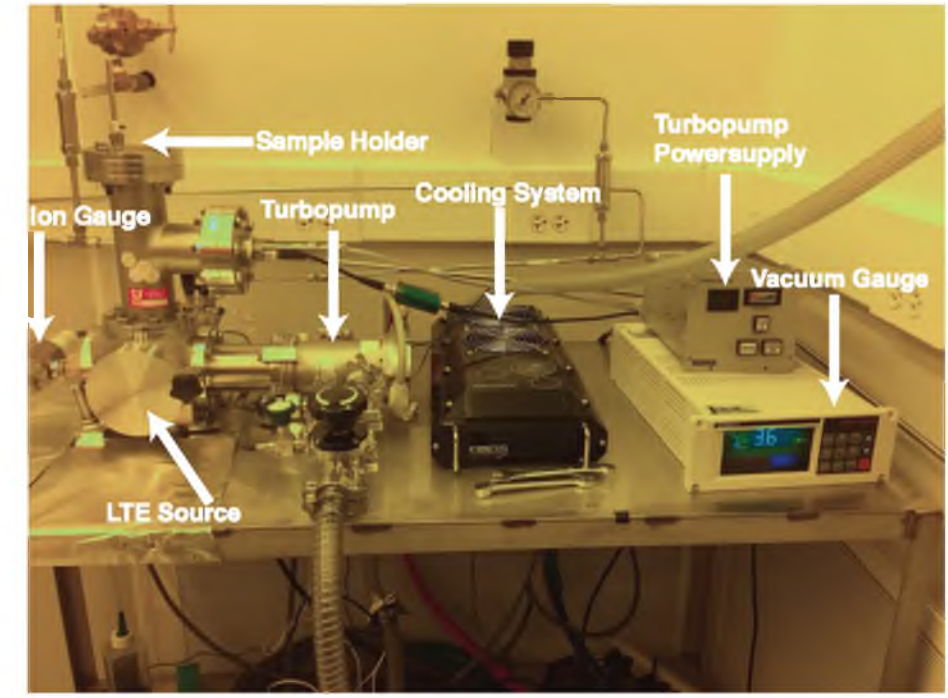

(a)

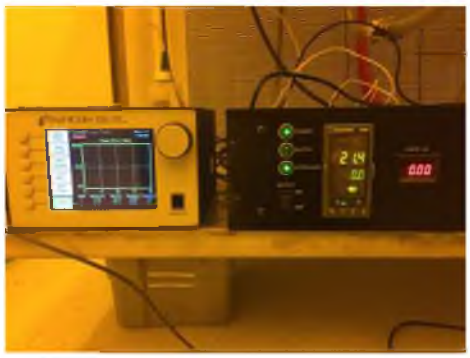

(b)

(c)

Figure 4.1: Complete custom evaporation system. (a) Overview of the custom evaporator system as well as the chamber, turbo molecular pump and power supply, cooling system, vacuum and ion gauges, and sample holder mount. (b) (left) INFICON® SQC-310 thin film deposition controller and (right) custom LTE power supply. (c) Varian® Triscroll 300 dry scroll pump.

(a) **(b)**

Figure 4.2: Solidworks® 3D rendering of LTE custom evaporator. (a) Complete system. (b) Exploded view showing sample holder.

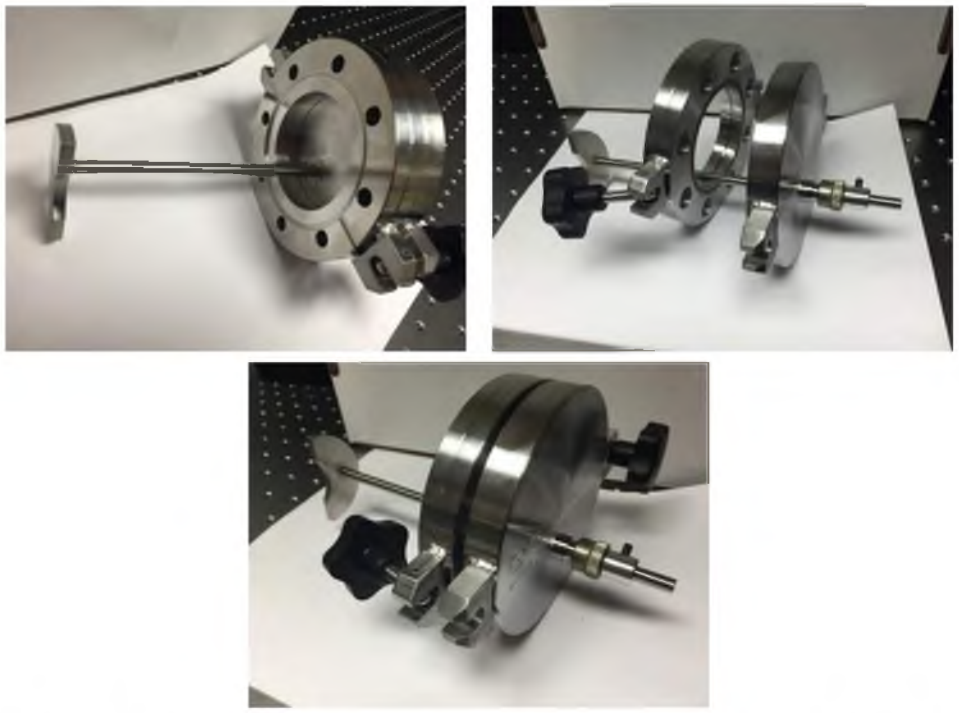

Figure 4.3: Custom Fast-Entry Door sample holder with dual-latch knobs.

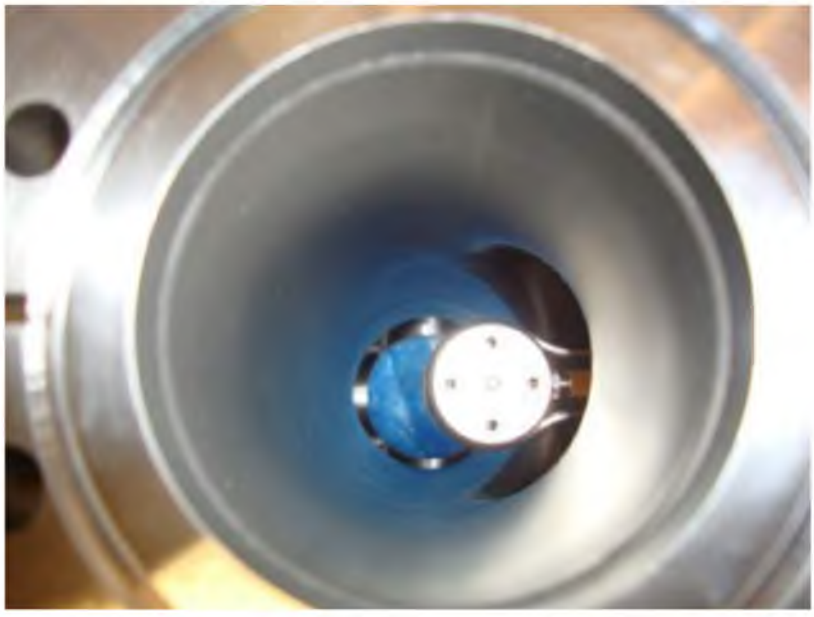

Figure 4.4: QCM in same place as sample holder substrate.

(a)

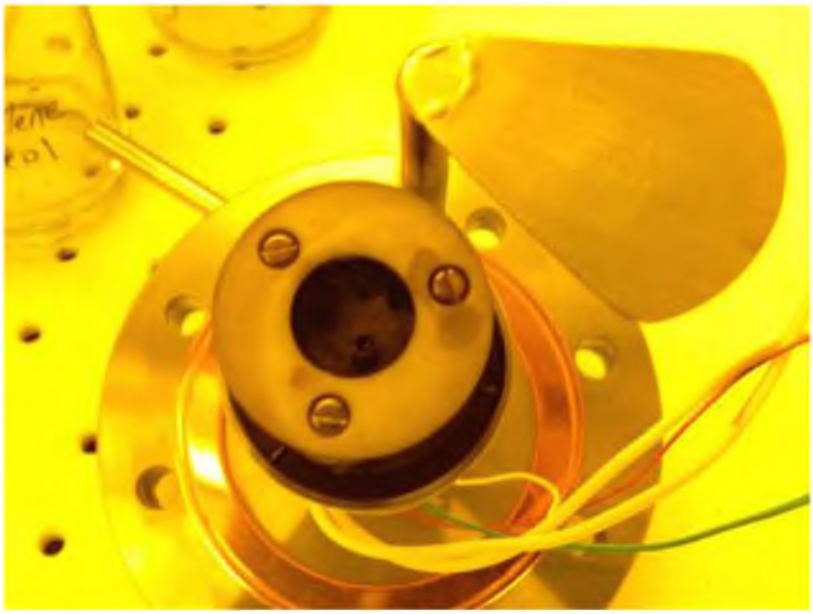

(b)

Figure 4.5: LTE source and custom shutter. (a) LTE source and tungsten basket. (b) Custom source shutter.

Figure 4.6: Aluminum oxide (Al_2O_3) crucible.

Figure 4.7: Alcatel ASM 180 TD Leak Detector.

CHAPTER 5

ELECTROCHEMISTRY AND SPECTROSCOPY

Compound **1** exists in two isomeric forms, open-ring (**1o**) and closed-ring (**1c**). Since this compound has an extended conjugation in **1c**, it can be selectively oxidized to a stable cation (**1ox**) as indicated in Scheme 5.1.

5.1 Experimental Setup

In many electrochemical techniques, the current-potential curves for the electrode reactions are measured and studied. These techniques are combined under the term voltammetry, and the current-potential curves are called voltammograms. The typical setup for the oxidation of our BTE samples in this work is shown in Figure 5.1. A potentiostat, supported by a voltage source, applies a potential between the 100nm thick platinum thin-film working electrode (WE) on which BTE is placed and the Platinum counter electrode (CE). A high-impedance Ag/AgCl quasi-reference electrode (QRE) is used to measure and control the potential precisely. The resulting current through the three-electrode electrochemical cell is then measured and recorded, together with the potential. With the appropriate working setup, the BTE can be investigated. Cyclic voltammetry (CV) was chosen as the electrochemical technique to study the redox reactions of the solution and thin-film forms of BTE.

5.1.1 BTE in Solution

The redox properties of the molecule are clearly critical to defining the feature sizes of the nanostructures. Therefore, we first characterized the redox properties of compound **1c** in solution by performing cyclic voltammetry at various scan rates, as illustrated in Figure 5.2 (a). The Faradic current is directly proportional to the scan rate, as shown in Figure 5.2 (b), indicating that the kinetics of the redox reactions were more adsorption controlled than diffusion limited.

5.1.2 BTE in Thin-Film Form

We then applied this principle to determine the appropriate oxidation conditions for **1c** in thin-film. Figure 5.3 (a) shows the oxidation current for a 40 nm-thick film of compound **1** that was first exposed to a standing wave 633 nm wavelength (HeNe) of period 400 nm for 3 hr and 5 min with a laser output power of 2.65mW. The oxidation potential was fixed at 0.81 V. As expected, the current shows an exponential decrease with time.[1] The total time of oxidation determines the width and depth of the final developed nanostructure. We characterized different oxidation times as illustrated by the atomic-force micrographs in Figure 5.3 (b) at an oxidation voltage of 0.85V determined from cyclic voltammetry.[2] The 50 nm-thick films were exposed to a standing wave at λ_2=647 nm (CW Kr-ion, Coherent Innova 301C) of period 400nm for 60secs at a power density of 0.95 mW/cm^2. As the oxidation time is increased from 10 min to 25 min, one can clearly see a loss of contrast as some of the regions comprised of **1o** get oxidized as well. The developer (5% IPA: 95% ethylene glycol) dissolves all oxidized portions. Larger oxidation times result in an uneven line and increased surface nonuniformities after development. Therefore, a careful choice of the oxidation conditions is critical to patterning high-quality nanostructures.

5.2 UV-visible Spectroscopy and Switching Cycles

In order to characterize the performance of compound **1** in thin-film, we evaporated 80 nm of **1o** onto an ITO-coated quartz slide.[2] As indicated in Figure 5.4 (a), UV-Vis absorption spectroscopy reveals distinct peaks for the three forms: **1o**, **1c**, and **1ox**. These spectra confirm the existence of stable isomeric forms. One important characteristic for lithography is the capability of compound **1** to undergo repeated switching without adverse effects. This is important for repeated patterning to create dense (as opposed to isolated) features. We switched the aforementioned quartz slide back and forth by exposing it to a UV lamp (center wavelength = 300 nm) and a Helium-Neon laser (λ_2 = 633 nm), respectively. Figure 5.4 (b) shows the resulting absorbance measured at 633 nm as a function of the switching cycle. A slight decrease of absorbance was noted for the first few cycles, presumably due to UV-induced photo-oxidation. The absorbance values were stable after the third cycle. This is a significant result!

5.3 In-situ Electrochemical Setup

The main goal of in-situ experimentation in the electrochemical method is performing electrochemical oxidation of the closed-form isomer, **1c**, in an O_2 purged environment. The cell was machined out of Teflon with an o-ring seal. Three windows were machined out to

allow for the attachment of anti-reflection (AR) coated windows for the exposures. Figure 5.5 (a-d) shows the design and fabricated in-situ electrochemical cell.

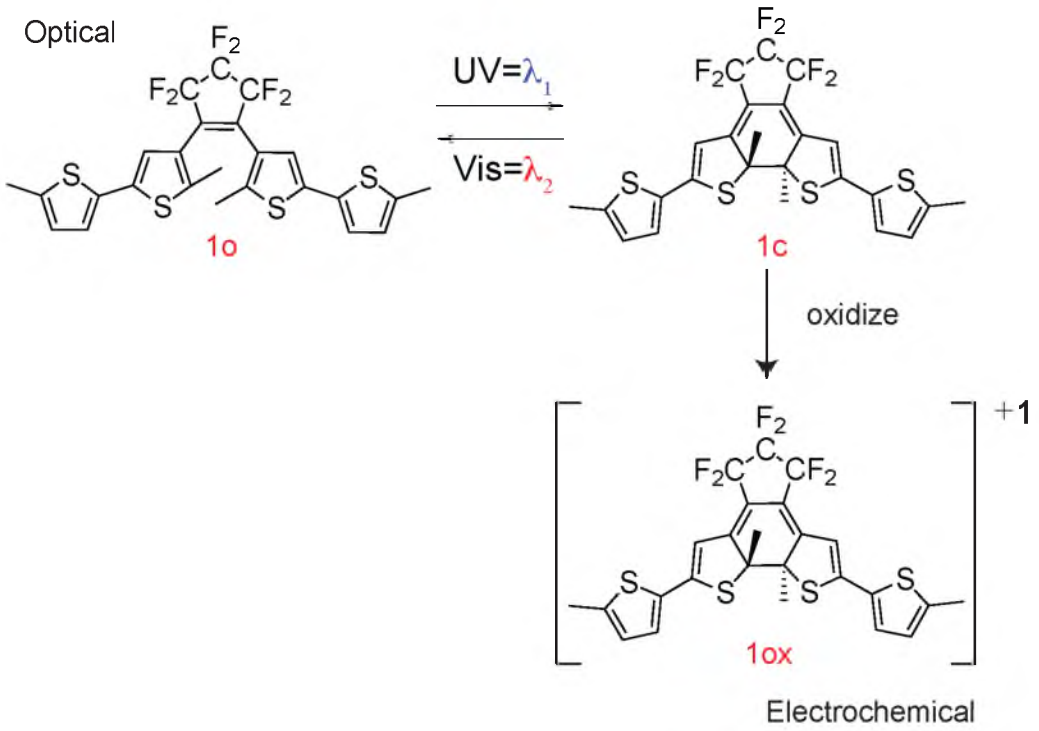

Scheme 5.1: Scheme of the photochromic molecule, compound **1**.

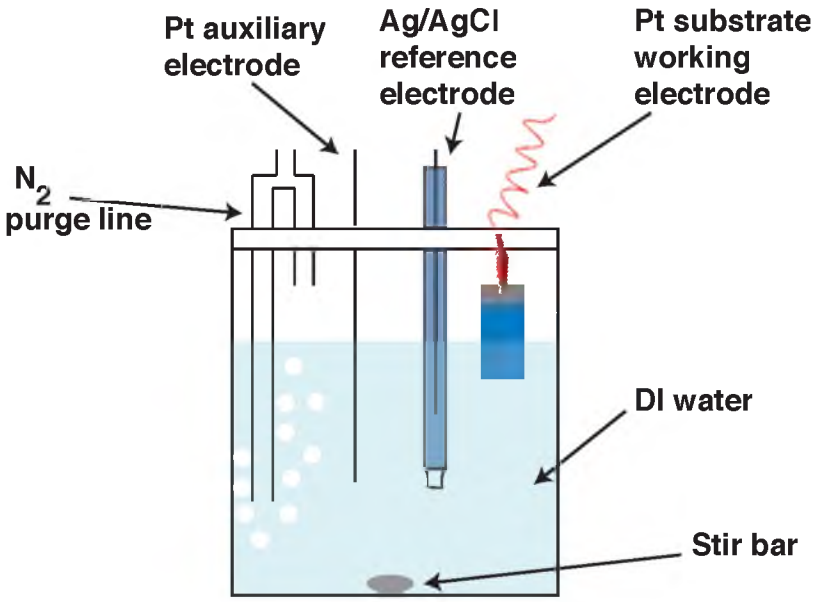

Figure 5.1: Three-electrode electrochemical cell

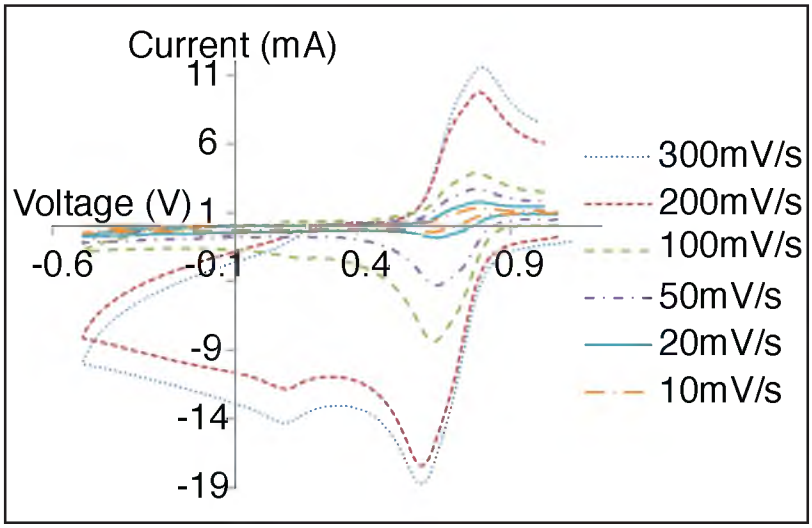

(a)

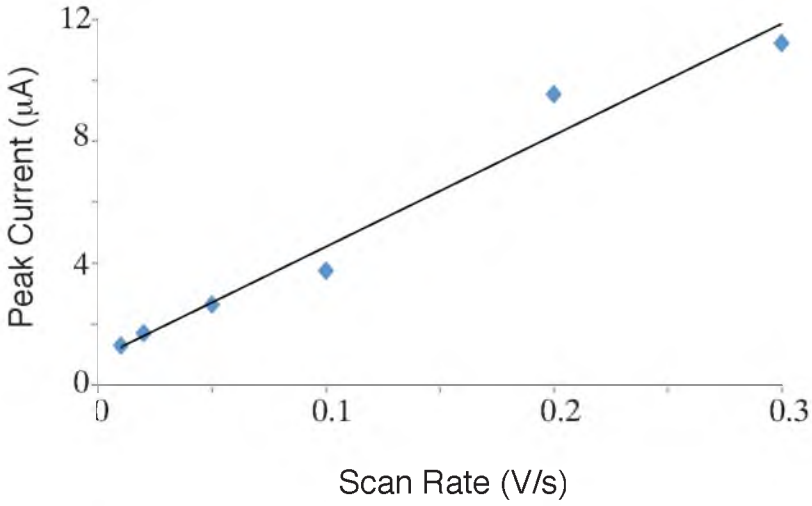

(b)

Figure 5.2: Characterization of the redox properties of compound **1** in solution form. (a) Cyclic voltammograms of **1c** in solution of 0.1M tetrabutylammonium hexafluorophosphate in dichloromethane at various scan rates. (b) Peak current shows a linear dependence on the scan rate.

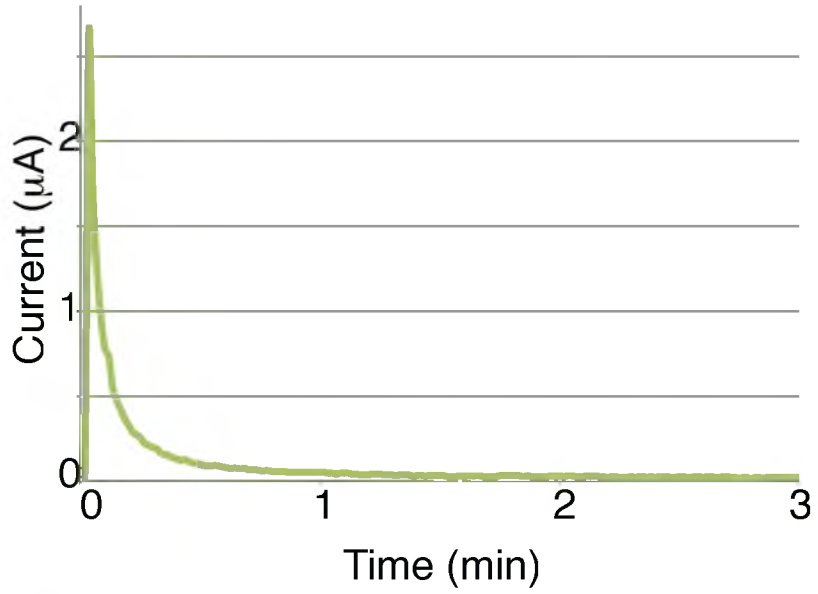

(a)

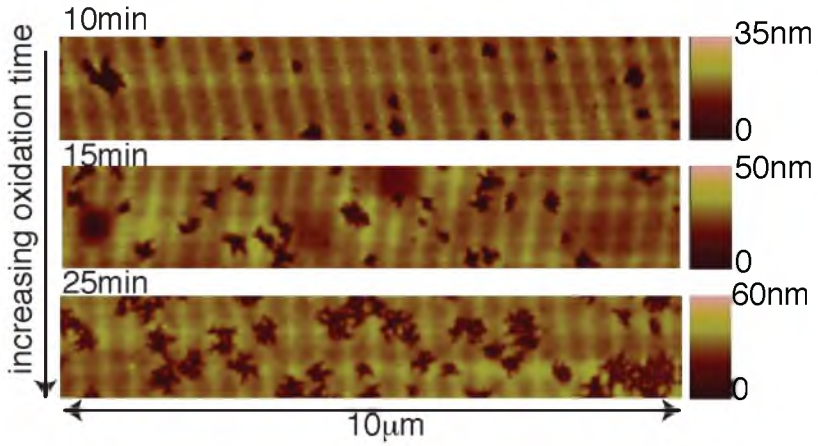

(b)

Figure 5.3: Characterization of the redox properties of compound **1** in thin-film form. (a) Oxidation current as a function of time for compound 1 in solid form for an oxidation potential of 0.81 V. (b) Atomic-force micrographs of lines after development for samples at various oxidation times.

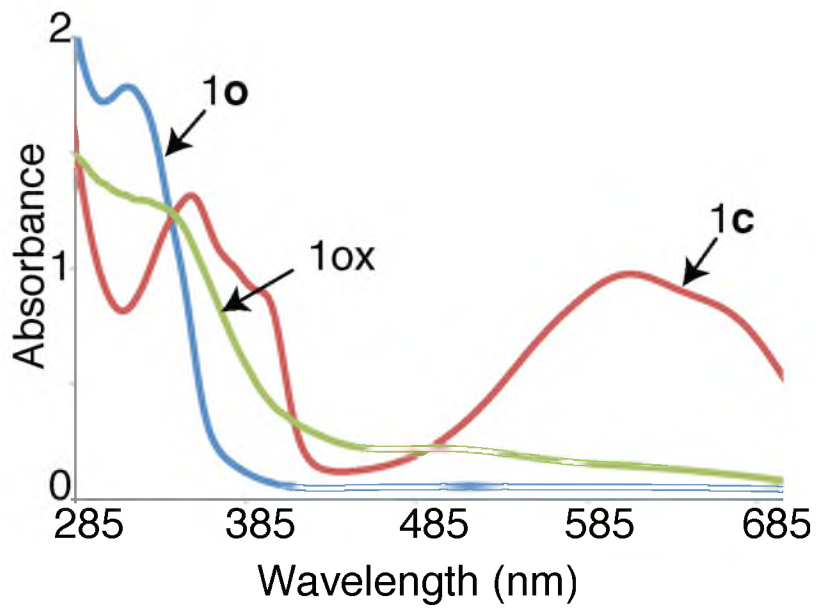

(a)

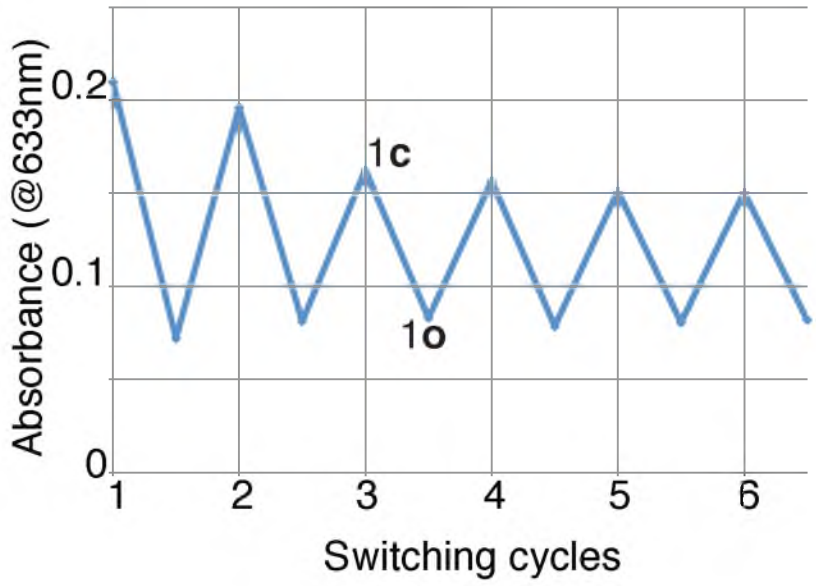

(b)

Figure 5.4: Characterization of compound **1** in thin-film. (a) UV-Vis absorbance spectroscopy of compound **1**. Compound **1c** shows a peak in the visible range, while compound **1o** has a peak in the UV. Both peaks disappear in the oxidized form. (b) Response to cyclic UV/Vis exposure. The absorbance at 633 nm is plotted as the sample is repeatedly exposed to UV and red light. The absorbance stabilizes after 3 cycles and remains approximately constant for tens of cycles.

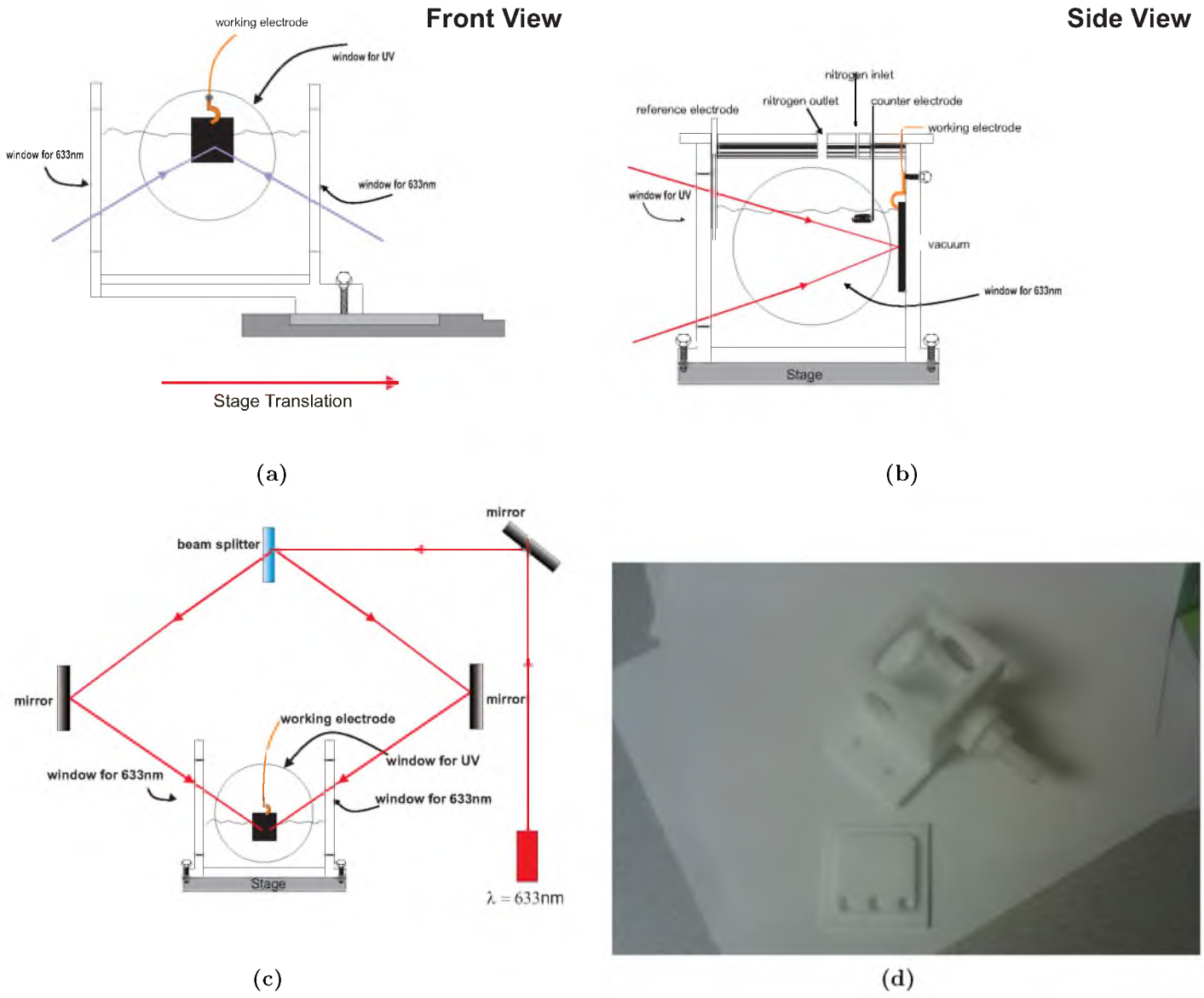

Figure 5.5: Electrochemical in-situ design and build. (a) Detailed design of stage translation. (b) Sideview showing top ports. (c) In-situ setup inside of Mach-Zhender interferometer (d) Fabricated in-situ setup made from teflon.

5.4 References

[1] A. J. Bard and L. R. Faulkner. *Electrochemical Methods: Fundamentals and Applications*. John Wiley & Sons, Inc, 2001.

[2] P. Cantu, N. Brimhall, T. L. Andrew et al. Subwavelength nanopatterning of photochromic diarylethene films. *Applied Physics Letters*, 100(18):183103, 2012.

CHAPTER 6

SUBWAVELENGTH NANOPATTERNING OF PHOTOCHROMIC DIARYLETHENE FILMS

Reprinted with permission from: P. Cantu, N. Brimhall, T.L. Andrew, R. Castagna, C. Bertarelli, and R. Menon. "Subwavelength nanopatterning of photochromic diarylethene films." *Applied Physics Letters*, vol. 100, pp. 183103-1 to 183103-3, 2012.

APPLIED PHYSICS LETTERS **100**, 183103 (2012)

Subwavelength nanopatterning of photochromic diarylethene films

Precious Cantu,[1] Nicole Brimhall,[1] Trisha L. Andrew,[2] Rossella Castagna,[3,4] Chiara Bertarelli,[3,4] and Rajesh Menon[1,a)]

[1]*Department of Electrical and Computer Engineering, University of Utah, Salt Lake City, Utah 84112, USA*
[2]*Department of Chemistry, Massachusetts Institute of Technology, Cambridge, Massachusetts 02139, USA*
[3]*Dipartimento di Chimica, Materiali e Ingegneria Chimica "Giulio Natta," Politecnico di Milano, P.zza Leonardo da Vinci 32, 20133 Milano, Italy*
[4]*Center for Nano Science and Technology @ PoliMi, Istituto Italiano di Tecnologia, Via Pascoli 70/3, 20133 Milano, Italy*

(Received 15 February 2012; accepted 16 April 2012; published online 1 May 2012)

The resolution of optical patterning is constrained by the far-field diffraction limit. In this letter, we describe an approach that exploits the unique photo- and electro-chemistry of diarylethene photochromic molecules to overcome this diffraction limit and achieve sub-wavelength nanopatterning. © *2012 American Institute of Physics*. [http://dx.doi.org/10.1063/1.4710547]

Top-down patterning of nanostructures is the key element that introduces functionality at the nanoscale. This is exemplified in numerous devices such as the complex geometries in nanoelectronics,[1] exquisite control of nanoscale dimensions in integrated optics,[2] geometries that impart photonic bandgaps in photonic crystals,[3] and subwavelength control of refractive index in metamaterials.[4] In almost all these examples, the nanopatterns are generated via scanning-electron-beam lithography (SEBL), where a focused beam of electrons is scanned over an electron-sensitive polymer resist. On the other hand, SEBL and related approaches are extremely slow. Photons, on the contrary, can create patterns extremely fast. However, they suffer from diffraction, and hence, are limited to features that are larger than about one-half the wavelength.[5]

Recently, a number of techniques have been proposed to circumvent this diffraction limit and achieve nanoscale resolution with optics.[6–9] Most of these methods are inspired by the use of photoswitchable states for deep sub-wavelength resolution in fluorescence imaging.[10] Similar techniques have also been extended to non-fluorescence imaging.[11] We recently proposed a novel alternative that extends these approaches to nanopatterning via the combined photo- and electrochemical switching of stable photochromic isomers.[12] In this letter, we elucidate the key material aspects that form the basis of this technique including the material stability, the electrochemical oxidation mechanisms, and the influence of the oxidation time on pattern contrast. Moreover, we show that the photochromic layer can be used as both a positive-tone and a negative-tone photoresist depending on developing conditions. The negative-tone approach allowed us to demonstrate isolated lines as narrow as $\lambda/16$.

We thermally evaporated thin-films of 1,2-bis[2-methyl-5-(5′-methyl-2′-thienyl)-3-thienyl]hexafluorocyclopentene (compound **1**) onto a 100 nm-thick platinum (Pt) film atop a silicon wafer.[13] The evaporated films ranged in thickness from 20 nm to 60 nm. As indicated in Fig. 1(a), compound **1** exists predominantly in either the closed form (**1c**) or the open form (**1o**). When exposed to red light, **1c** is converted to **1o**. When exposed to UV, **1o** is converted back to **1c**. Upon illuminating this film with a standing wave of wavelength $\lambda = 633$ nm, the molecules originally in form **1c** are converted into form **1o** except at the centre of the node, where they remain as **1c** (Fig. 1(c)).[12] By increasing the exposure time, the area of **1c** can be made arbitrarily small as long as the centre of the node is devoid of photons, i.e., as dark as possible. The isomers of the diarylethene molecule are thermally stable, which allows for a subsequent electrochemical-fixing step (Fig. 1(d)). Compound **1c** has a lower oxidation potential than **1o**.[14] Therefore, applying the appropriate oxidation potential will selectively oxidize only **1c**, resulting in a subwavelength region that is in the stable oxidized form, which is no longer photochromic. The remaining unoxidized molecules can participate in subsequent exposure-oxidation steps to create more areas that are in the oxidized form generating dense features.[12] The oxidized form therefore, is analogous to the latent image in conventional photolithography. After all exposures are completed, the oxidized form is selectively dissolved away to create nanoscale topography. As in conventional photolithography, the photochromic layer can act as a negative-tone resist when the unoxidized regions are selectively removed by a solution of pentane. Pentane is a nonpolar solvent, which selectively dissolves the neutral molecule with respect to the polar cation. As indicated in Fig. 1(e), isolated lines representing the removed portions as narrow as 39 nm ($\sim\lambda/16$) were clearly resolved. The photochromic layer can act as a positive-tone resist when the oxidized regions are selectively removed by a solution of 5% isopropanol (IPA) and 95% ethylene glycol resulting in lines shown in Fig. 1(f).

In order to characterize the performance of compound **1** in thin-film, we evaporated 80 nm of **1o** onto an ITO-coated quartz slide.[13] As indicated in Fig. 2(a), UV-Vis absorption spectroscopy reveals distinct peaks for the three forms: **1o**, **1c,** and oxidized. These spectra confirm the existence of stable isomeric forms. One important characteristic for lithography is the capability of compound **1** to undergo repeated switching without adverse effects. This is important for repeated patterning to create dense (as opposed to isolated) features. We switched the aforementioned quartz slide back and forth by exposing it to an UV lamp (center wavelength = 300 nm) and

a)Author to whom correspondence shoule be addressed. Electronic mail: rmenon@eng.utah.edu.

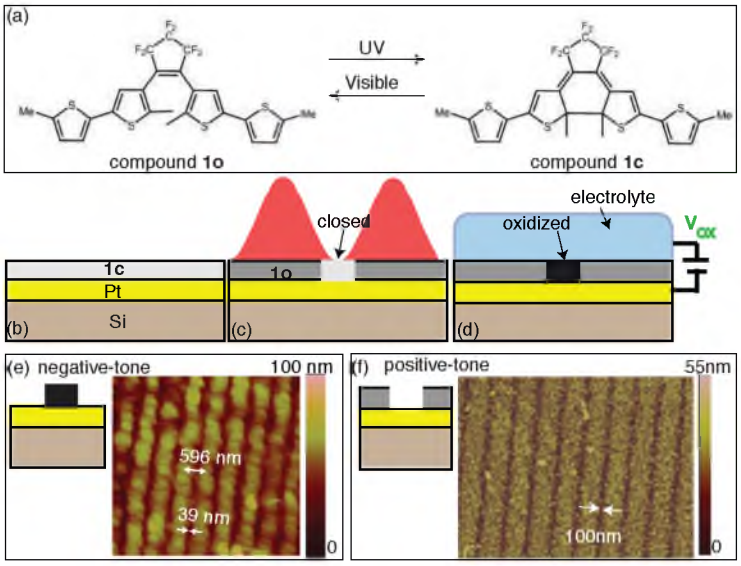

FIG. 1. (a) Photochromic molecule, compound **1** exists in open form, **1o** and the closed form, **1c**. (b) Sample for nanopatterning is comprised of a thin-film (20 nm-60 nm thick) of **1c** deposited on 100 nm of Pt on a silicon wafer. (c) When exposed to a standing wave at λ (red), **1c** becomes **1o** except at the node. (d) **1c** is preferentially oxidized electrochemically. (e) As a negative-tone resist, **1o** is selectively removed to form representative lines as narrow as 39 nm. (f) As a positive-tone resist, the oxidized form is selectively removed to form representative lines as narrow as 100 nm.

a Helium-Neon laser ($\lambda = 633$ nm), respectively. Figure 2(b) shows the resulting absorbance measured at 633 nm as a function of the switching cycle. A slight decrease of absorbance was noted for the first few cycles, presumably due to UV-induced photo-oxidation. The absorbance values were stable after the third cycle. The quality of the thermally evaporated films is extremely important for nanopatterning. It was noticed that the film uniformity degraded dramatically if exposed to air over prolonged periods of time as illustrated by the optical micrograph in Fig. 2(c). This sample was comprised of a 40 nm thick film of **1o** deposited on 100 nm of Pt. Following deposition, the sample was irradiated with UV to convert all molecules to **1c** in order to preserve film integrity.[12] The sample was stored in atmosphere and imaged after 24 h. The molecules of **1c** tend to form nanoscale islands, which introduce significant non-uniformities in the thickness of the layer, making it unusable for nanopatterning. This problem was solved by storing the samples under N_2 as indicated by a different sample shown in Fig. 2(d), again imaged 24 h after deposition of 40 nm of compound **1**.[13] This effect is therefore likely due to the partial oxidation of **1c** under ambient conditions. Nevertheless, the samples were stable enough so as to be able to conduct all exposure and development steps in air.

Compared to earlier methods in fluorescence imaging,[10] a fixing step is necessary for nanopatterning. This is achieved by selective oxidation of **1c** in an electrochemical cell.[13] The redox properties of the molecule are clearly critical to defining the feature sizes of the nanostructures. Therefore, we first characterized the redox properties of compound **1c** in solution by performing cyclic voltammetry at various scan rates as illustrated in Fig. 3(a). The Faradic current is directly proportional to the scan rate as shown in Fig. 3(b) indicating that the kinetics of the redox reactions were more adsorption controlled than diffusion limited. We then applied this principle to determine the appropriate oxidation conditions for **1c** in thin-film. Figure 3(c) shows the oxidation current for a 40 nm-

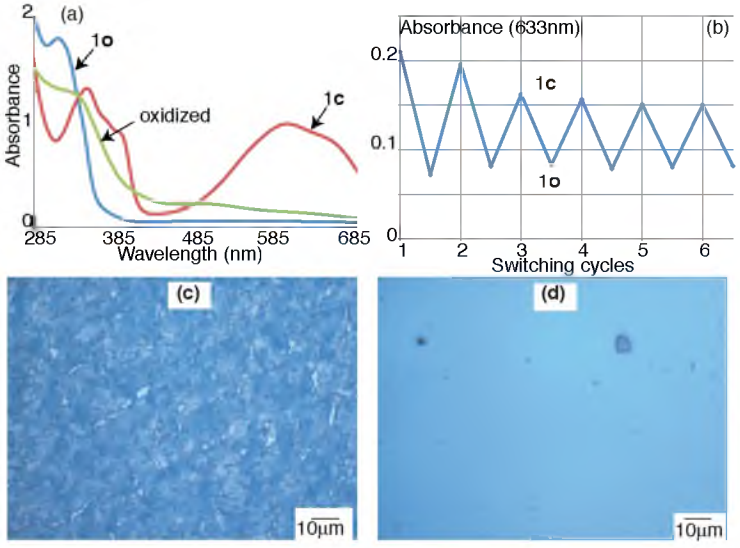

FIG. 2. Characterization of compound **1** in thin-film. (a) UV-Vis absorbance spectroscopy of compound **1**. Compound **1c** shows a peak in the visible range, while compound **1o** has a peak in the UV. Both peaks disappear in the oxidized form. (b) Response to cyclic UV/Vis exposure. The absorbance at 633 nm is plotted as the sample is repeatedly exposed to UV and red light. The absorbance stabilizes after 3 cycles and remains approximately constant for tens of cycles. Optical micrographs of samples with ~40 nm-thick films of **1c** 24 h after evaporation (c) when stored in air and (d) when stored under N_2.

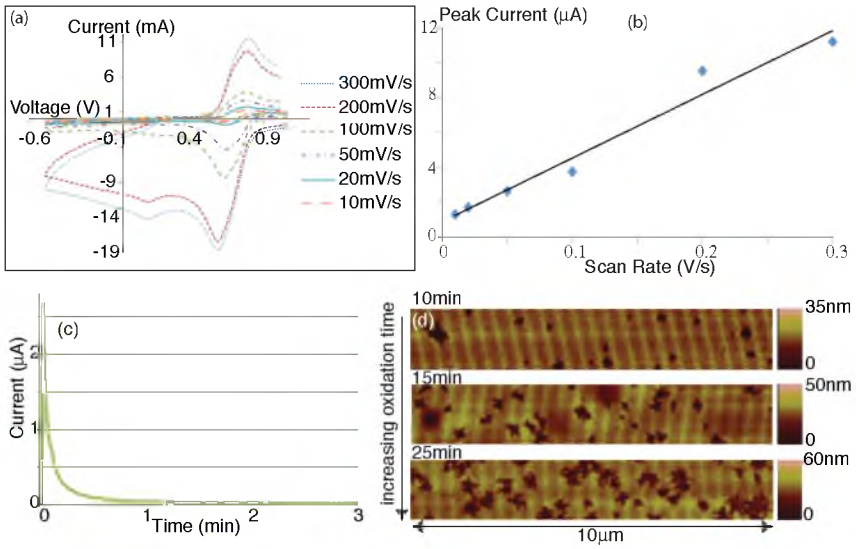

FIG. 3. Characterization of the redox properties of compound **1**. (a) Cyclic voltammograms of **1c** in solution of 0.1M tetrabutylammonium hexafluorophosphate in dichloromethane at various scan rates. (b) Peak current shows a linear dependence on the scan rate. (c) Oxidation current as a function of time for compound **1** in solid form for an oxidation potential of 0.81 V. (d) Atomic-force micrographs of lines after development for samples at various oxidation times.

thick film of compound **1** that was first exposed to a standing wave 633 nm wavelength (HeNe) of period 400 nm for 3 h and 5 min with a laser output power of ~2.65 mW. The oxidation potential was fixed at 0.81 V. As expected,[15] the current shows an exponential decrease with time. The total time of oxidation determines the width and depth of the final developed nanostructure. We characterized different oxidation times as illustrated by the atomic-force micrographs in Fig. 3(d) at an oxidation voltage of 0.85 V determined from cyclic voltammetry.[13] The 50 nm-thick films were exposed to a standing wave at $\lambda = 647$ nm (CW Kr-ion, Coherent Innova 301C) of period 400 nm for 60 s at a power density of 0.95 mW/cm^2. As the oxidation time is increased from 10 min to 25 min, one can clearly see a loss of contrast as some of the regions comprised of **1o** get oxidized as well. The developer (5% IPA: 95% ethylene glycol) dissolves all oxidized portions. Larger oxidation times result in uneven line and increased surface non-uniformities after development. Therefore, a careful choice of the oxidation conditions is critical to patterning high-quality nanostructures.

In conclusion, we characterized a photochromic molecule, compound **1** as a resist material for optical nanopatterning. By exposing a thin-film of this molecule with a standing wave, one of the isomers can be spatially localized. A subsequent electrochemical oxidation "fixes" this localized isomer. The unoxidized regions are free to be used for subsequent exposures. The molecule can be used as a negative-tone or a positive-tone resist with appropriate choice of a developer. Electrochemical oxidation conditions are critical to the quality of the patterns and we characterized the performance of the material under different oxidation conditions. In the specific method, we described here, a conducting electrode is required underneath the photochromic film. This constraint could be avoided if a compatible photo-oxidant could be found. Gated photochromism as the locking mechanism within a photo-reversible switching process has the potential to overcome the far-field diffraction limit with low intensities of light. Therefore, this approach has promise for the fast patterning of large area, two-dimensional complex geometries.

We thank Brian Baker, Kevin Hensley, and Charles Fisher for assistance in the Utah Nanofabrication facility, and Brian van Deveneer for assistance in the Surface Characterization Laboratory. P.C. acknowledges the University of Utah Nanotechnology Training Fellowship. C.B. acknowledges Fondazione Cariplo, which partly funded this work through Indixi Project (Bando "Ricerca scientifica e tecnologica sui materiali avanzati" 2011). R.M. acknowledges a NSF CAREER Award No. 1054899 and funding from the USTAR Initiative.

[1]H. Yan, H. S. Choe, S. Nam, Y. Hu, S. Das, J. F. Klemic, J. C. Ellenbogen, and C. M. Lieber, Nature (London) **470**, 240 (2011).
[2]V. V. Kotlyar, A. A. Almazov, S. N. Khonina, V. A. Soifer, H. Elfstrom, and J. Turunen, J. Opt. Soc. Am. A **22**(5), 849 (2005).
[3]C. C. Cheng, V. Arbet-Engels, A. Scherer, and E. Yablonovitch, Phys. Scr. **T68**, 17 (1996).
[4]N. Yu, P. Genevet, M. A. Kats, F. Aieta, J-P Tetienne, F. Capasso, and Z. Gaburro, Science **334**(6054), 333 (2011).
[5]E. Abbé, Arch. Mikrosc. Anat. Entwicklungsmech. **9**, 413 (1873).
[6]K. I. Willig, A. C. Stiel, T. Brakemann, S. Jakobs, and S. W. Hell, Nano Lett. **11**, 245 (2011).
[7]L. Li, R. R. Gattass, E. Gershgoren, H. Hwang, and J. T. Fourkas, Science **324**(5929), 910 (2009).
[8]L. Li and J.T. Fourkas, Mater. Today **10**(6), 30 (2007).
[9]T. F. Scott, B. A. Kowalski, A. C. Sullivan, C. N. Bowman, and R. R. McLeod, Science **324**, 913 (2009).
[10]S. W. Hell, Science **316**, 1153 (2007).
[11]H.-Y. Tsai, S. W. Thomas III, and R. Menon, Opt. Express **18**(15), 16014 (2010).
[12]N. Brimhall, T. L. Andrews, R. V. Manthena, and R. Menon, Phys. Rev. Lett. **107**, 205501 (2011).
[13]See supplementary material at http://dx.doi.org/10.1063/1.4710547 for experimental procedures for the deposition of the photochromic films, exposure, electrochemical oxidation and development. It also includes details of the optical-exposure system. Characterization procedures for the thin-films are also described.
[14]T. Saika, M. Irie, and T. Shimidzu, J. Chem. Soc., Chem. Commun. 2123 (1994).
[15]A. J. Bard and L. R. Faulker, *Electrochemical Methods, Fundamentals and Applications* (Wiley, New York, 2001).

Supporting Information

Sub-wavelength nano-patterning of photochromic diarylethene films

Precious Cantu[1], Nicole Brimhall[1], Trisha L. Andrew[2], Rossella Castagna[3,4], Chiara Bertarelli[3,4], and Rajesh Menon[1]

[1]Department of Electrical and Computer Engineering, University of Utah, Salt Lake City, UT 84112, USA. [2]Department of Chemistry, Massachusetts Institute of Technology, Cambridge, MA 02139, USA.
[3]Dipartimento di Chimica, Materiali e Ingegneria Chimica "Giulio Natta", Politecnico di Milano, P.zza Leonardo da Vinci 32, 20133 Milano, Italy
[4]Center for Nano Science and Technology @ PoliMi, Istituto Italiano di Tecnologia, Via Pascoli 70/3, 20133 Milano, Italy.

1. Procedure for the synthesis of 1,2-bis[2-methyl-5-(5'-methyl-2'-thienyl)-3-thienyl]hexafluorocyclopentene (compound 1)

5-Methylthiophene-2-boronic acid pinacol ester (0.638 g, 2.85 mmol, 0.7 ml), 1,2-bis-[2-methyl-5-chloro-3-thienyl]hexafluorocyclopentene[1] (0.500 g, 1.14 mmol), and $Pd(PPh_3)_4$ (0.107 g, 0.093 mmol) were placed in a reaction flask under argon atmosphere. Toluene (10 ml), THF (10 ml) and an aqueous 1M solution of Na_2CO_3 (5 ml) were subsequently added, and the solution was refluxed under argon for 24 hrs. Reaction was monitored by TLC. Due to the presence of both the unsubstituted and the mono-substituted species, amounts of boronic acid pinacol ester (100 mg) and $Pd(PPh_3)_4$ (13 mg, 0,01 mmol) were added to complete the reaction, and heating was continued for ca. 24 hrs. The reaction mixture was extracted with water and ether. The combined organic phases were dried over Na_2SO_4 and filtered. After solvent removal, the raw material was purified by flash chromatography on silica gel (ETP:DCM, 9:1) to afford 320 mg of **1** in 50% yield.

1H NMR (400 MHz, $CDCl_3$): d/ppm 7.01 (s, 2H), 6.90 (d, J = 3.5 Hz, 2H), 6.65 (dq, J = 3.5, 1.0 Hz, 2H), 2.47 (s, J = 0.8 Hz, 6H), 1.94 (s, 6H).

2. Evaporation process

Deposition of a uniform thin film over large areas with small organic molecules is of critical importance in order to achieve precise nanopatterning.[3] As the evaporation of small molecules is not a trivial process step, we have designed and fabricated a custom low temperature thermal evaporator to achieve relatively high vacuum, ~10^{-7} torr, to improve the quality of the thin films.

Fig. S1*: Image showing the custom low temperature thermal evaporator. It consists of a 4.5 inch six-way stainless steel cube with knife-edge (ConFlat) flanges to house the ion gauge, LTE source and electrical feedthroughs. Pumping is done by a Varian scroll pump and a 50 liter per second turbo molecular pump (Pfeiffer-Balzers TPH-O5).*

The silicon substrates were obtained by immersion in diluted hydrofluoric acid (HF:H_2O = 1:50) to etch away the native oxide layer. Next a 100nm layer of platinum was sputtered on using the TMV SS-40C-IV Multi Cathode Sputtering system. After sputtering the platinum-coated substrate it was found by a wettability test that the platinum surface was contaminated by a hydrophobic organic impurity. In order to rid the platinum surface of adsorbed contaminants, the surface was cleaned using Reactive Ion Etching (RIE). A conventional Oxford Plasma Lab 80 Plus RIE system was used. Oxygen gases were injected into the chamber through mass flow controllers with 200 W RIE chuck power, 20mT chamber pressure, and flow rates of 50 standard cubic centimeters per minute (sccm). After 1 minute etching, the surface was blown with nitrogen gas. Compound **1** was then thermally evaporated onto platinum-coated silicon substrates from an Al_2O_3 boat at 100°C using a

custom built low temperature thermal evaporator with a base pressure of $1x10^{-6}$ torr and a deposition rate of ~2 Å/second. During deposition a quartz crystal head monitor was used to adjust the monitored thickness of the films. After evaporation, the films were illuminated with short-wavelength UV light (UVP UVGL-25) for 5 minutes to fully convert the samples to the closed form. The film thicknesses were then measured with a Tencor P-10 Profilometer.

3. Optical Exposure System.

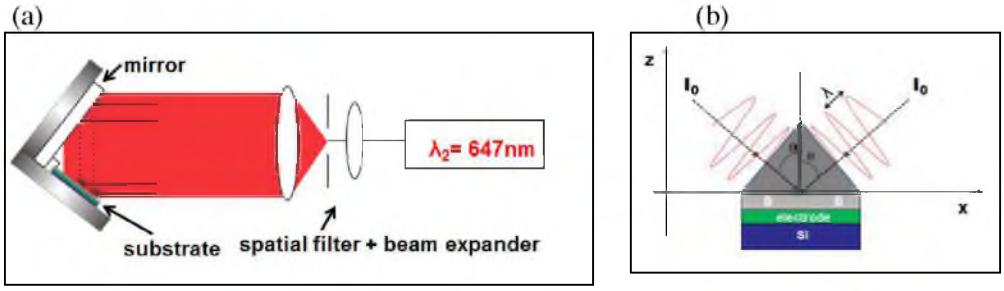

Fig. S2: *(a) Schematic of the experimental setup of the 647nm KrIon laser using a Lloyd's-mirror interferometer. (b) Standing wave of the beam incident on the sample with a period of 400nm.*

The He-Ne Lloyd's mirror interferometer was detailed previously.[2] A 712mW Kr-ion (Innova 300C Series I-301, TEM00 mode) laser at λ = 647nm was also used as a light source for Figure 3(d). A spatial filter allows the high frequency noise to be removed from the beam to provide a clean Gaussian profile. The center of the mirror and substrate assembly remained on the optical axis. Half of the expanded beam was reflected by a mirror and folded a portion of the wave front back onto itself. It served as two beams for recording patterns on the sample. When the mirror is fixed perpendicular to the substrate, θ is equal to the stage rotation angle. The horizontal standing wave interference period can be calculated as $\lambda/(2\sin\theta)$, where θ is the half angle of intersection between the two incident beams and λ the laser wavelength.

4. Electrochemistry

Electrochemical cyclic voltammetry measurements were performed using a DY2000 Electrochemical Workstation in a conventional three-electrode electrochemical cell. Analyte

concentrations were 1.784 nM in anhydrous dichloromethane containing 0.1M tetra-butylammonium hexafluorophosphate ($TBAPF_6$). A platinum button microelectrode was employed as a working electrode; a Pt wire counter electrode and a Silver/SilverNitrate quasi-reference electrode were employed. Cyclic voltammograms of **1c** in solution were obtained at sweep rates between 10 mV/s and 300 mV/s.

Electrochemical oxidation experiments of compound **1c** in thin film form were performed using a Bioanalytical Systems CV-37 Voltammograph in a conventional three-electrode electrochemical cell. Platinum-coated silicon substrate, a Pt wire and an Ag/AgCl saturated KCl were employed as the working electrode, counter electrode and quasi-reference electrode, respectively. All experiments were carried out in DI water as the electrolyte, which was deoxygenated with purified nitrogren for 20 minutes.

5. Development Process

The oxidized form has increased solubility in polar solvents. After electrochemical selective oxidation of the molecule from **1c** to **1ox**, the samples were then developed in a solution of 5% isopropanol and 95% ethylene glycol for 60 seconds. The samples were then carefully rinsed in de-ionized water and dried under N_2. Finally, the resulting structures were imaged by atomic force microscopy (AFM) using a commercial instrument (Bruker Dimension ICON-PT) operating in Peakforce QNM tapping mode. In the case of negative-tone, the unoxidized isomers were dissolved in pentane.

6. UV-Vis absorbance spectroscopy

To investigate the behavior of the compound **1** in thin film form during the process of oxidation and reduction, changes in the spectroscopic properties of the material were monitored as a change in the redox reactions by UV-Vis spectroscopy. For the UV-Vis measurements 80 nm of compound **1** was evaporated onto ITO-coated microscope slides (SPI Supplies 06402-AF). The compound **1o** was obtained by illuminating an evaporated film with a 4 mW He-Ne laser (λ = 633nm) for three hours. The compound **1c** was obtained by

illuminating an evaporated film with short-wavelength UV light (UVP UVGL-25) for 30 minutes. The oxidized form was obtained by illuminating an evaporated film with short-wavelength UV light (UVP UVGL-25) for 30 minutes, immersing the sample in 0.04M NaCl, and oxidizing at 0.5 V (vs. Ag/AgCl) for 30 minutes with the ITO substrate as the working electrode and a platinum counter electrode.

The wavelength of the light was scanned from 300 nm to 800 nm, using a Perkin-Elmer Lambda 20 spectrophotometer. The background spectra were recorded with a blank ITO slide. The three forms of compound **1** in thin-film form also have distinct absorption peaks, showing that they are separate stable species. The compound **1o** has a distinct peak at 324 nm, the compound **1c** has a distinct peak at 618 nm, and the broad absorption band at 452 nm is the fingerprint of the oxidized form. The absorption spectra of the BTE molecule in the three forms in thin film are shown in Fig. 2(a).

7. AFM surface roughness measurements

The surface roughness was studied with an atomic force microscope (Bruker Dimension ICON-PT) in Peakforce QNM tapping mode using a scan window of 1 x 1 μm^2. Because the roughness values are influenced by tip, scan size, and scan conditions, the parameters of the measurements were kept identical from sample to sample. Images of 512 x 512 pixels were acquired at a scan rate of 1Hz. All measurements were made at room temperature (25°C). Fig. S3 shows the surface morphology of thin-films of compound **1**. The surface roughness of the thin-film was calculated in terms of root mean square (rms) value by using Veeco Nanoscope Analysis software. The rms value of the film roughness is estimated to be 0.325 nm. R_a values, defined as the mean value of the surface relative to the center plane were also calculated using equation S1:

$$R_a = \frac{1}{L_x L_y} \int_0^{L_y} \int_0^{L_x} |f(x,y)| dx dy \quad \text{(S1)}$$

where $f(x,y)$ is the surface relative to the center plane and L_x and L_y are the dimensions of the surface. The R_a value was estimated to be 0.260 nm.

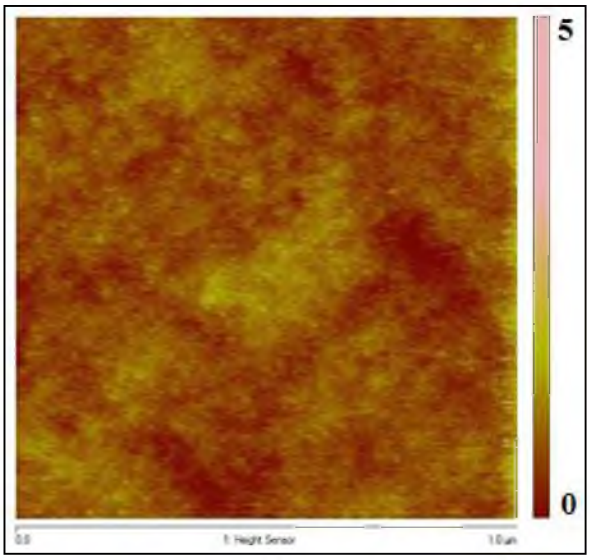

Fig. S3: *AFM image of 40nm thick film of* ***1c*** *.*

The AFM images depicted in Fig. S4 illustrate the long-term stability of the samples. The study of AFM surface morphology of the **1c** film scanned 8 weeks after the date of deposition exhibited the same properties in terms of surface morphology and roughness as did the samples on the date of deposition. This demonstrates that these films deposited by low temperature thermal evaporation technique have consistent morphology and long-term stability. The reproducibility was also verified by studying samples prepared in different batches. The samples were stored under N_2 to prevent ambient oxidation.

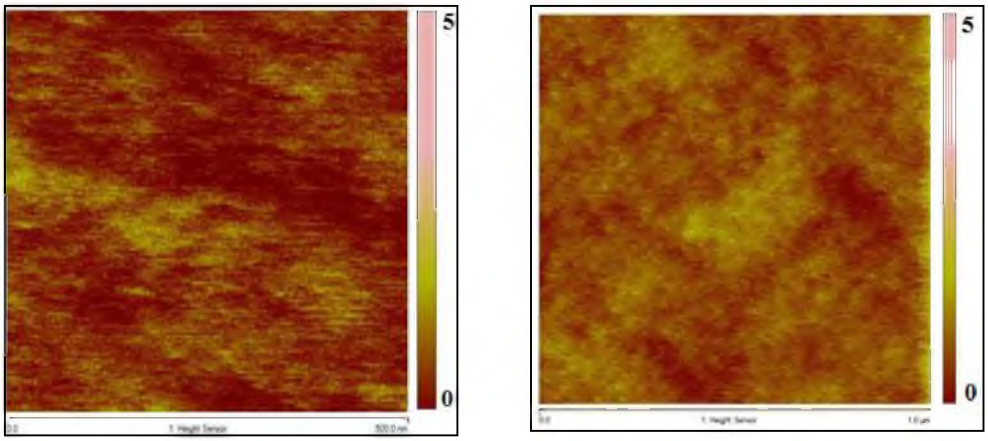

***Fig. S4**: Illustrating film stability of **1c**. The AFM scanning image of 40nm thin-film (Left) on deposited date, (Right) after 8 weeks from the deposited date. The samples were stored under N_2.*

References

[1] S. Hermes, G. Dassa, G. Toso, A. Bianco, C. Bertarelli, G. Zerbi, *New fast synthesis route for symmetric and asymmetric phenyl-substituted photochromic dithienylethenes bearing functional groups such as alcohols, carboxylic acids, or amines*, Thetrahedron Lett. 50, 1614- 1617 (2009).

[2] N.Brimhall, et al, *Breaking the Far-Field Diffraction Limit in Optical Nanopatterning via Repeated Photochemical and Electrochemical Transitions in Photochromic Molecules*, Physical Review Letters. 107, 205501 (2011).

[3] R. Carbonell and J. Kim, *Deposition of Small Organic Molecules by the Displacement of Two Immiscible Supercritical Phases*, Langmuir 22, 2117-2129 (2006).

CHAPTER 7

NANOPATTERNING OF DIARYLETHENE FILMS VIA SELECTIVE DISSOLUTION OF ONE PHOTOISOMER

Reprinted with permission from: P. Cantu, T.L. Andrew, and R. Menon. "Nanopatterning of diarylethene films via selective dissolution of one photoisomer." *Applied Physics Letters*, vol. 103, pp. 173112–1 to 173112–4, 2013.

APPLIED PHYSICS LETTERS 103, 173112 (2013)

Nanopatterning of diarylethene films via selective dissolution of one photoisomer

Precious Cantu,[1] Trisha L. Andrew,[2] and Rajesh Menon[1,a)]
[1]Department of Electrical and Computer Engineering, University of Utah, Salt Lake City, Utah 84112, USA
[2]Department of Chemistry, University of Wisconsin-Madison, Madison, Wisconsin 53706, USA

(Received 30 September 2013; accepted 11 October 2013; published online 24 October 2013)

The ability to pattern nanometric features on various substrates with high throughput, accuracy, and uniformity is the key driving force enabling novel applications in nanophotonics, nanoelectronics, nano-electro-mechanical systems, and nanofluidics. Patterning via Optical Saturable Transitions (POST) is an optical nanopatterning technique that circumvents the far-field diffraction limit by exploiting the linear switching properties of thermally stable photochromic molecules. Previously, POST was enabled by an electrochemical oxidation "locking step." In this letter, we report an electrode-free "locking step" that exploits the difference in solubility between the two isomeric states of a photochromic molecule in a polar solvent. The reported method obviates the need for a conducting underlayer and also reduces the number of required steps. Using this method, we demonstrated isolated lines of width $\sim\lambda/4$ and spacing between features as small as $\sim\lambda/2.5$ for an exposure wavelength of λ. [http://dx.doi.org/10.1063/1.4826925]

Nanopatterning with optical wavelengths has many potential applications in the research, development, and manufacture of electronic, optical, and photonic devices.[1–4] Currently, geometries at the nanoscale are patterned primarily via serial writing tools such as scanning-electron-beam lithography, scanning-ion-beam lithography, and scanning-probe lithography. Although these tools offer high resolution and flexibility, their slow writing speeds prevent patterning of nanostructures over large areas. On the contrary, optical lithography can be extremely fast. However, its resolution is limited by diffraction.[5–7] Several techniques such as photo-induced deactivation (RAPID)[8] lithography, multiphoton absorption polymerization,[9] absorbance-modulation-optical lithography (AMOL),[10] and two-photon continous flow lithography (TP-CFL)[11] have been proposed to circumvent this far-field diffraction limit. The first two of these suffer from poor image contrast and require high light intensities, which limit their potential for parallelizability and high throughput. AMOL is limited to surface (2-D) patterning and in its current implementation also suffers from the requirement of high light intensities.[10] The last approach is not easily scalable to large volumes. Recently, we developed patterning via optical saturable transitions (POST) as an alternative technique for sub-diffraction-limited patterning.[5] POST exploits the photoisomerization at low light intensities of photochromic molecules, namely, diarylethenes, to create sub-diffraction-limited nanoscale patterns. Periodic features with sub-wavelength resolution have been reported before using other photochromic molecules,[12] namely, azobenzene polymers. However, the *cis* isomer of azobenzene is thermally unstable compared to the *trans* isomer and will spontaneously relax back to the *trans* form. This thermal isomerization reaction limits the subwavelength resolution limit achievable with azobenzene photochromes.[12] Diarylethenes have an advantage over azobenzenes as they are thermally stable at room temperature. Also, since only single-photon transitions are involved, POST does not have the restriction of high light intensity to achieve nanoscale resolution.

In POST, a thin layer of photochromic molecules acts as the pattern-recording material. The principle of operation is related to nanoscale fluorescence imaging where the samples are labeled with photoswitchable fluorophores such as in stimulated-emission-depletion microscopy (STED).[13,14] In STED, a focused round spot first excites the fluorophores in a diffraction-limited region. Subsequently, a focused ring-shaped spot at a longer wavelength de-excites the molecules through stimulated emission in this region except at the center of the ring. Only fluorophores in the center of the ring remain in the excited state and spontaneously emit photons. This light-emitting region can be substantially smaller than the far-field diffraction limit. The one key difference in nanopatterning is that a "locking" step is necessary to fix the sub-wavelength region and isolate it from further optical processing.[14] The specific sequence of steps for POST is described next.

In the POST process, a thin film of a photochromic molecule is first thermally evaporated onto a silicon substrate. In our experiments, the photochromic molecule is 1,2-bis(5, 5′-dimethyl-2,2′-bithiophen-4-yl) perfluorocyclopent-1-ene (compound 1 in Fig. 1(a)). This layer is analogous to the pattern-recording material or the resist in conventional lithography. The layer is uniformly illuminated with a short-wavelength UV lamp (UVGL-25, Analytika Jena AG), which converts all molecules to the closed-ring isomer (compound 1c). Next, the sample is exposed to a standing wave at $\lambda_2 = 647$ nm (Kr-ion laser, Coherent Innova 301C). This exposure converts all molecules except at the nodes to the

a)Email: rmenon@eng.utah.edu

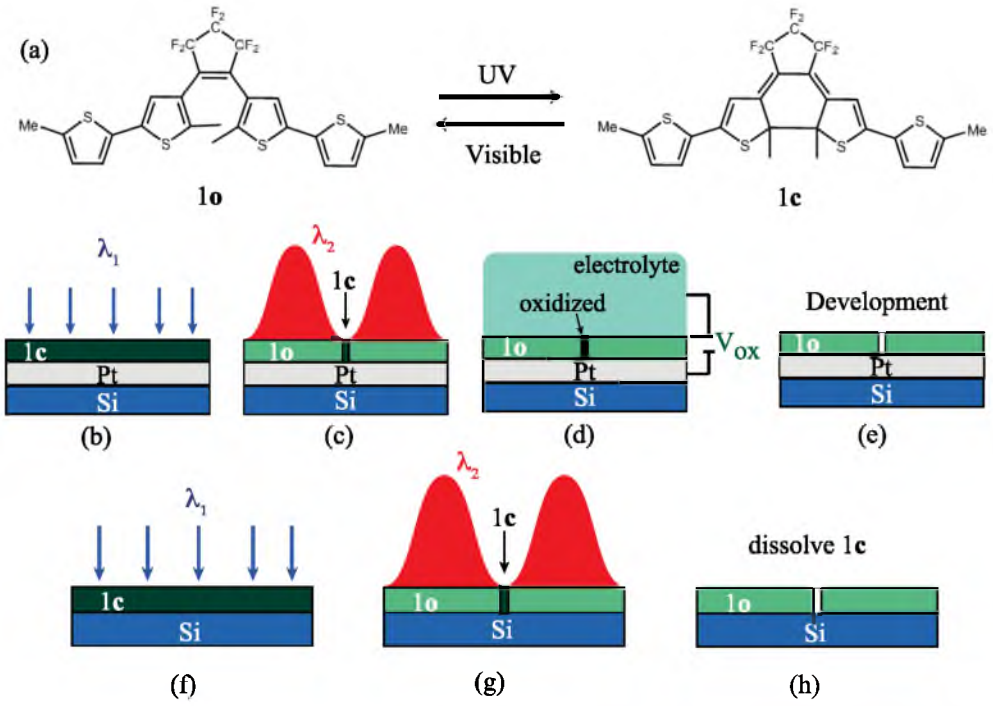

FIG. 1. (a) Photochromic molecule (compound 1) used as recording medium in POST. Compound 1 exists as an open-ring isomer 1o and a closed-ring isomer 1c. (b)–(e) Sequence of steps for conventional POST. (f)–(h) Sequence of steps for the new dissolution-based method.

open-ring isomer (compound 1o). Increasing this exposure time decreases the width of the regions that remain as 1c beyond the far-field diffraction limit. In conventional POST (Figs. 1(b)–1(e)), electrochemical oxidation selectively oxidizes 1c while 1o remains unchanged. The oxidized 1c is subsequently developed in a polar solvent mixture of 5%(wt.) isopropyl alcohol and 95%(wt.) ethylene glycol. We recently discovered that it is possible to selectively dissolve away 1c in 100%(wt.) ethylene glycol without affecting 1o. This step essentially achieves the "locking" of the pattern as illustrated in Figs. 1(f)–1(h). Note that this approach uses one less step than the conventional method. Furthermore, the conventional method requires a 100-nm-thick film of platinum underneath compound 1 to serve as the working electrode in a three-electrode electrochemical cell.[5,6] This, in turn, requires an additional evaporation step during sample preparation. Furthermore, it introduces challenges for pattern transfer into the underlying substrate after patterning. This approach reduces the number of required steps, is more general, and has the potential to be integrated into conventional optical-projection lithography, where water immersion is typically used.[15]

Compound 1o closes its central ring under UV irradiation, leading to a completely π-conjugated current path along the long axis of the molecule. Visible light irradiation of compound 1c opens the ring, breaking the conjugation length in half.[16] The central fluorocarbon tether acts as a through-space electron density-withdrawing group and introduces a dipole in both isomers of compound 1. The longer π-conjugation length, i.e., larger conjugated electron density, in the closed form leads to a larger dipole moment than for the broken π-system of the open form. This makes the closed-ring isomer 1c comparatively more polar and, therefore, more soluble in a polar solvent such as ethylene glycol.

To verify this selective solubility on the macro scale, we thermally evaporated a ~22 nm thick layer of compound 1 at 100 °C and a base pressure of 1×10^{-6} Torr onto a clean silicon substrate and exposed half the sample to uniform illumination at $\lambda_2 = 647$ nm (CW Kr-ion, Coherent Innova 301C) for 10 min with an output laser power of ~38 mW at an incident intensity of 2.15 mW/cm^2. This converts half the sample to 1o while the other half remains as 1c. The entire sample was then immersed in 100%(wt.) ethylene glycol for time intervals ranging from 5 min to 105 min, as illustrated in Fig. S2 of the supplementary material.[17] The remaining film thicknesses in both regions were measured with a Tencor P-10 profilometer after each immersion step. The results plotted in Fig. 2(a) confirm that while 1c is dissolved away, 1o remains mostly unaffected even after 105 min of immersion. The dissolution rate of 1c is 0.0565 nm/min while that of 1o is negligible. The ratio of the dissolution rate of 1c to that of 1o is higher than 20:1.[17]

Figure 2(b) shows the atomic-force micrographs of three grating patterns that were created in ~29 nm-thick film of compound 1 atop a silicon substrate. Using a Lloyd's mirror interferometer, the samples were exposed to a standing wave of period 540 nm at λ_2 647 nm (incident intensity 2.1 mW/cm^2) for 647 s. The samples were immersed in 100%(wt.) ethylene glycol for varying times. Subsequently, each sample was rinsed in deionized water and dried with N_2. From these two plots, one can clearly see the agreement of the dissolution rates of the closed-ring isomer 1c, in the macro-scale (Fig. 2(a)) with that at the nanoscale (Fig. 2(b)).

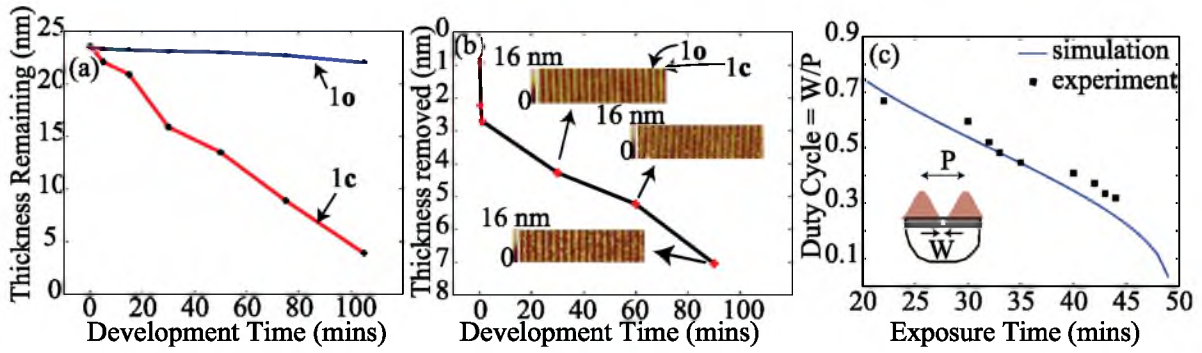

FIG. 2. (a) Macro-scale solubility of 1c and 1o in 100%(wt.) ethylene glycol. (b) Relative solubility of 1c vs 1o at the nanoscale (Inset: atomic-force micrographs of 3 development times). (c) Linewidth vs exposure time for a single exposure and development. The simulated curve is shown as a solid line while the experimental data are shown using solid squares. A sinusoidal illumination with period 526 nm was assumed.

In order to explain these observations, Density-Functional Theory (DFT) calculations were performed with the B3LYP functional and a standard 6-31G(d) basis set. The molecular geometries of both 1o and 1c were first optimized to a thermodynamic ground state and the electronic properties of both compounds then calculated using the Gaussian software interface. The ab initio calculated dipole moments for the open (1o) and closed (1c) forms are 5.65 D and 13.39 D, respectively. Details of this simulation are included in the supplementary material.[17] The higher dipole moment of 1c indicates that the closed-ring isomer is more polar and, therefore, comparatively more soluble in polar solvents. Again, this calculated trend agrees with the experimental observations that the closed-ring form, 1c, is more soluble compared to the open-ring form, 1o, in polar ethylene glycol.

Assuming an incident sinusoidal illumination, we can readily simulate the resulting feature size. In Fig. 1(c), this feature size as a fraction of the period of the illumination (526 nm in our experiments), i.e., the duty cycle, is plotted as a function of the exposure time using the solid black line. The experimentally measured values are shown using squares. Using the exposure threshold as the only fitting parameter, we can show that this simple model can accurately explain our experimental results. The smallest experimentally obtained duty cycle was 0.3, corresponding to a linewidth of $\sim$158 nm or $\sim\lambda/4$. More precise control of the exposure time should enable even smaller features. Note that as the exposure time is increased, the simulation indicates that feature size should be reduced significantly below the far-field diffraction limit.

Since the photochromic film can readily recover to its original state upon exposure to UV, it is straightforward to extend the idea to multiple exposures. This is, of course, required for creating dense patterns.[5] Here, we show feasibility of this approach by performing two exposures of the same standing wave, but with a $\sim$45° rotation in between (Fig. 3). Each exposure was conducted on the Lloyd's-mirror interferometer, with a standing wave of period, 540 nm at $\lambda_2 = 647$ nm (incident intensity = 2.1 mW/cm^2) for 1 min.

After the first exposure, the sample was immersed in 100%(wt.) ethylene glycol for 30 min and exposed to short-wavelength UV lamp (UVGL-25, Analytika Jena AG) for 3 min to convert the molecules to the original closed-ring isomer 1c. The sample was then rotated approximately 45° relative to the optics, and a second exposure to the standing wave was performed. Again, the sample was immersed in 100%(wt.) ethylene glycol for 30 min. After each development, the sample was rinsed in deionized water and dried with N_2. The corresponding atomic-force micrograph resolves lines with spacing as small as $\sim$260 nm or $\sim\lambda/2.5$, which is less than half of the period of the standing wave. The significant line-edge roughness evident in Fig. 3 (right) is likely due to the partial oxidation of 1c under ambient condtions.[6] Improving the uniformity of the patterns requires that the exposure and development process be conducted under an inert atmosphere.

In conclusion, we introduced an approach to sub-diffraction-limited nanopatterning using low light intensities that exploits the solubility difference between photoswitchable

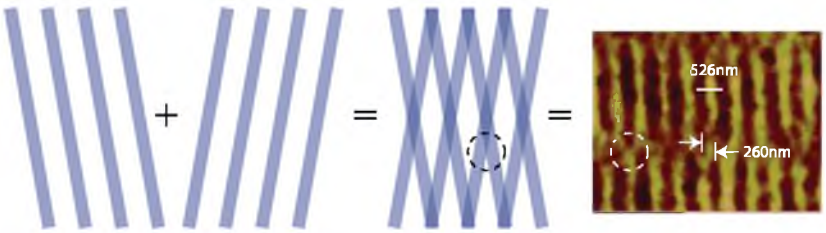

FIG. 3. Experimental demonstration of a double-exposure. Left: Schematic showing orientation of sample for double-exposure using POST. Right: Atomic-force micrograph of the resulting pattern. The atomic-force micrograph reveals the smallest spacing between the features as $\sim$260 nm, which is approximately half the period of the illuminating standing wave.

molecules and demonstrated the patterning of lines of width $\lambda/4$. We have also demonstrated isolated lines with resolvable features as small as $\lambda/2.5$, which is less than the far-field diffraction limit. This technique reduces the number of steps by avoiding an electrochemical oxidation as well as the requirement for a platinum working-electrode. Further optimization of the exposure and immersion parameters should lead to significantly reduced feature spacings. By extending the approach to 2D and even 3D, patterns of complex geometries may be readily patterned as well.

We thank Charles Fisher for assistance in the Utah Nanofabrication facility and Brian van Deveneer for assistance in the Surface Characterization Laboratory. P.C. acknowledges the NSF GRFP under Grant No. 0750758. P.C. acknowledges the University of Utah Nanotechnology Training Fellowship. R.M. acknowledges a NSF CAREER Award No. 1054899 and funding from the USTAR Initiative.

[1]X. Xie, Y. Liu, M. Zhang, J. Zhou, and K. S. Wong, Physica E **44**, 1109–1126 (2012).
[2]J. Leroy, A. Crunteanu, A. Bessaudou, F. Cosset, C. Champeaux, and J. C. Orlianges, Appl. Phys. Lett. **100**, 213507 (2012).
[3]D. W. Carr, L. Sekaric, and H. G. Craighead, J. Vac. Sci. Technol. B **16**, 3821 (1998).
[4]O. Wilhelmi, S. Reyntjens, C. Mitterbauer, L. Roussel, D. J. Stokes, and D. H. W. Hubert, Jpn. J. Appl. Phys. **47**(6), 5010–5014 (2008).
[5]N. Brimall, T. L. Andrew, R. V. Manthena, and R. Menon, Phys. Rev. Lett. **107**, 205501 (2011).
[6]P. Cantu, T. L. Andrew, R. Castagna, C. Bertarelli, and R. Menon, Appl. Phys. Lett. **100**, 183103 (2012).
[7]E. Abbé, Arch. Mikrosk. Anat. Entwichlungsmech. **9**, 413 (1873).
[8]L. Li, R. R. Gattass, E. Gershgoren, H. Hwang, and J. T. Fourkas, Science **324**(5929), 910–913 (2009).
[9]L. Li and J. T. Fourkas, Mater. Today **10**(6), 30 (2007).
[10]T. L. Andrew, H. Y. Tsai, and R. Menon, Science **324**(5929), 917–921 (2009).
[11]S. C. Laza, M. Polo, A. A. R. Neves, R. Cingolani, A. Camposeo, and D. Pisignano, Adv. Mater. **24**, 1304–1308 (2012).
[12]H.-Y. Tsai, S. W. Thomas III, and R. Menon, Opt. Express **18**(15), 16015 (2010).
[13]S. W. Hell, Science **316**, 1153 (2007).
[14]S. W. Hell, Phys. Lett. A **326**, 140 (2004).
[15]M. Switkes and M. Rothschild, J. Vac. Sci. Technol. B **19**, 2353 (2001).
[16]Y. Kim, T. J. Hellmuth, D. Sysoiev, F. Pauly, T. Pietsch, J. Wolf, A. Erbe, T. Huhn, U. Groth, U. E. Steiner *et al.*, Nano Lett. **12**, 3736–3742 (2012).
[17]See supplementary material at http://dx.doi.org/10.1063/1.4826925 for the modeling method, fabrication techniques, and dissolution characterization.

Supporting Information

Nanopatterning of diarylethene films via selective dissolution of one photoisomer

Precious Cantu[1], Trisha L. Andrew[2], and Rajesh Menon[1]

[1]Department of Electrical and Computer Engineering, University of Utah, Salt Lake City, UT 84112, USA.

[2]Department of Chemistry, University of Wisconsin-Madison, Madison, WI 53706, USA

1. Sample Preparation

The silicon substrates were cleaned by immersion in diluted hydrofluoric acid ($HF:H_2O$ = 1:50) to etch away the native oxide layer and dried with N_2. To remove any hydrophobic adsorbed contaminents, the surface was cleaned using Reactive Ion Etching (RIE) (Oxford Plasma Lab 80 Plus RIE). Oxygen gases were injected into the chamber through mass flow controllers with 200 W RIE chuck power, 20mT chamber pressure, and flow rates of 50 standard cubic centimeters per minute (sccm). After 1 minute etching, the surface was blown with nitrogen gas. The photochromic molecule was then thermally evaporated from an Al_2O_3 boat at 100 degrees Celsius using a custom built low temperature thermal evaporator with a base pressure of $1x10^{-6}$ Torr and a deposition rate of ~1.32 Å/second. After evaporation, the films were illuminated with short-wavelength UV lamp (UVGL-25, Analytika Jena AG) for 3 minutes to fully convert the samples to the closed-ring isomer, **1c**. The film thicknesses were then measured with a Tencor P-10 Profilometer measuring ~29nm.

2. Demonstration of effectiveness of dissolution method

To demonstrate the effectiveness of our method, we produced 1D-grating patterns fabricated by interference lithography. Figure S1 shows the characterization of different development times and exposure times as illustrated by the atomic-force micrographs for a ~22nm-thick film of compound **1** that was exposed to a standing wave λ_2 = 633nm wavelength (CW 05-

LHP-151, Melles-Griot) of period 600 nm for 240 minutes and 314 minutes with an output laser power of ~2.7mW. As exposure to the polar solvent (100%(wt) ethylene glycol) is increased from 15 seconds to 60 seconds, one can clearly see the increased contrast. The lines are well defined with a width of about λ/2.4 (265 nm) for an immersion time of 60 seconds for the 314 minutes exposure. As the immersion time is reduced to 30 seconds, the linewidth decreases slightly. When the immersion time is 15 seconds, it is clear that not all the closed-ring isomer, **1c**, has been removed, which significantly reduces the contrast of the printed lines.

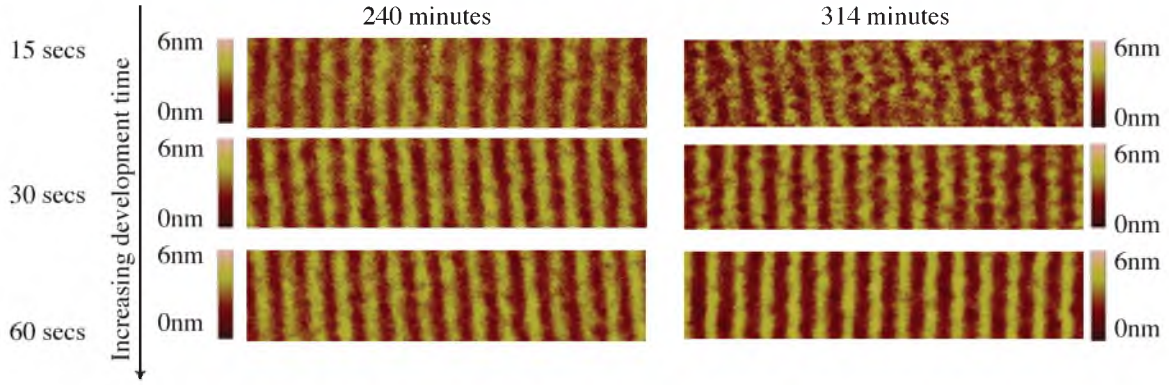

Fig. S1*: Atomic force micrographs of isolated lines after various development times for exposure times of 240mins and 314mins.*

3. Density Functional Theory Calculations

The results of the density functional theory calculations of the two photochromic isomers is illustrated in Scheme S1.

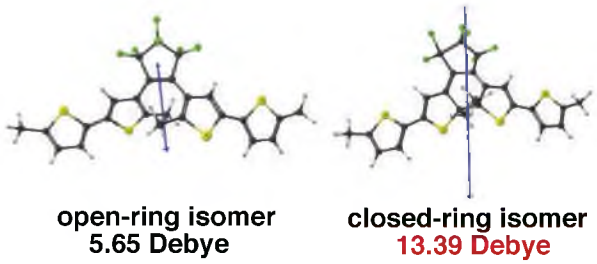

Scheme S1: *Dipole moments of the open (**1o**) and closed (**1c**) ring isomers of photochrome BTE. The dipole moment vectors are superimposed on the geometry-optimized molecular structures of the respective isomers. Calculations were performed with the Gaussian software interface [1] using the B3LYP functional and a standard 6-31G(d) basis set.*

4. Dissolution Characterization

A schematic of the experiment to characterize the macro-scale dissolution of compound **1** is shown in Fig. S2.

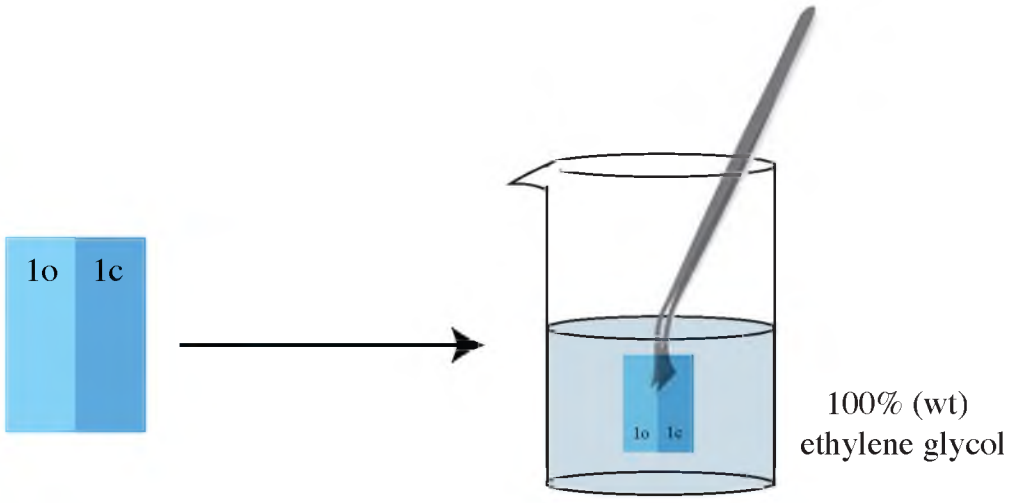

Fig. S2: *Schematic of setup for dissolution of compound **1** in 100%(wt) ethylene glycol.*

The resulting plot showing the thickness of the layer remaining as a function of immersion time is shown in Fig. S3.

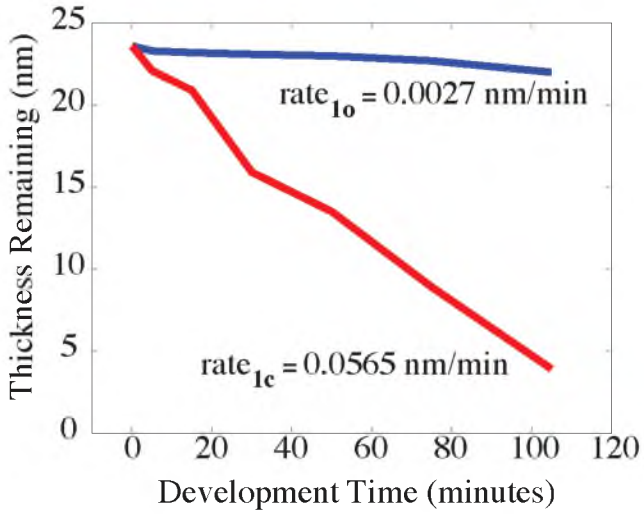

Fig. S3: *Plot of thickness remaining of the closed-ring, **1c**, and open-ring, **1o**, forms as a function of dissolution time in 100%(wt) ethylene glycol.*

References

[1] Gaussian 09, Revision C.01, M. J. Frisch, G. W. Trucks, H. B. Schlegel, G. E. Scuseria, M. A. Robb, J. R. Cheeseman, G. Scalmani, V. Barone, B. Mennucci, G. A. Petersson, H. Nakatsuji, M. Caricato, X. Li, H. P. Hratchian, A. F. Izmaylov, J. Bloino, G. Zheng, J. L. Sonnenberg, M. Hada, M. Ehara, K. Toyota, R. Fukuda, J. Hasegawa, M. Ishida, T. Nakajima, Y. Honda, O. Kitao, H. Nakai, T. Vreven,J. A. Montgomery, Jr., J. E. Peralta, F. Ogliaro, M. Bearpark, J. J. Heyd, E. Brothers, K. N. Kudin, V. N. Staroverov, T. Keith, R. Kobayashi, J. Normand, K. Raghavachari, A. Rendell, J. C. Burant, S. S. Iyengar, J. Tomasi, M. Cossi, N. Rega, J. M. Millam, M. Klene, J. E. Knox, J. B. Cross, V. Bakken, C. Adamo, J. Jaramillo, R. Gomperts, R. E. Stratmann, O. Yazyev, A. J. Austin, R. Cammi, C. Pomelli, J. W. Ochterski, R. L. Martin, K. Morokuma, V. G. Zakrzewski, G. A. Voth, P. Salvador, J. J. Dannenberg, S. Dapprich, A. D. Daniels, O. Farkas, J. B.Foresman, J. V. Ortiz, J. Cioslowski, and D. J. Fox, Gaussian, Inc., Wallingford CT, 2010.

CHAPTER 8

PATTERNING VIA OPTICAL SATURABLE TRANSFORMATIONS: A REVIEW AND SIMPLE SIMULATION MODEL

Reprinted with permission from: P. Cantu, T.L. Andrew, and R. Menon. "Patterning via Optical-Saturable Transformations: A review and simple simulation model." *Applied Physics Letters*, vol. 105, pp. 193105-1 to 193105-5, 2014.

APPLIED PHYSICS LETTERS **105**, 193105 (2014)

Patterning via optical-saturable transformations: A review and simple simulation model

Precious Cantu,[1] Trisha L. Andrew,[2] and Rajesh Menon[1,a)]
[1]*Department of Electrical and Computer Engineering, University of Utah, Salt Lake City, Utah 84112, USA*
[2]*Department of Chemistry, University of Wisconsin-Madison, Madison, Wisconsin 53706, USA*

(Received 13 August 2014; accepted 6 November 2014; published online 13 November 2014)

Most of the nanoscale fabrication in the semiconductor industry is based on patterning with scanning-electron beam lithography (SEBL). Although this approach is very versatile and has very high resolution, it is intrinsically a serial writing process, and therefore, relatively slow. Our group has been investigating alternative nano-fabrication techniques, adapted from ideas of saturating optical transitions such as those used in stimulated emission-depletion microscopy and related methods, and optical interference lithography. Linewidths and resolutions on the scale of a few tens of nanometers and below are highly desirable for various applications in nanotechnology. However, the spatial resolution of optical lithography is restricted by diffraction. In the past, we developed absorbance modulation to overcome this limit. This approach utilizes photochromic molecules that can be optically switched between two thermally stable states, one opaque and the other transparent. However, absorbance modulation is limited to surface (2-D) patterning. Here, we report on an alternative approach that exploits unique combinations of spectrally selective reversible and irreversible photochemical transitions to achieve deep subwavelength resolution with potential extension to 3-dimensions. This approach, which we refer to as patterning via optical-saturable transformations have the potential for massive parallelism, enabling the creation of nanostructures and devices at a speed far surpassing what is possible with SEBL. The aim of our research is to translate the success in circumventing Abbe's diffraction limit in optical microscopy to optical lithography. © *2014 AIP Publishing LLC*. [http://dx.doi.org/10.1063/1.4902024]

Today the role of optical lithography is of key importance in the fabrication of nanoscale structures, with particular relevance to the semiconductor industry, however, it is limited by diffraction. Advancements in alternative optical lithography techniques that circumvent this diffraction limit will enable applications of nanopatterning, such as 3-dimensional fabrication of nanostructures for biological applications. In this article, we review a class of optical lithographic techniques that achieve deep sub-wavelength resolution using photoswitchable molecules. We call this approach Patterning via Optical-Saturable Transformations (POST).[1]

In POST, a thin layer of photochromic molecules is used as the pattern-recording material. The principle of operation is related to nanoscale fluorescent imaging where the samples are labeled with photoswitchable fluorophores such as in stimulated emission-depletion (STED) microscopy.[2] In STED, a focused round spot first excites the fluorophores in a diffraction-limited region (Fig. 1(b)). Subsequently, a focused ring-shaped spot at a longer wavelength de-excites the molecules through stimulated emission in this region except at the center of the ring (Fig. 1(c)). Only fluorophores in the center of the ring remain in the excited state and spontaneously emit photons (Fig. 1(d)). This light-emitting region can be substantially smaller than the far-field diffraction limit. In nanopatterning, a "locking" step is necessary to fix the sub-wavelength region, and isolate it from further optical processing. The photochromic molecule used in POST exists in two isomeric states. One of the isomers may be selectively and irreversibly converted ("locked") into a 3rd state (Fig. 1(e)). An illustration of the sequence of steps in POST is shown in Figs. 1(f)–1(p).

The photochromic layer is originally in one homogeneous state as shown in Fig. 1(f). When this layer is exposed to a focused node at λ_2, it converts into the second isomeric state (shown in red) everywhere except in the near vicinity of the node. By controlling the exposure dose, the size of the unconverted region may be made arbitrarily small (Fig. 1(h)). A subsequent locking step "locks" in the pattern (Fig. 1(i)). Next, the layer is exposed uniformly to λ_1, which converts everything except the locked region back to the original state (shown in white in Fig. 1(k)). The sequence of steps may be repeated with a displacement of the sample relative to the optics, resulting in two "locked spots" whose spacing is smaller than the far-field diffraction limit (Fig. 1(p)). Therefore, any arbitrary geometry may be patterned in a "dot-matrix" fashion.

It is clear from the previous discussion that the locking step is the key difference between nanoscopy and nanoscale patterning. We have pursued two alternative paths to achieve this locking behavior. Clearly, the molecule that is used for recording will determine the specific approach. In our examples, we used a diarylethene molecule, specifically (1, 2-bis(5, 5′-dimethyl-2, 2′-bithiophen-yl) perfluorocyclopent-1-ene. Colloquially, we refer to this compound as BTE. BTE exists in two isomeric forms as illustrated in Fig. 2(a).

The closed-ring isomer has an extended conjugation of its π electron cloud, which allows the closed-ring isomer to have a lower oxidation potential than the open-ring isomer.[3]

a)Email: cantu@eng.utah.edu

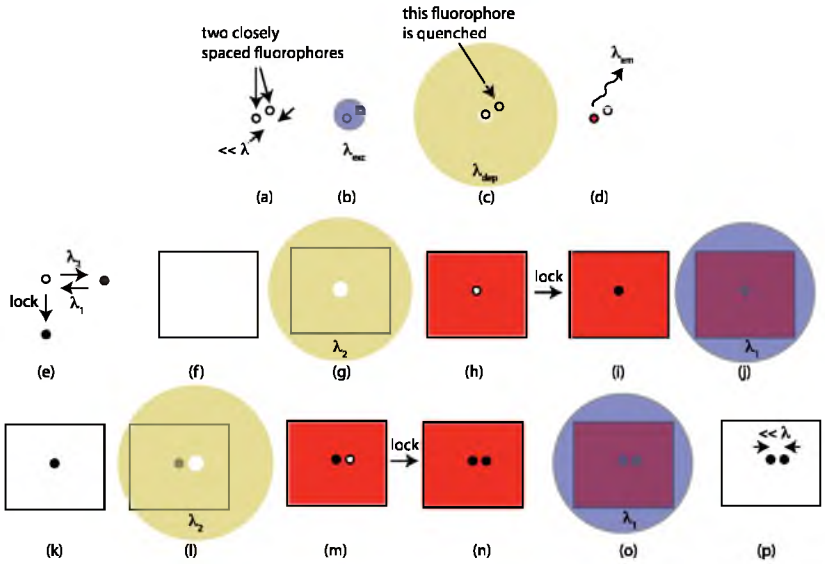

FIG. 1. (a)–(d) Schematic of stimulated-emission-depletion microscopy. (e)–(p) Schematic of POST.

Our first approach to "locking" therefore relies on the selective oxidation of the closed-ring isomer.

The locking step is achieved by electrochemical oxidation of the closed-ring isomer into a stable cation. This product cation is preferentially soluble in a polar solvent compared to the unoxidized isomers. Therefore, it allows us to convert the locked regions into topographic nanoscale patterns after all the exposures are completed. The idea is illustrated in Fig. 2(b).

The sample is comprised of a clean silicon wafer onto which a 100 nm-thick film of Pt is evaporated. Subsequently, about 20 nm of BTE is thermally evaporated on top of the Pt.

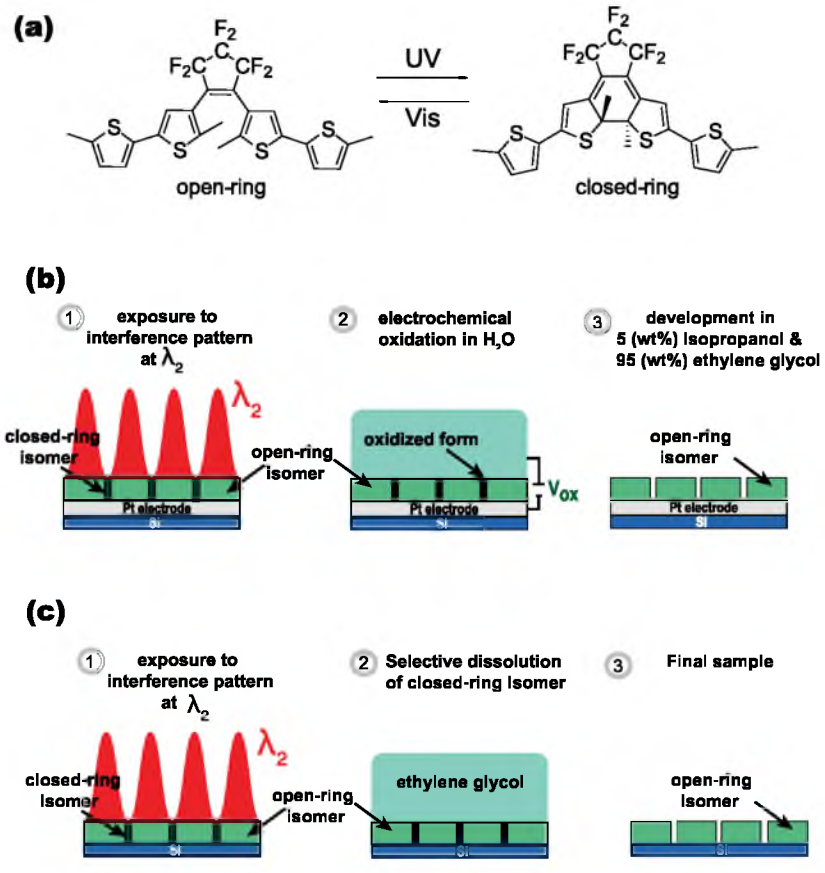

FIG. 2. (a) Schematic of photochromic molecule (BTE) used in POST. (b) Electrochemical oxidation as the locking step in POST. (c) Isomer-selective dissolution as the locking step.

Prior to use, all the BTE is converted into the closed-ring form. In step 1, the sample is exposed to a standing wave at a visible wavelength ($\lambda_2 = 633$ nm), where all the BTE is converted to the open-ring form except in very narrow lines near the vicinity of the nodes of the standing wave. For a single-exposure experiment, the sample is then placed in an electrochemical cell and oxidized at about 0.5 V. This converts only the closed-ring isomer into a cation, while the open-ring isomer is unaffected. Finally, in step 3, the sample is developed in a mixture of 95 (wt. %) ethylene glycol and 5 (wt. %) isopropanol, which dissolves away the cations. Most of the unoxidized BTE remains. This results in nanoscale grooves as illustrated. The width of these grooves is no longer determined primarily by the far-field diffraction limit (which in this case should be half the period of the exposing standing wave). The details of this experiment and related approaches have been described previously by Brimhall *et al.* and Cantu *et al.*[1,4]

An alternative approach to the locking mechanism has also been identified. The idea is based upon the selective dissolution of one of the isomers of the BTE. This has the advantage of not requiring a conductive Pt layer, which might be problematic in some devices. Also, it combines the two steps of locking and development into a single dissolution step. The idea is illustrated in Figure 2(c).

We have recently realized that two isomers of BTE have drastically different solubility rates in ethylene glycol. Hence, it allowed us to realize preliminary experimental results from this approach.[5]

We have recently developed a simple model to describe POST, which allows us to explain the observed experimental results well. The salient features of this model and related simulation analysis are summarized here.

The geometry of the problem is illustrated in Fig. 3(a). The propagation of light is from top to bottom (in the positive Z direction). A two-dimensional geometry is assumed. This is consistent with our experiments, where a 1-D standing wave is used for exposure. The chemical rate equation

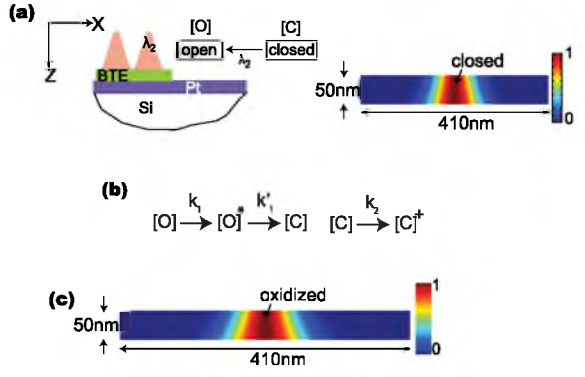

FIG. 3. (a) Model for simulating the exposure step. An example of the output of the simulation showing the relative concentrations of the two isomers within the layer. Scale bar represents normalized concentration of closed-ring isomer. (b) Electrochemical oxidation of the two isomers of BTE. (c) Normalized concentration of the oxidized-closed form of BTE. Oxidation was performed after the exposure in (a).

for the reaction from the closed-form [C] (which is the initial form of all molecules) to the open-form [O] is given by

$$-\frac{\partial[C]}{\partial t} = [C]I\varepsilon_c\phi_{C\to O} - [O]I\varepsilon_o\phi_{O\to C}, \tag{1}$$

where [C] and [O] are the molar concentrations of the closed and open form isomers, respectively, ε is the molar absorptivity, ϕ is the quantum efficiency, and I is the intensity of the exposure. The differential form of the Beer-Lambert law gives us the following equation:

$$\frac{\partial I}{\partial z} = -(\varepsilon_O[O] + \varepsilon_C[C])I\,. \tag{2}$$

From conservation of matter, we have

$$[O] + [C] = [C_0]. \tag{3}$$

$[C_0]$ is the initial concentration of the closed form (the only form present at the beginning). The boundary condition is $I(x, z = 0, t) = I_0(x)$, the incident illumination intensity and the initial condition are $[C_0](x, z, t = 0) = [C_0]$. For BTE, we can make the further assumption that $\phi_{O\to C}$ is 0, since visible photons do not have sufficient energy to initiate the ring-closing reaction. Since $\varepsilon_O \ll \varepsilon_C$, we can ignore ε_O in the system of equations as well. We can solve the resulting system of partial differential equations using standard finite-element methods as a function of space (x,z) and time (t).

A representative solution for the concentration distributions of open- and closed-ring isomers as a function of depth is illustrated in Fig. 3(a). A standing wave of period 600 nm and $\lambda_2 = 633$ nm was assumed for the incident illumination. Material parameters were all used from Andrew *et al.*[6] The thickness of the BTE layer was assumed to be 50 nm.

The electrochemical oxidation of BTE proceeds along two different paths as illustrated below. The closed-ring isomer oxidizes to a stable cation. The open-ring isomer oxidizes to a meta-stable state that can undergo photocyclization reaction and form the closed-ring isomer.[3] Here, we model these two reactions with four rate equations, Fig. 3(b)

$$\frac{\partial[O]^*}{\partial t} = k_1[O] - k_1'[O]^*, \tag{4}$$

$$\frac{\partial[C]^+}{\partial t} = k_2[C], \tag{5}$$

$$\frac{\partial[C]}{\partial t} = -k_2[C] + k_1'[O]^*, \tag{6}$$

$$\frac{\partial[O]}{\partial t} = -k_1[O]. \tag{7}$$

The solutions for this system of rate equations is

$$[O] = [O_0]e^{-k_1 t}, \tag{8}$$

$$[O]^* = \frac{[O_0]k_1}{k_1 - k_1'}e^{-k_1' t}\left\{1 - e^{-(k_1 - k_1')t}\right\}, \tag{9}$$

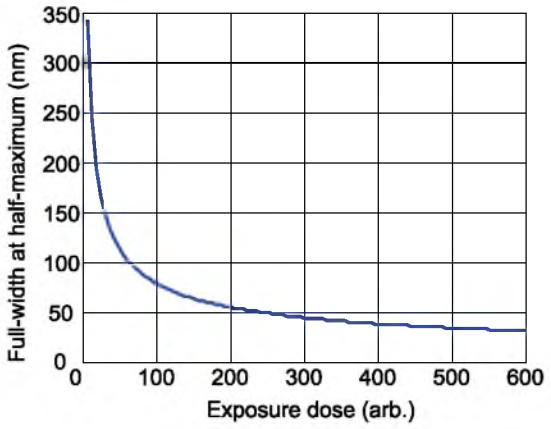

FIG. 4. Full-width at half-maximum of a developed line as a function of exposure dose. The exposure conditions were the same as in Fig. 3(a) except the period of the standing wave, which was 610 nm.

$$[C] = [C_0]e^{-k_2 t} + \frac{k_1 k_1'}{k_1 - k_1'} e^{-k_2 t} \times \left\{ \frac{1 - e^{-(k_1' - k_2)t}}{k_1' - k_2} - \frac{1 - e^{-(k_1 - k_2)t}}{k_1 - k_2} \right\}, \quad (10)$$

$$[C]^+ = [C_0] + [O_0] - ([C] + [O] + [O]^*). \quad (11)$$

The last equation comes from the conservation of matter. Note that the subscript 0 refers to the concentration after exposure and prior to oxidation. Figure 3(c) shows an example simulation that illustrates the concentration distribution of the oxidized closed form. The rate constants need to be experimentally determined. Our previous work elucidated some of these rate constants.[1] In the simulations here, we assumed that $k_1 = 3 \times 10^{-4}\text{min}^{-1}$ and $k_2 = 1.4 \times 10^{-2}\text{min}^{-1}$. Since the rate of oxidation of the closed form is over 2 orders of magnitude higher than that of the open form, we can ignore k_1. Furthermore, if the oxidation is performed for a time that is substantially larger than $\frac{1}{k_2}$, all the closed form will be oxidized without oxidizing any of the open form. This is consistent with Fig. 3(c), where the distribution of the closed-oxidized form is almost identical to the distribution of the closed-form in Fig. 3(a).

For simplicity, we assumed that the unoxidized forms are not dissolved in the developer, while the closed-oxidized form is completely dissolved. This is a good approximation as described earlier in Brimhall *et al.*[1] Therefore, one would expect the final feature profile within BTE to resemble Fig. 3(c), where the red regions are removed after development. Indeed, we reported in Brimhall *et al.* that careful scanning-electron microscopy of the developed lines reveal a clear undercut as predicted by the simulations here.[1]

One important point to note is that the simulation model described here can be used to model POST with either locking approaches. In the case of locking using solubility differences, the oxidation simulation is not required. We can see that Figs. 3(a) and 3(c) look almost identical. This suggests that in both locking approaches, one can use only the exposure model as long as the electrochemical oxidation is performed long enough and the solubility difference between the open and closed forms is large.

We applied the model developed in Modeling and Simulation section to elucidate several key aspects of POST. First, one would expect the linewidth of the developed feature to decrease with exposure dose, since the feature is defined via the optical node. Figure 4 shows the simulation of the full-width at half-maximum (FWHM) of a developed line as a function of exposure dose to the optical standing wave. A steep decrease is seen and the FWHM continues to decrease monotonically with increasing exposure dose.

It is clear that the darkness of the optical node is critical for high contrast in POST. This idea is illustrated by simulating the effect of exposure on a BTE film by a standing wave with a perfect node (on the left) and an imperfect node (on the right) in Fig. 5. As the exposure time increases (top to bottom), for both cases, the region that remains in the closed form gets smaller. This is consistent with Fig. 4. However, for the imperfect node, noise in the node starts to convert some of closed form into the open form, which degrades the image of the patterned region. Eventually, this limits the resolution of the technique.

In this paper, we briefly reviewed the approaches that are enabling optical nanopatterning beyond the far-field diffraction limit. The basic principle is inspired by the idea of saturating an optical transition with a focal ring, which has been implemented in microscopy. However, in order to extend this principle to patterning, a "locking" mechanism is required. We described two distinct approaches to this locking mechanism. We also developed

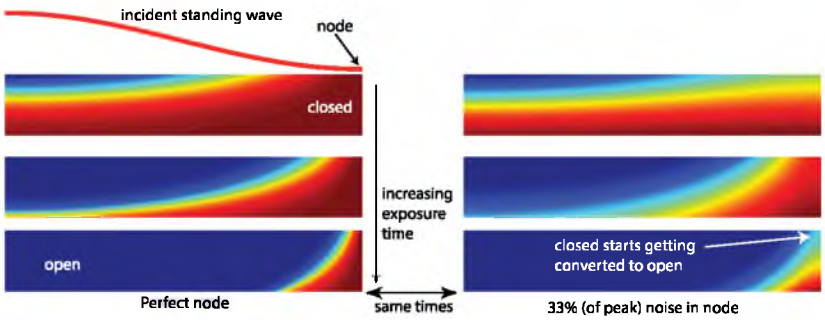

FIG. 5. Simulation of BTE isomer distribution after exposure for a standing wave with a perfect node (on the left) and for the same standing wave with a node containing noise intensity of about 33% of the peak intensity.

a simple model that simulates the steps and discussed the impact of the key parameters, particularly the quality of the node.

P.C. acknowledges the NSF GRFP under Grant No. 0750758. P.C. acknowledges the University of Utah Nanotechnology Training Fellowship. R.M. acknowledges a NSF CAREER Award No. 1054899 and funding from the USTAR Initiative. The authors thank H.I. Smith, C. Bertarelli and R. Castagna for fruitful discussion.

[1]N. Brimhall, T. L. Andrew, R. V. Manthena, and R. Menon, Phys. Rev. Lett. **107**, 205501 (2011).
[2]S. W. Hell, Science **316**, 1153 (2007).
[3]A. Peters and N. R. Branda, Chem. Commun. **8**, 954–955 (2003).
[4]P. Cantu, T. L. Andrew, R. Castagna, C. Bertarelli, and R. Menon, Appl. Phys. Lett. **100**, 183103 (2012).
[5]P. Cantu, T. L. Andrew, and R. Menon, Appl. Phys. Lett. **103**, 173112 (2013).
[6]T. L. Andrew, H. Y. Tsai, and R. Menon, Science **324**(5929), 917–921 (2009).

CHAPTER 9

PATTERNING VIA OPTICAL SATURABLE TRANSITIONS – FABRICATION AND CHARACTERIZATION

Reprinted with permission from: P. Cantu, T.L. Andrew, and R. Menon. "Patterning via Optical Saturable Transitions - Fabrication and Characterization." *Journal of Visualized Experiments*, vol. 94, e52449, 2014.

jove Journal of Visualized Experiments www.jove.com

Video Article

Patterning via Optical Saturable Transitions - Fabrication and Characterization

Precious Cantu[1], Trisha L. Andrew[2], Rajesh Menon[1]

[1]Department of Electrical and Computer Engineering, The University of Utah

[2]Department of Chemistry, The University of Wisconsin-Madison

Correspondence to: Precious Cantu at cantu@eng.utah.edu

URL: http://www.jove.com/video/52449
DOI: doi:10.3791/52449

Keywords: Physics, Issue 94, Optics, nanomaterials, fabrication, nanolithography, optical nanolithography, sub-wavelength diffraction

Date Published: 12/11/2014

Citation: Cantu, P., Andrew, T.L., Menon, R. Patterning via Optical Saturable Transitions - Fabrication and Characterization. *J. Vis. Exp.* (94), e52449, doi:10.3791/52449 (2014).

Abstract

This protocol describes the fabrication and characterization of nanostructures using a novel nanolithographic technique called Patterning via Optical Saturable Transitions (POST). In this technique the chemical properties of organic photochromic molecules that undergo single-photon reactions are exploited, enabling rapid top-down nanopatterning over large areas at low light intensities, thereby, allowing for the circumvention of the far-field diffraction barrier.[4] Simple, cost-effective, high throughput and resolution alternatives to nanopatterning are being explored, such as, two-photon polymerization[5,6], beam pen lithography (BPL)[7], scanning electron beam lithography (SEBL), and focused ion beam (FIB) patterning. However, multi-photon approaches require high light intensities, which limit their potential for high throughput and offer low image contrast. Although, electron and ion beam lithographic processes offer increased resolution, the serial nature of the process is limited to slow writing speeds, which also prevents patterning of features over large areas. Beam-pen lithography is an approach towards parallel near-field optical lithography. However, the gap between the source of the beam and the surface of the photoresist needs to be controlled extremely precisely for good pattern uniformity and this is very challenging to accomplish for large arrays of beams. Patterning via Optical Saturable Transitions (POST) is an alternative optical nanopatterning technique for patterning sub-wavelength features[1-3]. Since this technique uses single photons instead of electrons, it is extremely fast and does not require high light intensities[1-3], opening the door to massive parallelization.

Video Link

The video component of this article can be found at http://www.jove.com/video/52449/

Introduction

Optical lithography is of key importance in the fabrication of nanoscale structures and devices. Increased advancements in novel lithography techniques has the ability to enable new generations of novel devices.[8-11] In this article, a review is presented of a class of optical lithographic techniques that achieve deep sub-wavelength resolution using novel photoswitchable molecules. This approach is called Patterning via Optical-Saturable Transitions (POST).[1-3]

POST is a novel nanofabrication technique that uniquely combines the ideas of saturating optical transitions of photochromic molecules, specifically (1,2-bis(5,5'-dimethyl-2,2'-bithiophen-yl))perfluorocyclopent-1-ene. Colloquially, this compound is referred to as BTE, **Figure 1**, such as those used in stimulated emission-depletion (STED) microscopy[12], with interference lithography, which makes it a powerful tool for large-area parallel nanopatterning of deep subwavelength features onto a variety of surfaces with potential extension to 2- and 3-dimensions.

The photochromic layer is originally in one homogeneous state. When this layer is exposed to a uniform illumination of λ_1, it converts into the second isomeric state (**1c**), **Figure 2**. Then the sample is exposed to a focused node at λ_2, which converts the sample into the first isomeric state (**1o**) everywhere except in the near vicinity of the node. By controlling the exposure dose, the size of the unconverted region may be made arbitrarily small. A subsequent fixing step of one of the isomers may be selectively and irreversibly converted (locked) into a 3rd state (in black) to lock the pattern. Next, the layer is exposed uniformly to λ_1, which converts everything except the locked region back to the original state. The sequence of steps may be repeated with a displacement of the sample relative to the optics, resulting in two locked regions whose spacing is smaller than the far-field diffraction limit. Therefore, any arbitrary geometry may be patterned in a "dot-matrix" fashion.[1-3]

Protocol

NOTE: perform all the following steps under cleanroom class 100 conditions or better.

1. Sample Preparation

1. Clean a 2" diameter silicon wafer with Buffered Oxide Etch (BOE) solution (6 parts 40% NH_4F and 1 part 49% HF) for 2 min (**Caution: Hazardous chemicals**). Choose this etch time to remove any organics or contaminants on the surface. Rinse with deionized (DI) water for approximately 5 min. Dry wafer with dry N_2.
   NOTE: Never work alone when using HF. Always wears eye protection with face shield and personal protective equipment (PPE) in case of spills. Post guidelines for the use and handling of HF waste in the lab where the etching is performed.
   NOTE: Steps 1.2 to 1.7 are for electrochemical *locking* only. If performing locking via dissolution proceed to Step 2.
2. To lay down the working electrode, sputter 100 nm of Platinum (Pt) onto the clean 2" diameter silicon wafer.
3. Before etching the platinum thin film, clean the RIE chamber of any impurities or leftover photoresist from previous dry etches.
4. Pump down the chamber until a base pressure of 1×10^{-5} Torr is achieved. Make sure that the RF power is set to 200 W and the flow rates for the oxygen and argon are set to 50 sccm and 10 sccm respectively. Ignite the Ar/O_2 plasma and run for at least 1 hr.
5. Turn off the Ar/O_2 plasma and allow the chamber vent for approximately 10 min.
6. To etch the platinum thin film surface, load the sample into the RIE chamber and pump the chamber down to a base pressure of 1×10^{-5} Torr. This time set the argon flow rate to 0 sccm. Ignite the O_2 plasma and let this process run for 30 min.
7. Turn off the O_2 plasma and let the chamber vent for 10 min.

2. Thermal Evaporation of Photochromic Molecule Using Custom Low Temperature Evaporator (LTE)

1. Fill AlO_2 boat with 30 mg of BTE and load into custom LTE source (**Figure 6**).
2. Load silicon wafer into sample mount.
3. Seal chamber ports and pump chamber down to a base pressure of 1×10^{-6} Torr.
4. Evaporate the BTE at a setpoint temperature of 100 °C, with a film thickness of 30 nm.
5. Immediately after evaporation, flood illuminate the sample to 5 min of UV to transform the BTE material to the closed form, **1c**.
6. In order to define the sample size, cleave a small piece of the wafer using a diamond scribe to scratch a line from the edge of the silicon surface. Grab the wafer on both sides of the scratch line and bend the wafer downwards until it breaks along the crystal plane.
7. Perform profilometer measurements to validate BTE thin film thickness. To do this, scratch the sample using a fine edge tweezers. Measure the step height from this scratch, which is the difference in height between the right and left cursor position.
   NOTE: Inaccuracies in film thickness will result in discrepancies in exposure dose.
8. Store remaining sample in N_2 filled glovebox.

3. Exposures

NOTE: Perform all exposures under inert atmosphere conditions to prevent degradation of sample.

1. Cleave the sample by following the same procedure as outlined in step 2.6.
2. Load sample in inert atmosphere sample holder.
3. Mount inert sample holder on stage. Purge sample with N_2.
4. Expose the sample to the desired exposure time using an interferometer, such as the one shown in **Figure 8**.

4. Electrochemical Oxidation Using Three Electrode Cell

NOTE: Perform electrochemistry under inert atmosphere conditions to prevent degradation of sample.

1. Clamp a clean glass vial on top of the hot plate. Place a clean stirring bar in the vial. Turn on the stirrer.
2. Clean a new copper clip with methanol. Clean the platinum counter electrode with methanol.
3. Using a clean copper clip, clip the sample through one of the holes in the Teflon vial cap. Make sure to clip onto the exposed platinum only.
4. Place the Teflon vial cap onto the vial. Clip the red lead onto the platinum counter electrode and the black lead onto the copper clip holding the sample.
5. Using a clean syringe, fill the vial with filtered deionized (DI) water through the second hole in the Teflon vial cap. Fill as high without immersing any of the bare platinum on the sample.
6. Bubble nitrogen through the water for 3-5 min. Turn off the nitrogen.
7. Place the reference electrode in the second hole in the Teflon vial cap. Clip the white lead onto the reference electrode. Check to make sure none of the bare platinum on the sample is immersed.
8. Using a voltammograph, set the oxidation voltage to 0.5 V/sec.
9. After the desired oxidation time has elapsed, turn the power to the voltammograph off.
10. Remove the red, black, and white clips from the platinum counter electrode, copper clip, and reference electrode.
11. Expose the sample to UV for 5 min.

5. Sample Development — Electrochemical *Locking*

NOTE: Perform development under inert atmosphere conditions to prevent degradation of sample.

1. Develop the sample in filtered 5 (wt%) isopropanol, 95 (wt%) ethylene glycol for the desired amount of time. Note: Typically 50 nm samples are developed for 30-60 sec while 80 nm samples are developed for 60-180 sec.

2. Dry sample with dry N_2.
3. Immediately expose sample to 5 min of UV.

6. Sample Development — Dissolution *Locking*

NOTE: Perform development under inert atmosphere conditions to prevent degradation of sample.

1. Using 100 ml of ethylene glycol in a clean glass beaker, develop the exposed sample for the desired development time.
2. Dry sample with dry N_2. Immediately expose sample to 5 min of UV.

7. Multiple Exposures

1. If performing multiple exposures repeat steps 3-6 with a translation of the sample relative to the optics.

Representative Results

Fabricated samples:

Different oxidation times were characterized as illustrated by the atomic-force micrographs in **Figure 3** at an oxidation voltage of 0.85 V determined from cyclic voltammetry. The 50 nm-thick films were exposed to a standing wave at λ = 647 nm of period 400 nm for 60 sec at a power density of 0.95 mW/cm^2. As the oxidation time is increased from 10 min to 25 min, one can clearly see a loss of contrast as some of the regions comprised of **1o** get oxidized as well. The developer (5 (wt%) isopropanol: 95 (wt%) ethylene glycol) dissolves all oxidized portions. Larger oxidation times result in uneven line and increased surface non-uniformities after development. Therefore, a careful choice of the oxidation conditions is critical to patterning high-quality nanostructures.[2]

The higher dipole moment of the closed form of the molecule, **1c**, as compared to the open form, **1o**, allows for the closed form to be more soluble in polar solvents. This is represented in **Figure 4**, where half of the sample was converted to the closed form, **1c**, and the other half was converted to the open form, **1o**. The sample was then developed in 100 (wt%) ethylene glycol for several different development times and then the thickness of the film remaining was measured using a profilometer. From this graph the high selectivity of the dissolution *locking* step is seen. To remove the residual layer of the closed form, 1c, a reactive ion etching (RIE) process as used in nanoimprint lithography could be used.[13]

Since the photochromic film can readily recover to its original state upon exposure to UV, it is straightforward to extend the idea to multiple exposures. This is, of course, required for creating dense patterns. Here, the feasibility of this approach is shown by performing two exposures of the same standing wave, but with a ~45° rotation in between (**Figure 5**). Each exposure was conducted on the Lloyd's-mirror interferometer, with a standing wave of period, 540 nm at λ = 647 nm (incident intensity ~2.1 mW/cm^2) for 1 min. After the first exposure, the sample was immersed in 100 (wt%) ethylene glycol for 30 min and exposed to short-wavelength UV lamp for 5 min to convert the molecules to the original closed-ring isomer **1c**. The sample was then rotated approximately 45° relative to the optics, and a second exposure to the standing wave was performed. Again, the sample was immersed in 100 (wt%) ethylene glycol for 30 min. After each development, the sample was rinsed in deionized water and dried with N_2. The corresponding atomic-force micrograph resolves lines with spacing as small as ~260 nm or λ/2.5, which is less than half of the period of the standing wave.[3]

To verify the efficacy of the sample holder, several exposures were performed to see if the line edge roughness had improved. Assuming an incident sinusoidal illumination, the resulting feature size can be readily simulated. In **Figure 7**, this feature size is plotted as a function of the exposure time using the solid blue line. The experimentally measured values are shown using crosses. Using the exposure threshold as the only fitting parameter, it is shown that this simple model can accurately explain our experimental results. The smallest experimentally obtained feature size was ~85 nm, corresponding to a linewidth of ~λ/7.4. More precise control of the exposure time should enable even smaller features. Note that as the exposure time is increased, the simulation indicates that feature size should be reduced significantly below the far-field diffraction limit. From the scanning electron microscope (SEM) images, it is shown that the line-edge roughness has improved with the use of the inert atmosphere sample holder.

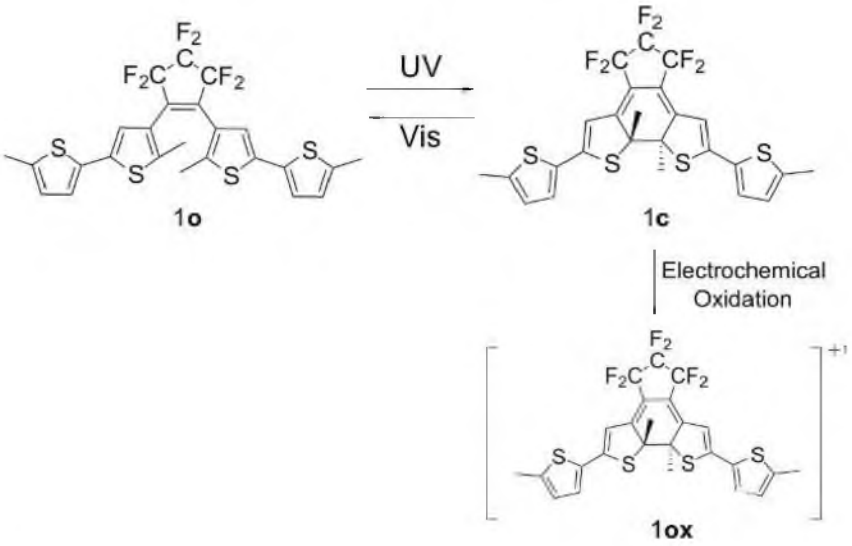

Figure 1. Organic photochromic molecule structure. Compound **1** exists in open form, **1o** and the closed form, **1c**. Electrochemical oxidation selectively converts **1c** to **1ox**.

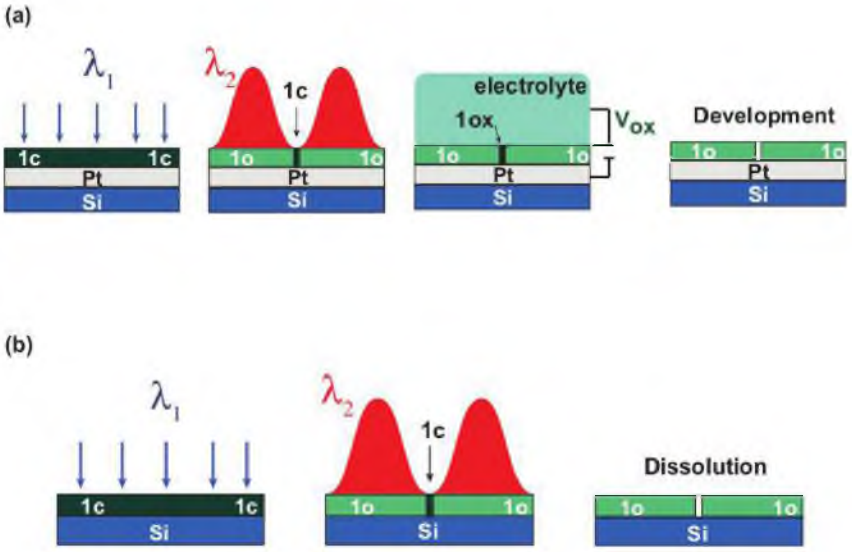

Figure 2. POST technique. Exposure and patterning "locking" steps required for recording feature. (**A**) Electrochemical oxidation. (**B**) Dissolution of one photoisomer.

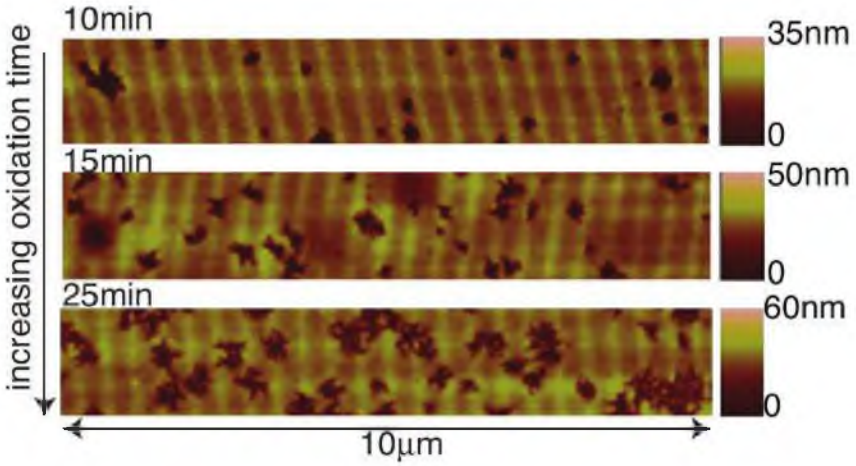

Figure 3. Isolated features. Atomic force micrographs of lines after development for samples at various oxidation times.[2] Thin-film thickness of ~50 nm. Reprinted with permission from [Cantu, P., *et al.* Subwavelength nanopatterning of photochromic diarylethene films. *App. Phys. Lett.* **100**(18), 183103]. Copyright [2012], AIP Publishing LLC. Please click here to view a larger version of this figure.

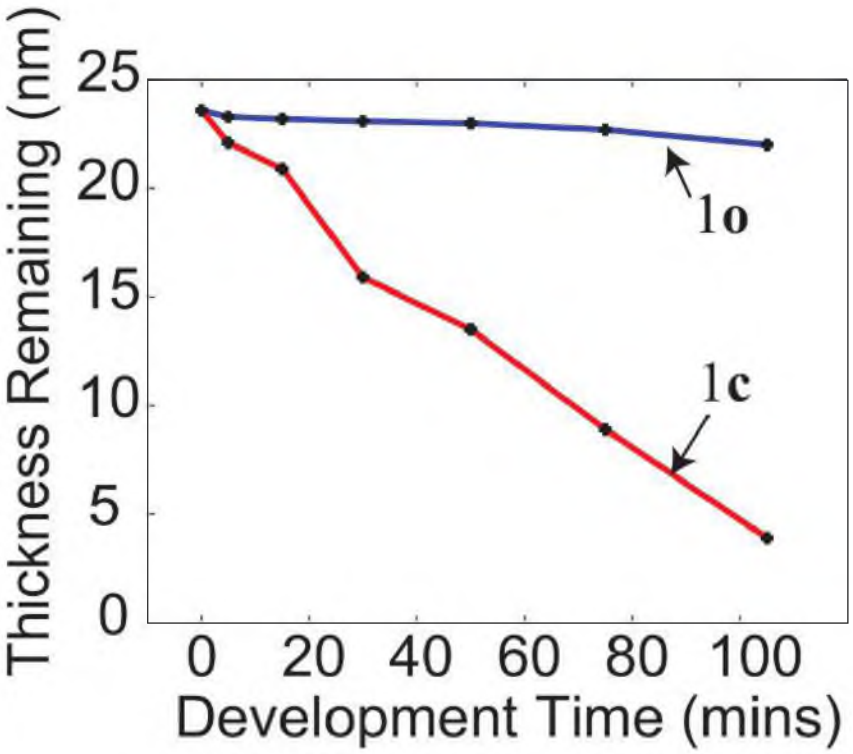

Figure 4. Dissolution rate. This figure shows the Macro-scale solubility of **1c** and **1o** in 100 (wt%) Ethylene glycol.[3] Thin-film thickness of ~29 nm. Reprinted with permission from [Cantu, P., *et al.* Nanopatterning of diarylethene films via selective dissolution of one photoisomer. *App. Phys. Lett.* **103**(17) 173112]. Copyright [2013], AIP Publishing LLC.

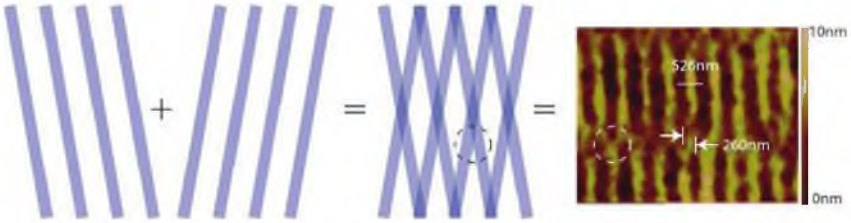

Figure 5. Experimental demonstration of a double-exposure. Left: Schematic showing orientation of sample for double-exposure using POST. **Right:** Atomic force micrograph of the resulting pattern. The atomic force micrograph reveals the smallest spacing between the features as ~260nm, which is approximately half the period of the illuminating standing wave.[3] Reprinted with permission from [Cantu, P., *et al.* Nanopatterning of diarylethene films via selective dissolution of one photoisomer. *App. Phys. Lett.* **103**(17) 173112]. Copyright [2013], AIP Publishing LLC. Please click here to view a larger version of this figure.

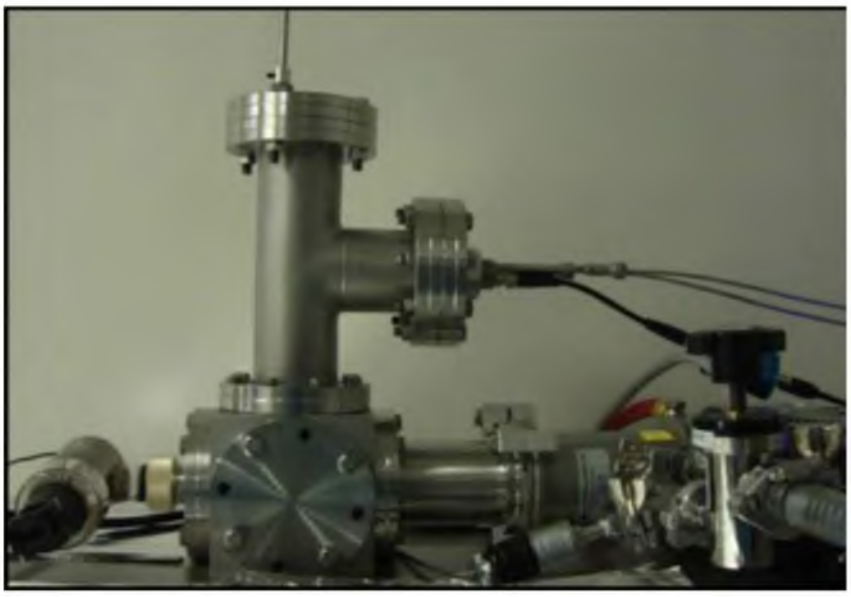

Figure 6. Custom evaporator. Image of the low temperature thermal evaporator (LTE) used in the POST technique.[2] Reprinted with permission from [Cantu, P., *et al.* Subwavelength nanopatterning of photochromic diarylethene films. *App. Phys. Lett.* **100**(18), 183103]. Copyright [2012], AIP Publishing LLC.

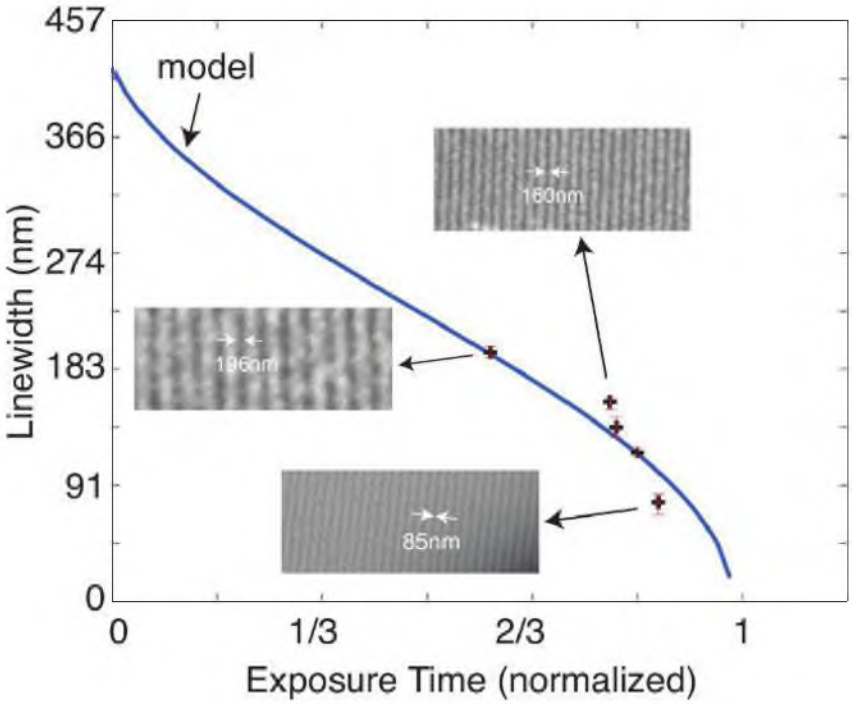

Figure 7. Linewidth vs exposure time for a single development and exposure. The incident simulated sinusoidal illumination is shown as a solid blue line, while the experimental data is shown using crosses. A sinusoidal illumination with period of 457 nm was assumed. Inset: SEM images. Please click here to view a larger version of this figure.

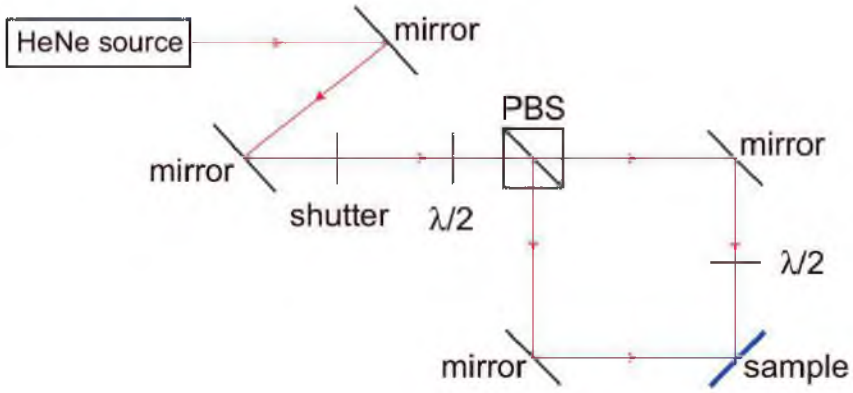

Figure 8. Schematic of the Mach-Zehnder interferometry setup used for exposures. The first half-wave plate is used to control the power in each arm. The second half-wave plate is used to control the polarization.

Discussion

The fabrication, experimental setup and related operational procedures of Patterning via Optical Saturable Transitions (POST) have been described. By exploiting the linear switching properties of thermally stable photochromic molecules, POST offers new perspectives on circumventing the far-field diffraction limit.[1-4]

Previously long-term storage requirement of the samples was solved by storing the samples under N_2, directly after the initial evaporation.[2] However, the significant line-edge roughness evident in the gratings, **Figures 3** and **5**, is likely due to the formation of oxidized products of **1c** in the presence of air.[2] Improving the uniformity of the patterns requires that the exposure and development process be conducted under an inert

atmosphere. To address the exposures done in ambient conditions, a custom inert atmosphere sample holder was designed and fabricated. The sample holder needed to provide a rigorous inert gas blanketing of the air-sensitive BTE in closed form, **1c** and maintain an excellent seal for sufficient time to obtain the appropriate exposure conditions. The holder was configured so that it could be easily modified for various optical configurations.

One way to address the exposure of the sample to atmosphere would be to design and fabricate an *in-situ* setup. The main goal of *in-situ* experimentation in both the electrochemical and dissolution method is performing the exposure, electrochemical oxidation, and development in an O_2 purged environment. Having the experiments performed *in-situ* would aid in the yield and quality of the desired nanostructures.

Currently the extension of this super-resolution technique, POST, to 3-dimensions, which would provide a promising approach to nanofabrication of nanoporous scaffolds, which act as supports for the initial cell attachment and subsequent tissue formation in biological tissue engineering (TE) is being investigated. The nanolithographic technique used to fabricate these initial scaffolds must produce a high yield and be at a low cost in order to produce any significant impact.[14]

There are, however, some limitations to the POST technique. The need for a separate locking mechanism (electrochemical or dissolution) requires an immersion-type setup. This could add associated complexities and cost if performed *in-situ*. Also, the need for a platinum layer for the electrochemical locking step (see **Step 1.2**) might preclude some already patterned substrates or devices. The organic compound (BTE), which is used as the recording medium, requires a relatively complex synthesis, which may add to the cost of the technique initially. However, with increased volumes, the cost should decrease.

Disclosures

The authors have nothing to disclose.

Acknowledgements

Thanks to Michael Knutson, Paul Hamric, Greg Scott, and Chris Landes for helpful discussions and assistance related to the custom inert atmosphere sample holder and assistance in the University of Utah student machine shop. P.C. acknowledges the NSF GRFP under Grant No. 0750758. P.C. acknowledges the University of Utah Nanotechnology Training Fellowship. R.M. acknowledges a NSF CAREER Award No. 1054899 and funding from the USTAR Initiative.

References

1. Brimhall, N., Andrew, T.L., Manthena, R.V., Menon, R., Breaking the far-field diffraction limit in optical nanopatterning via repeated photochemical and electrochemical transitions in photochromic molecules. *Physical Review Letters.* **107** (20), 205501, doi:10.1103/PhysRevLett.107.205501 (2011).
2. Cantu, P., *et al.* Subwavelength nanopatterning of photochromic diaryethene films. *Applied Physics Letters.* **100** (18), 183103, doi:10.1063/1.4710547 (2012).
3. Cantu, P., Andrew, T.L., Menon, R., Nanopatterning of diarylethene films via selective dissolution of one photoisomer. *Applied Physics Letters.* **103** (17), 173112, doi:10.1063/1.4826925 (2013).
4. Abbe, E., Beitrage zur Theorie des Mikroskops und der mikroskopischen Wahrnehmung. *Archiv fur mikroskopische Anatomie.* **9** (1), 413-418, doi:10.1007/BF02956173 (1873).
5. Li, L., *et al.* Achieving λ/20 resolution by one-color initiation and deactivation of polymerization. *Science.* **324** (5929), 910-913, doi:10.1126/science.1168996 (2009).
6. Fischer, J., Freymann, G. von, and Wegener, M., The materials challenge in diffraction-unlimited direct-laser-writing optical lithography. *Advanced Materials.* **22**(32), 3578-3582, doi: 10.1002/adma.201000892 (2010).
7. Mirkin, C. A., *et al.* Beam pen lithography. *Nature Nanotechnology.* **5**, 637-640, doi:10.1038/nnano.2010.161 (2010).
8. Xie, X., *et al.* Manipulating spatial light fields for micro- and nano-photonics. *Physica E: Low-dimensional Systems and Nanostructures.* **44**, 1109–1126, doi:10.1016/j.physe.2011.12.020 (2012).
9. Leroy, J., *et al.* High-speed metal-insulator transition in vanadium dioxide films induced by an electrical pulsed voltage over nano-gap electrodes. *Applied Physics Letters.* **100**(21), 213507, doi:10.1063/1.4721520 (2012).
10. Carr, D., Sekaric, L. and Craighead, H. Measurement of nanomechanical resonant structures in single-crystal silicon. *Journal of Vacuum Science & Technology B.* **16**(6), 3821–3824, doi:10.1116/1.590416 (1998).
11. Wilhelmi, O., *et al.* Rapid prototyping of nanostructured materials with a focused ion beam. *Japanese Journal of Applied Physics.* **47**(6), 5010–5014, doi:10.1143/JJAP.47.5010 (2008).
12. Hell, S.W., Far-field optical nanoscopy. *Science.* **316** (5828), 1153-1158, doi:10.1126/science.1137395 (2007).
13. Chou, S.Y., Krauss, P.R., and Renstrom, P.J., Nanoimprint lithography. *Journal of Vacuum Science & Technology B.* **14**, 4129, doi:/10.1116/1.588605 (1996).
14. Guillemette, M.D., *et al.* Surface topography induces 3D self-orientation of cells and extracellular matrix resulting in improved tissue function. *Integrative Biology.* **1** (2), 196-204, doi: 10.1039/b820208g (2009).

jove Journal of Visualized Experiments www.jove.com

Materials List for:

Patterning via Optical Saturable Transitions — Fabrication and Characterization

Precious Cantu[1], Trisha L. Andrew[2], Rajesh Menon[1]

[1]Department of Electrical and Computer Engineering, The University of Utah

[2]Department of Chemistry, The University of Wisconsin-Madison

Correspondence to: Precious Cantu at cantu@eng.utah.edu

URL: http://www.jove.com/video/52449
DOI: doi:10.3791/52449

Materials

Name	Company	Catalog Number	Comments
Isopropanol	Fisher Scientific	P/7500/15	CAUTION: flammable, use good ventilation and avoid all ignition sources.
Buffered Oxide Etch			
Methanol	Ricca Chemical	48-293-2	CAUTION: flammable, use good ventilation and avoid all ignition sources.
Ethylene Glycol	Sigma-Aldrich	324558	CAUTION: Harmful if swallowed
Silicon wafer			
Diamond Scribe			
Glass Beakers			
Tweezers	Ted Pella	5226	
Reactive Ion Etching System	Oxford	Plasma Lab 80 Plus	
Inert Atmosphere Sample Holder	Proprietary In-house Designed		
Polarizing beamsplitter cube	Thorlabs	PBS052	
HeNe Laser	Melles Griot	25-LHP-171	CAUTION: Wear safety glasses
Half-wave plates	Thorlabs	WPH05M-633	
Thermal Evaporator	Proprietary In-house Designed		
TMV Super	TM Vacuum Products	TMV Super	
Voltammograph	Bioanalytical Systems	CV-37	
Shortwave UV lamp 365 nm	UVP Analytik Jena Company	UVGL-25	CAUTION: Wear UV safety glasses

CHAPTER 10

NANORESOLUTION VIA NANOTRANSLATION (NRNT)

10.1 Principle of NRNT

This chapter describes a method for creating and imaging nanoscale patterns using long-wavelength photons and systems that utilize this method. This is enabled by photoswitchable materials that can be toggled in a repeatable and robust fashion between two distinct states by exposure to two distinct wavelengths of light (or other external stimuli). While stepping (or scanning) the sample in between exposures by exploiting the extreme precision that is now available in mechanical translation, one can design illumination patterns that *erase* previous exposures, thereby creating patterns that are far smaller than the diffraction. Such patterns may be *fixed* for patterning or imaged for microscopy as described here. Nowadays, once can displace a piezoelectric stage by a few nanometers with an absolute precision of a few picometers. Such a capability when combined with the photoswitchability of photochromic molecules allows one to potentially create sub-10nm nanostructures with just visible and near-UV light.

Optical imaging and patterning are limited by the far-field diffraction limit. This means that it is not possible to image patterns or create patterns that are spaced by a distance closer than $\sim\lambda/2$, where λ is the wavelength of the illumination. Significant effort is currently being made to overcome this limit via fluorescence switching for microscopy and by photoswitchable molecules for lithography. Here, we propose to extend these approaches with a simple modification, which considerably simplifies the entire process.

An example of the basic scheme of switching the recording material between 3 states, **A**, **B**, and **C**, is shown on the top in Figure 10.1. When material in form **A** absorbs a photon of wavelength λ_1, it turns into form **B**. When form **B** absorbs a photon of wavelength λ_2, it turns back to form **A**. Form **B** can be selectively converted in an irreversible manner

to form **C** via a *locking* step. This could be achieved in many ways including using a photochemical reaction, electrochemical oxidation, chemical oxidation, or simply dissolving it away or other means.

The sequence of steps that allows for sub-diffraction-limited patterning is shown in the bottom of Figure 10.1. In this example, we begin in step 1 with a substrate (not shown) that is coated with the material all in form **B**. In step 2, this is exposed to a standing wave at λ_2, which results in interspersed regions of **B** and **A** as shown. Note that the particular shape of the illuminating wave can be substantially different as long it results in some interspersed pattern of **A** within **B**. Also, we have only shown a 1D representation of the process. Later, we will show examples of the 2D and 3D processes as well. In step 3, the substrate is moved relative to the illumination by δ_1 and the exposure is repeated. The second illumination is shown to be the same as in step 2, but it can be substantially different. The objective is to result in sub–diffraction-limited regions of **B** interspersed in **A** as shown. The width of the **B** region is approximately given by P/2 δ_1 in this example, where P is the period of the standing wave. In step 4, the *locking* mechanism is invoked to convert all **B** regions to **C**. In step 5, a uniform exposure to λ_1 converts all material (except those that are locked into **C**) back into form **B**. In step 6, the sample is displaced relative to the illumination so as to convert regions surrounding **C** into **A**. In step 7, the sample is displaced relative to the illumination by δ_2 as shown and the exposure is repeated. Note that this results in a small region of **B** that is placed next to the first **C** region with a spacing that is determined primarily by the difference between the displacements δ_1 and δ_2. Since mechanical displacement can be far more accurate and precise compared to the diffraction limit, sub-diffraction-limited patterning is achieved. In step 8, regions in **B** are locked to **C**. The steps 6-8 are repeated until the desired pattern geometry is achieved. Note that by changing the relative displacement, it is possible to change the spacing between each **C** region in an arbitrary manner. Furthermore, although we have shown a periodic pattern in our example, it is obvious that any pattern (nonperiodic or periodic) could be used as long as we can create a pattern of **A** and **B** regions. As a last step, the regions in **C** could be dissolved away to result in topographical patterns. It is also possible to dissolve away regions of **A** or **B** while allowing **C** to remain (not shown in our example).

Figure 10.2 shows the details of the steps 2 and 3. The sample is displaced relative to the illumination by a distance, D. Then, the second exposure converts much of the **B** to **A** except at the right edge (in this example). By making D close to P/2, substantially narrow regions of **B** can be formed. We assumed a simple threshold model for exposure

in this example. This means that those regions that receive energy (dose) higher than the threshold are completely converted into the **A** form, while those regions that receive energy (dose) below this threshold remain in the original form (**A** or **B**). In practice, the threshold may not be so binary and a transition region that is a mixture of **A** and **B** will exist at the boundaries between the two regions. The normalized image slope at the pattern boundary will primarily determine this transition region. This is analogous to conventional optical lithography.

It is also possible to pattern patterns with many different linewidths in one exposure-displacement-exposure cycle as illustrated in Figure 10.3. In this example, we constrained the illumination to standing waves, which are relatively easy to generate. But any other waveform (or set of waveforms) periodic or not may also be used. In this example, we adjust the period and the relative phase shift between the two illuminations to result in a final pattern that has a combination of very narrow regions and wide regions. Any arbitrary pattern can be decomposed into sinusoids and techniques as proposed here can be applied. Note that the width of the smallest region is still determined primarily by the relative displacement between the exposures.

The idea of using standing waves of various periods to create complex geometries is explored further in Figure 10.4. Here, we have not used the displacement. Just changing the period as shown could also result in sub–diffraction-limited patterns. Note that in some cases, it might be easier to change the period rather than move the substrate relative to the illumination.

Figure 10.5 shows the proposed method in 2-dimensions (2D). In this specific example, we start with a simple checkerboard pattern of **A** and **B**. This can be achieved by exposing the material to λ_2 illumination that has a checkerboard intensity distribution. In the next step, the substrate is displaced relative to the illumination in the X-direction (horizontal) by Dx. This results in narrow strips whose width in the X-direction is Px/2 – Dx, where Px is the period of the checkerboard in the X-direction. Next, the sample is displaced relative to the illumination in the Y or vertical direction by Dy. This exposure results in narrow points of **B**, whose size is approximately given by (Px/2-Dx) X (Py/2-Dy). Note that in this example, the points are arranged in a hexagonal lattice.

Following the sequence of exposures illustrated in Figure 10.5, the hexagonal lattice of points in **B** form can be locked into the **C** form as shown in Figure 10.6. This is followed by a reset exposure that creates a region of **B** surrounding the previously locked **C** regions. The edges (in this example, the bottom and right edges) of the **B** regions must be chosen

carefully as they define the locations of the next exposure points.

One of the key challenges in patterning with a node as is done in this approach is that the quality of the pattern is intimately linked to the darkness of the node. If there is noise in the node, then the image contrast suffers. This effect is illustrated in Figure 10.7 (a). As exposure time is increased, the region that is supposed to receive no exposure (corresponding to the node of the incident standing wave) actually receives some noise photons. This converts the material from **B** to **A**, creating a low-contrast image. If the exposure is performed long enough, it is possible to completely eliminate the chemical image as illustrated. One approach to mitigating this problem is to place the material on the surface of a transparent substrate (such as a quartz or glass slide). Then, if the exposures are conducted through the opposite side, even a low-contrast image may be developed to result in narrow topography, as illustrated in Figure 10.7 (b).

This problem of low contrast may be solved in a different manner as well. We can take a low-contrast image from Figure 10.7 (a) and expose it to a uniform beam at λ_1 for a short time such that one converts a very thin layer at the top surface to **B** as shown in Figure 10.8 (b). By following this exposure with an exposure to λ_2, it is possible to increase the contrast of the final chemical image. The same result may also be achieved by exposing both wavelengths simultaneously to the material as shown in Figures 10.8 (b) and (c). In Figure 10.8 (c), λ_1 is exposed as a standing wave whose phase is π shifted to that of λ_2. The principles in Figures 10.7 and 10.8 can be applied to all the above methods including those illustrated in Figures 10.1-10.6, where we introduce either a sequential exposure of λ_1 followed by λ_2 or simultaneously use both wavelengths.

10.2 Systems for Implementing this Approach

Many different optical systems may be utilized to implement the proposed method. In one-dimension, many of the conventional interferometers will work well. Figure 10.9 illustrates several possible options. In all cases, we need to utilize two wavelengths either sequentially or simultaneously. Figure 10.9 (a) shows a simple Mach-Zehnder configuration. Figure 10.9 (b) shows a Lloyds-mirror interferometer and Figure 10.9 (c) shows the same interferometer for both beams. The sample is mounted on a stage so as to be able to generate dense and arbitrary 1D geometries. Simple 2D geometries may also be achieved by adding a rotational stage and/or a 2D (X-Y) stage. Figure 10.9 shows two possible optical systems that can implement the method in 2D. The basic idea is to use a spatial-light modulator (SLM) to create patterns within the λ_2 beam either in transmission (**a**) or in reflection (**b**).

When the patterns are required simultaneously as in Figure 10.8 (c), it is possible to use time–multiplexing and apply distinct patterns to the two beams (not shown). An imaging system (which could be a microscope objective, for instance) can focus all the patterns into a small region on the substrate as shown.

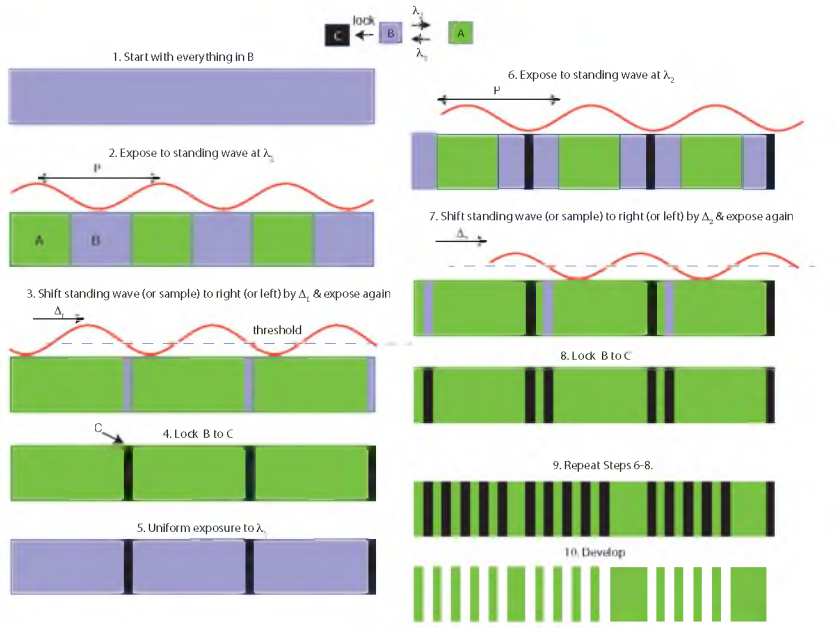

Figure 10.1: POST general process. Top: Scheme of reactions for proposed approach. Bottom: Sequence of steps that results in sub–diffraction-limited patterning.

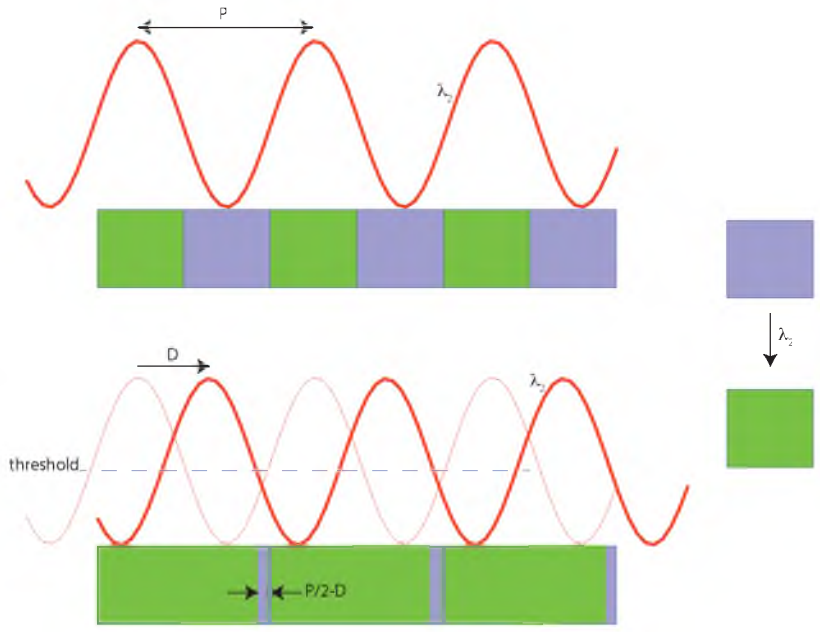

Figure 10.2: By shifting the standing wave, it is possible to reduce the size of the regions that are in **B** (violet) form. The original standing wave is shown by a lighter red curve in the bottom.

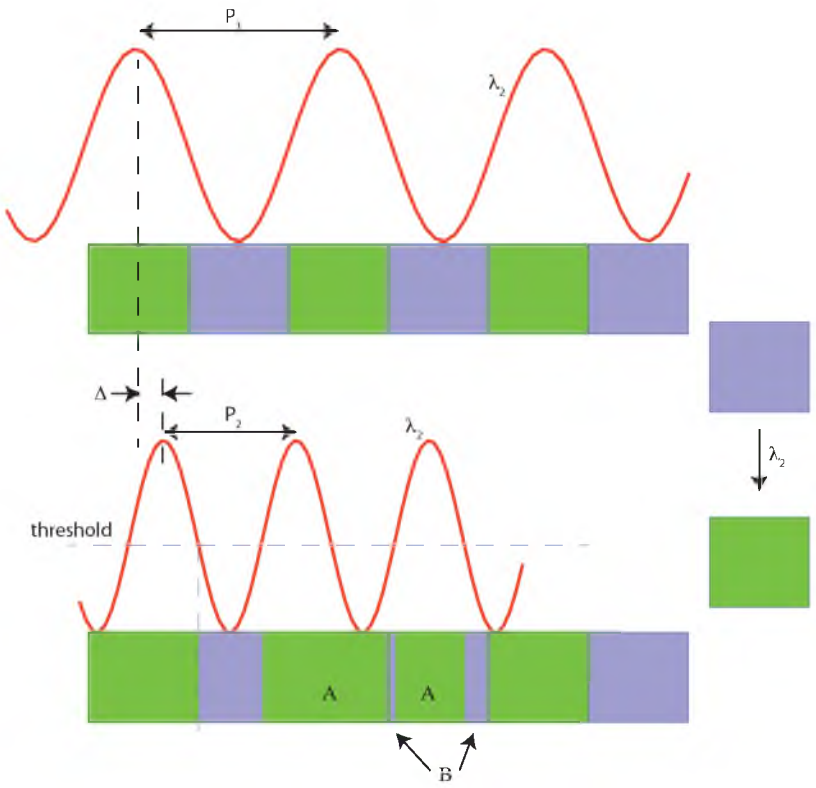

Figure 10.3: Creating patterns of various sizes.

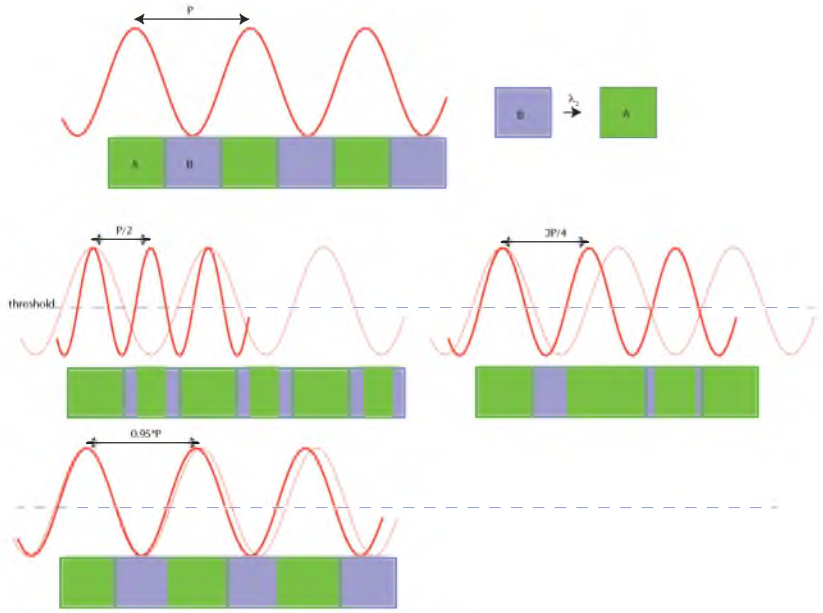

Figure 10.4: Varying the period of the standing wave without relative displacement can also result in sub-diffraction-limited features. In the bottom figures, the original standing wave is shown by a lighter red curve.

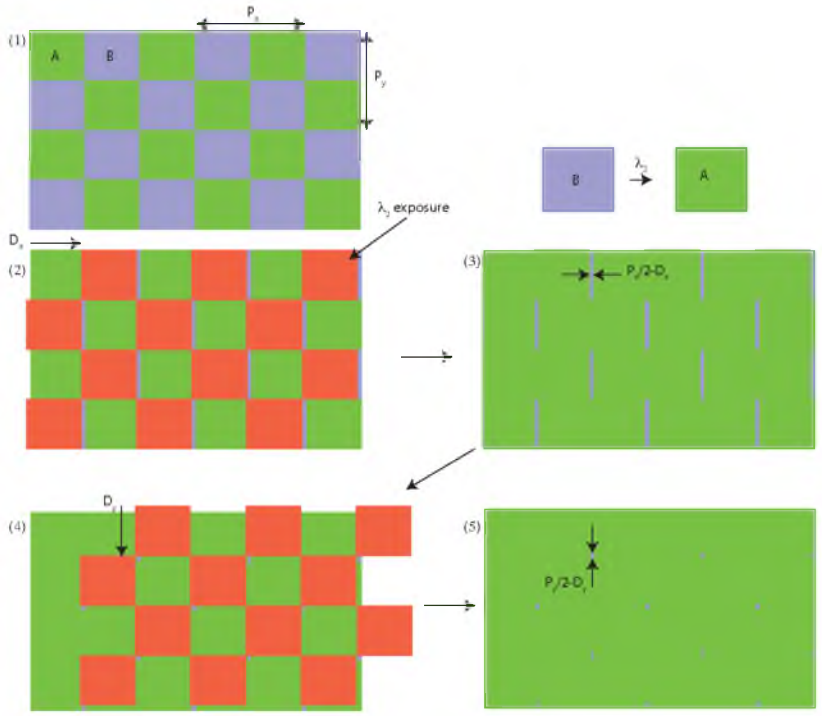

Figure 10.5: Patterning 2D geometries.

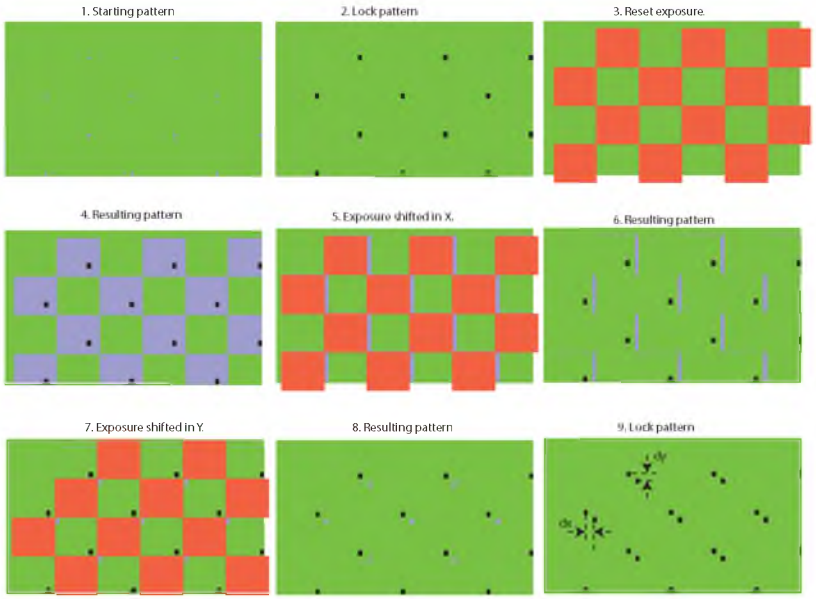

Figure 10.6: Patterning dense features in 2D.

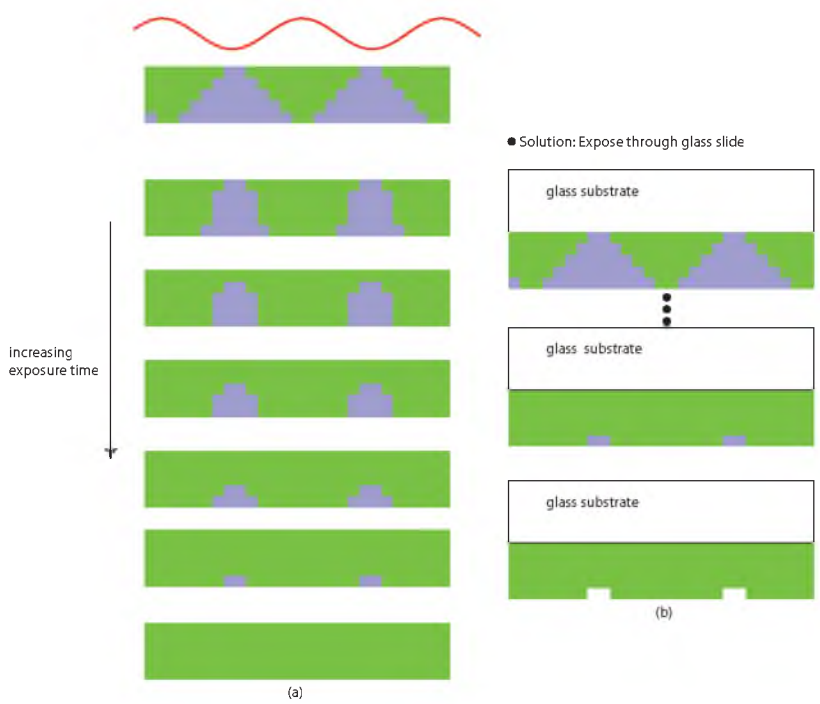

Figure 10.7: Noisy node. (a) If the standing wave quality is poor, image contrast may be deteriorated. (b) This problem may be solved by exposing through the back of a glass slide. In the bottommost panel, the sample is developed to showcase the narrow topography.

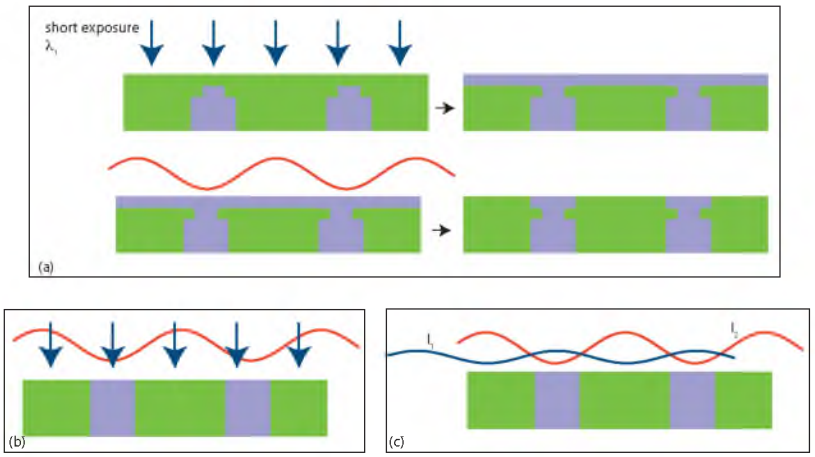

Figure 10.8: Low–contrast images. (a) By exposing the low-contrast image from Figure 10.7(a) to a uniform illumination at λ_1 for a relatively short period of time, it is possible to increase the image contrast as shown. (b) The same result can be achieve by exposing both wavelengths simultaneously. (c) The λ_1 illumination may also be a standing wave whose phase is π shifted with respect to the λ_2 standing wave. In cases (b) and (c), the intensities of λ_1 and λ_2 must be chosen carefully based on the quantum efficiencies of the respective transformations.

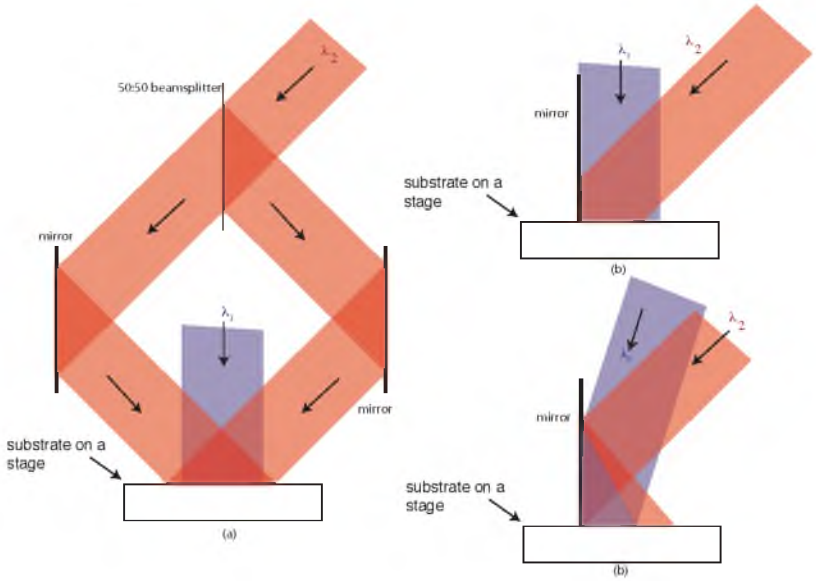

Figure 10.9: Possible optical systems that can implement the method in 1D.

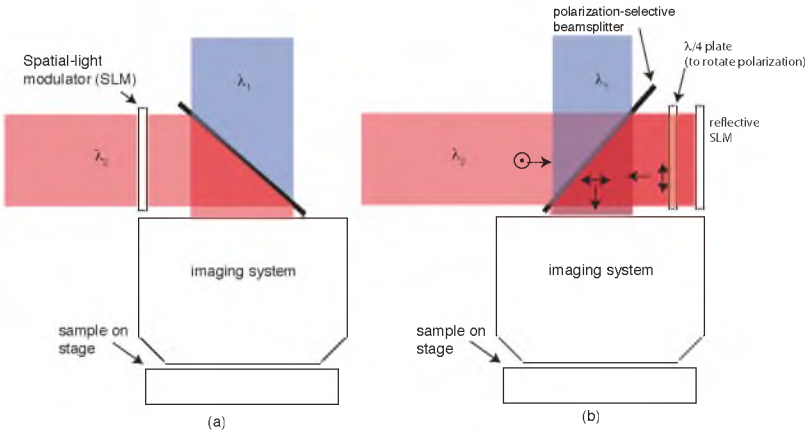

Figure 10.10: Possible optical systems that can implement the method in 2D.

10.3 References

[1] T. L. Andrew, H.-Y. Tsai, and R. Menon, "Confining light to deep subwavelength dimensions to enable optical nanopatterning," *Science*, vol. 324, no. 5929, pp. 917–921, 2009.

[2] N. Brimhall, T. L. Andrew, R. V. Manthena, and R. Menon, "Breaking the far-field diffraction limit in optical nanopatterning via repeated photochemical and electrochemical transitions in photochromic molecules," *Physical Review Letters*, vol. 107, p. 205501, Nov. 2011.

[3] US Patent 8 143 601, 2012.

[4] US Patent 7 989 151, 2011.

[5] US Patent 7 666 580, 2010.

[6] US Patent 7 667 819, 2010.

[7] US Patent 7 713 684, 2010.

[8] US Patent 7 714 988, 2010.

[9] US Patent 20 100 248 159, 2010.

APPENDIX A

LABVIEW®: OPTICAL SHUTTER AND TRANSLATION STAGE CONTROLLER CODE

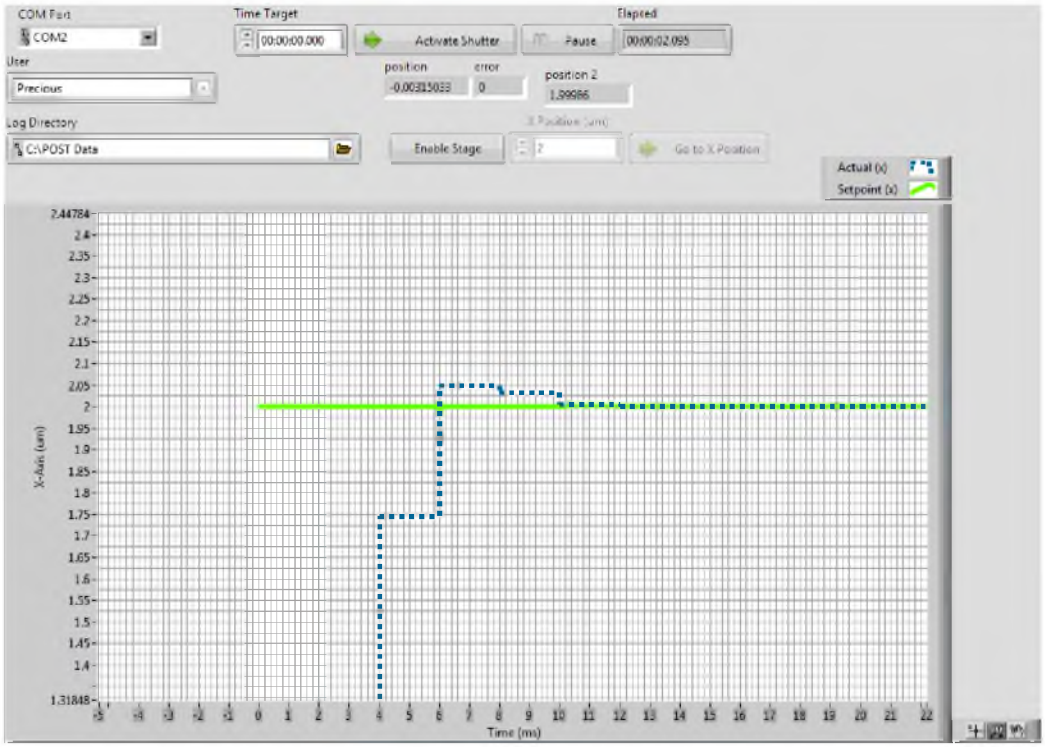

Figure A.1: Shutter and Stage controller user interface.

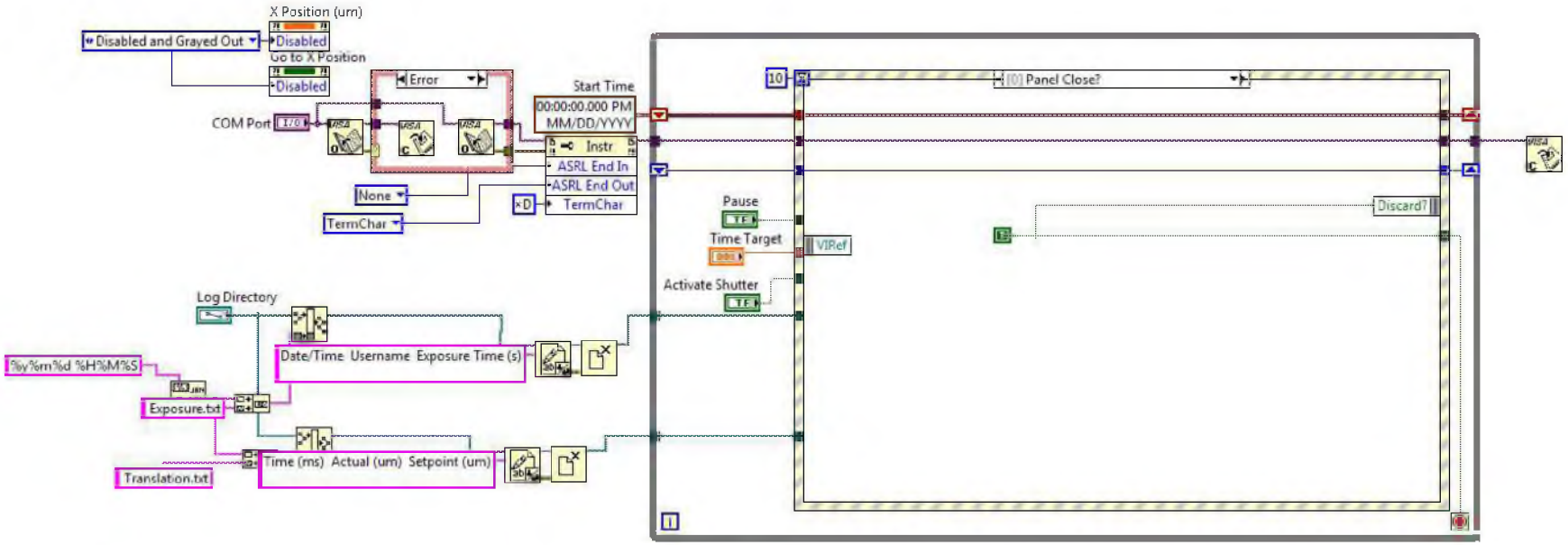

Figure A.2: Main shutter controller VI. This program is a large state machine.

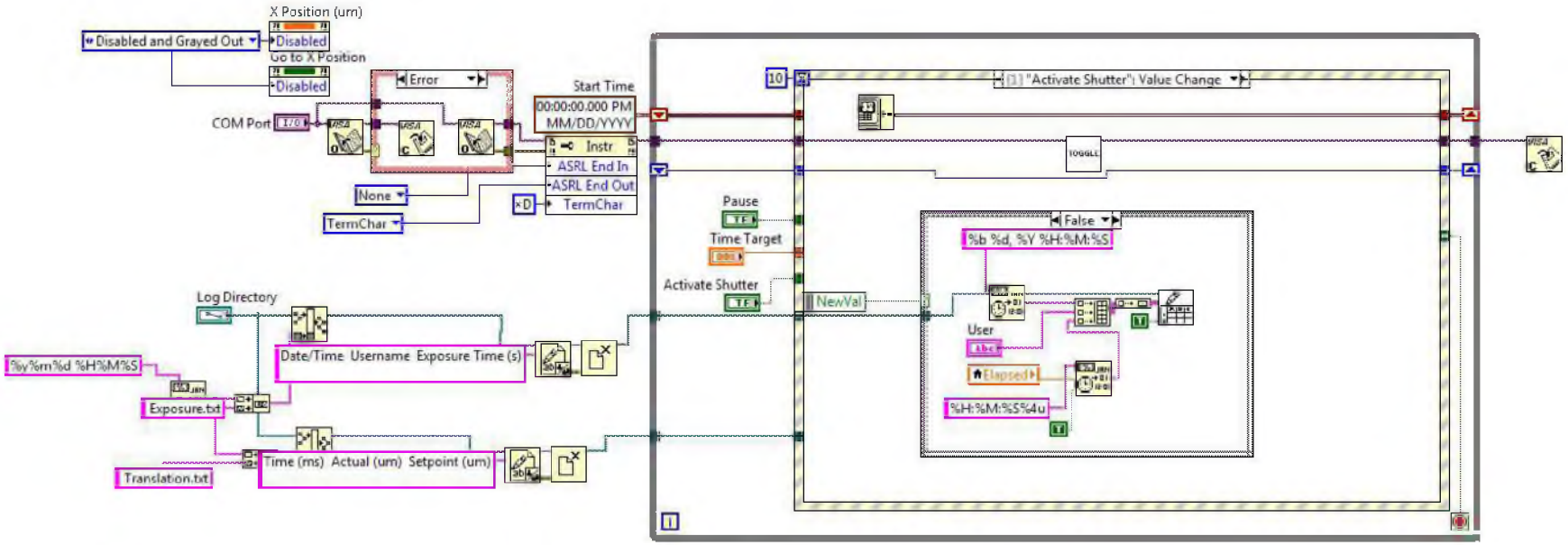

Figure A.3: Shutter controller VI to activate the shutter.

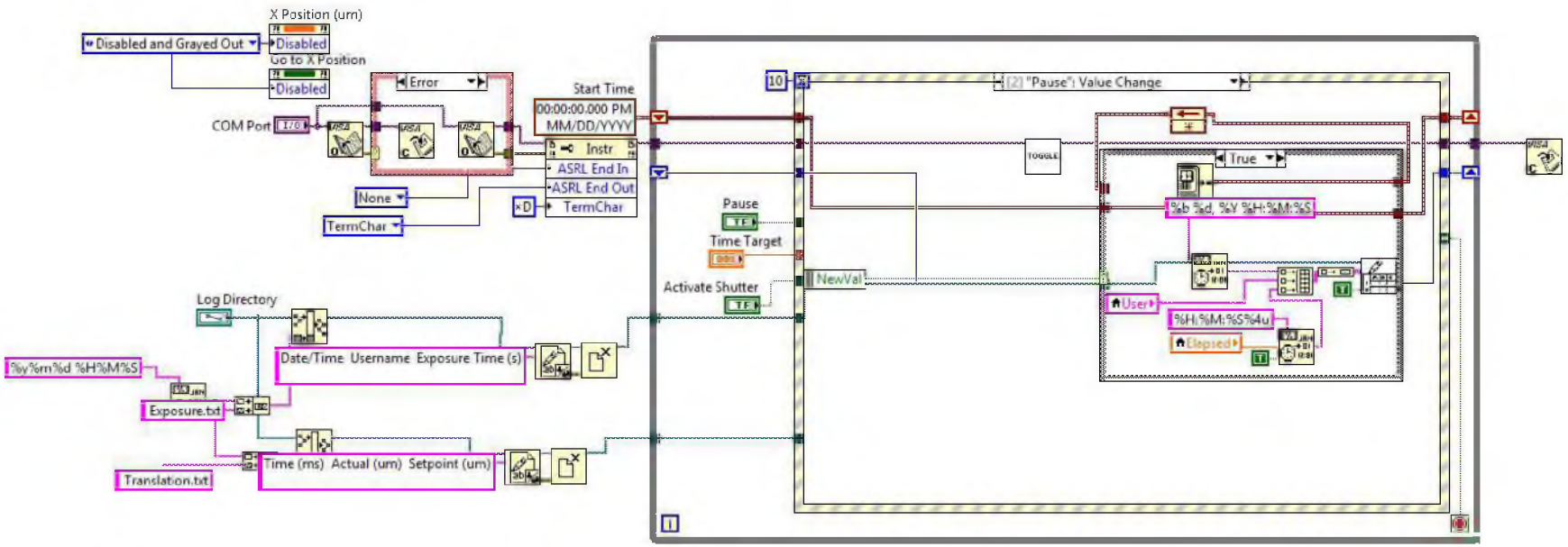

Figure A.4: Shutter controller VI to pause the shutter.

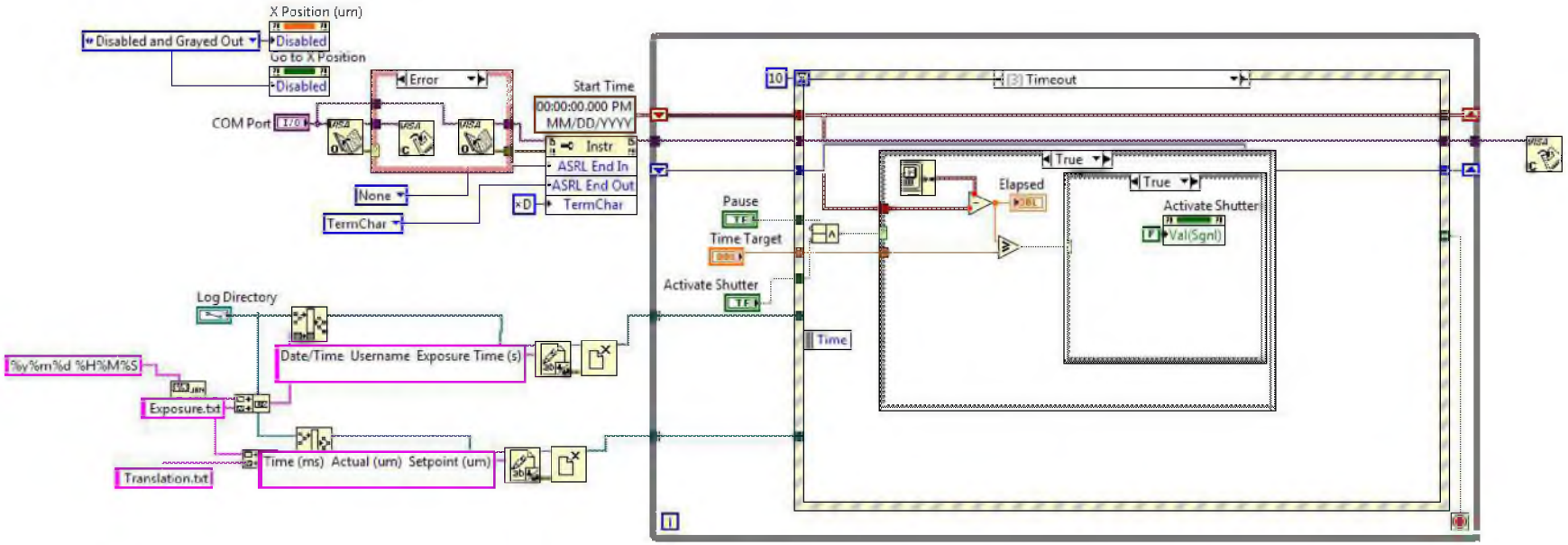

Figure A.5: Shutter controller VI to stop the shutter.

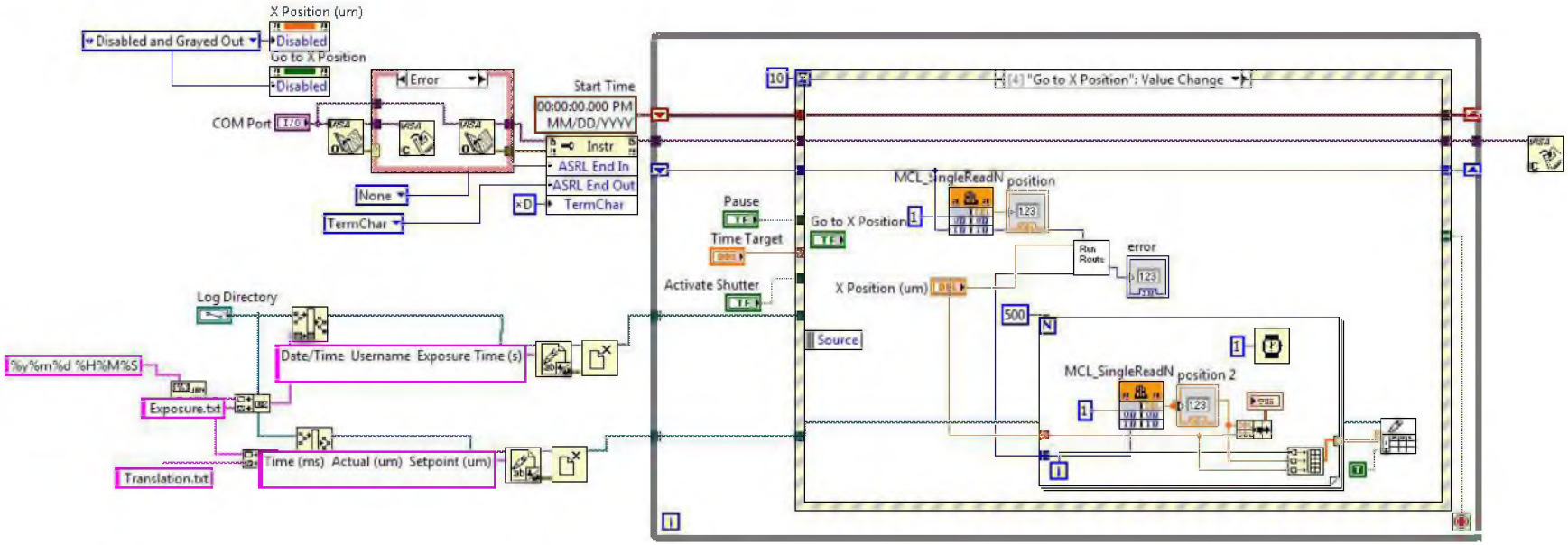

Figure A.6: Stage translation controller VI to control the X-position.

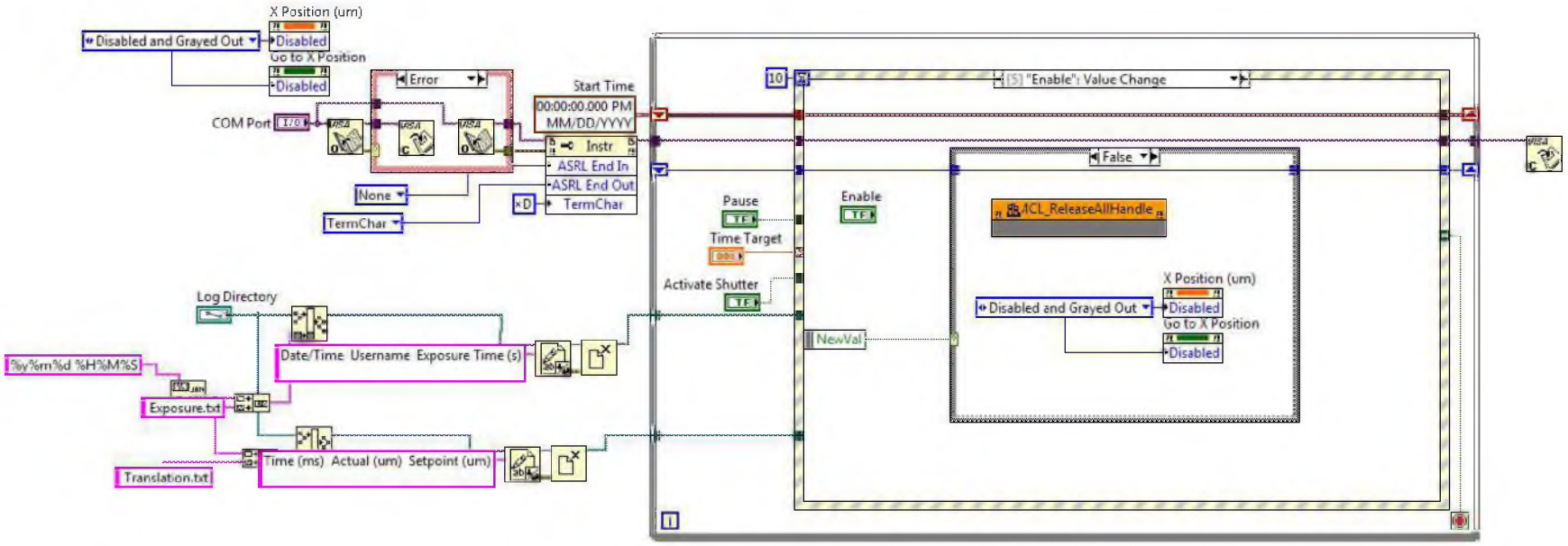

Figure A.7: Stage translation controller VI to enable the stage.

APPENDIX B

DAQFACTORY®: CYCLIC VOLTAMMETRY SETUP CODE

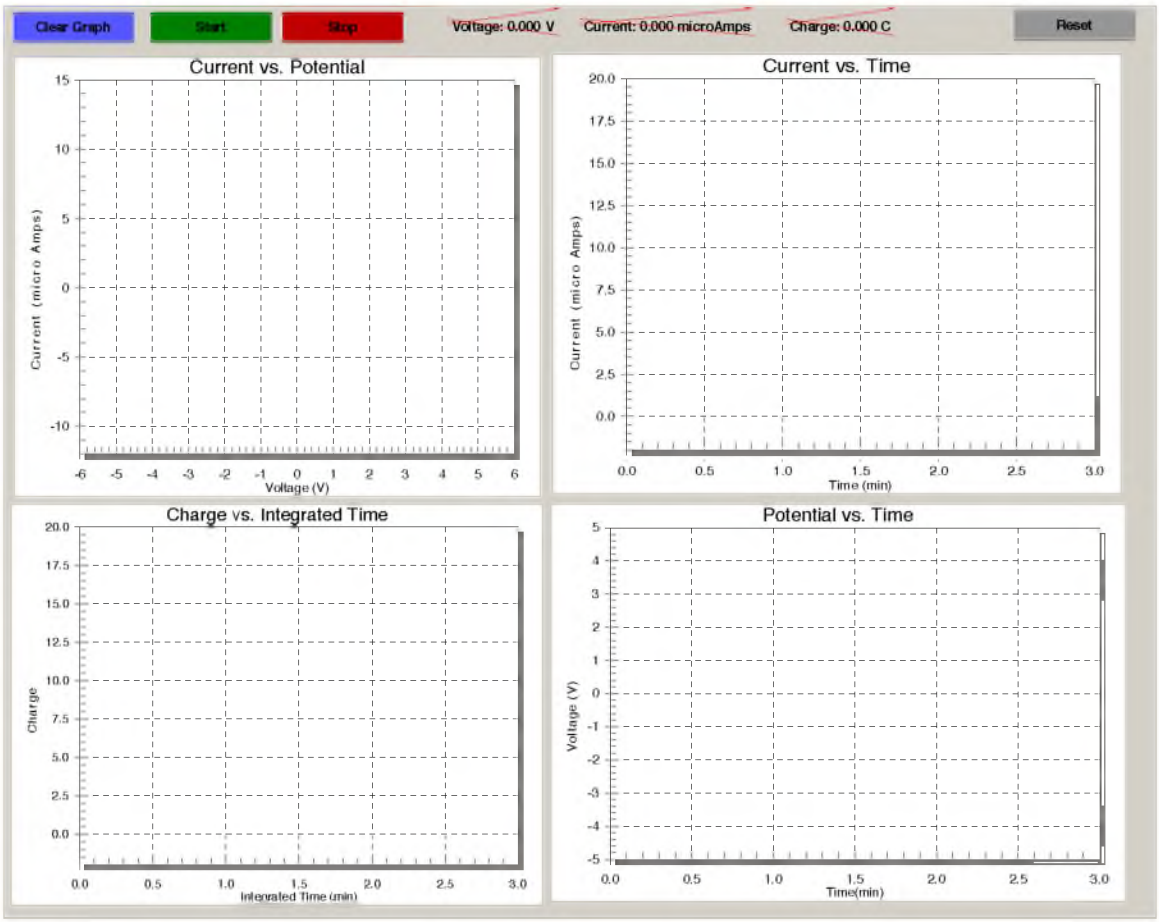

Figure B.1: Cylic voltammetry (CV) user interface.

Setup4.ctl - StartStream

```
1   // standard initialization:
2   using("device.labjack")
3   include("c:\Program Files (x86)\LabJack\Drivers\labjackud.h")
4   // setup stream:
5   // set scan rate:
6   AddRequest(0, LJ_ioPUT_CONFIG, LJ_chSTREAM_SCAN_FREQUENCY, 1000, 0, 0)
7   // setup channels to stream:
8   AddRequest(0, LJ_ioCLEAR_STREAM_CHANNELS, 0, 0, 0, 0)
9   AddRequest(0, LJ_ioADD_STREAM_CHANNEL, 0, 0, 0, 0)
10  AddRequest(0, LJ_ioADD_STREAM_CHANNEL, 1, 0, 0, 0)
11  AddRequest(0, LJ_ioADD_STREAM_CHANNEL, 3, 0, 0, 0)
12
13
14  GoOne(0)
15  // start the stream:
16  global scanrate = 0
17  eGet(0,LJ_ioSTART_STREAM, 0, @scanrate, 0)
18  // scanrate now has the actual scanrate, which you can display on the screen if you want.
```

Setup4.ctl - StopStream

```
1
2   ePut(0,LJ_ioSTOP_STREAM, 0, 0, 0)
```

Figure B.2: Streaming code for CV experiments.

APPENDIX C

ENGINEERING SCHEMATICS: HIGH VACUUM SYSTEM

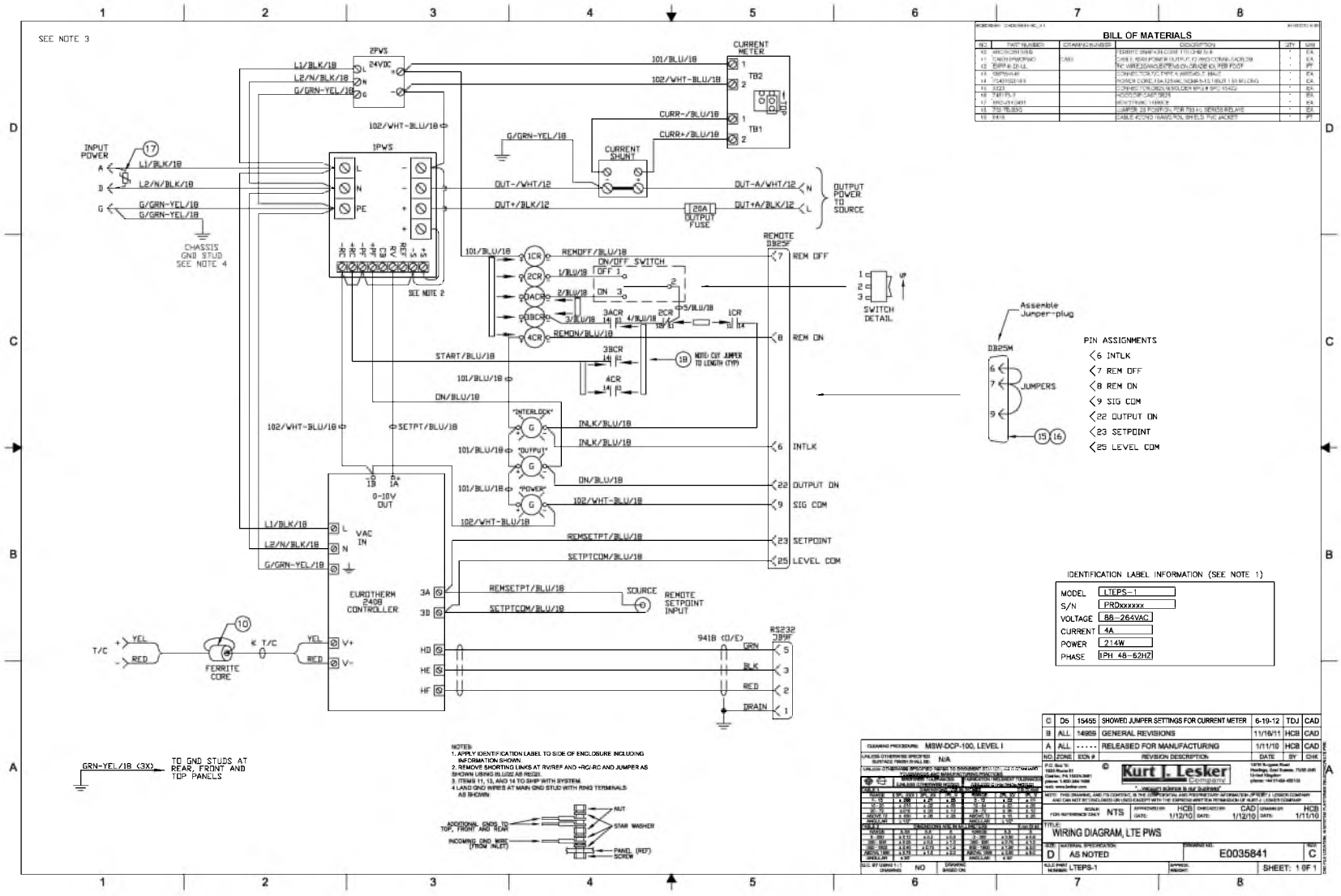

Figure C.1: LTE sourse power controller diagram.

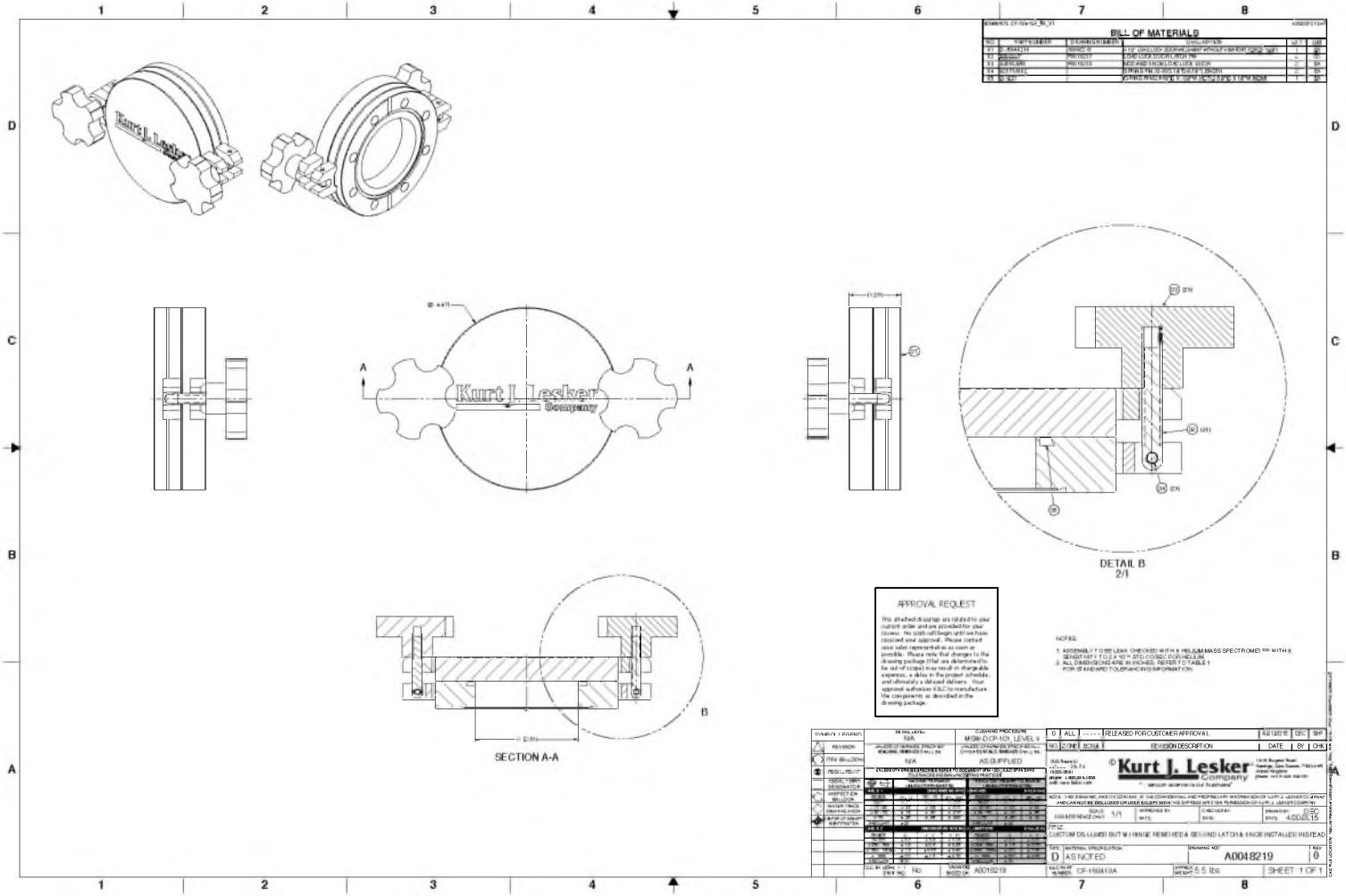

Figure C.2: Custom double latch-knobs sample holder.

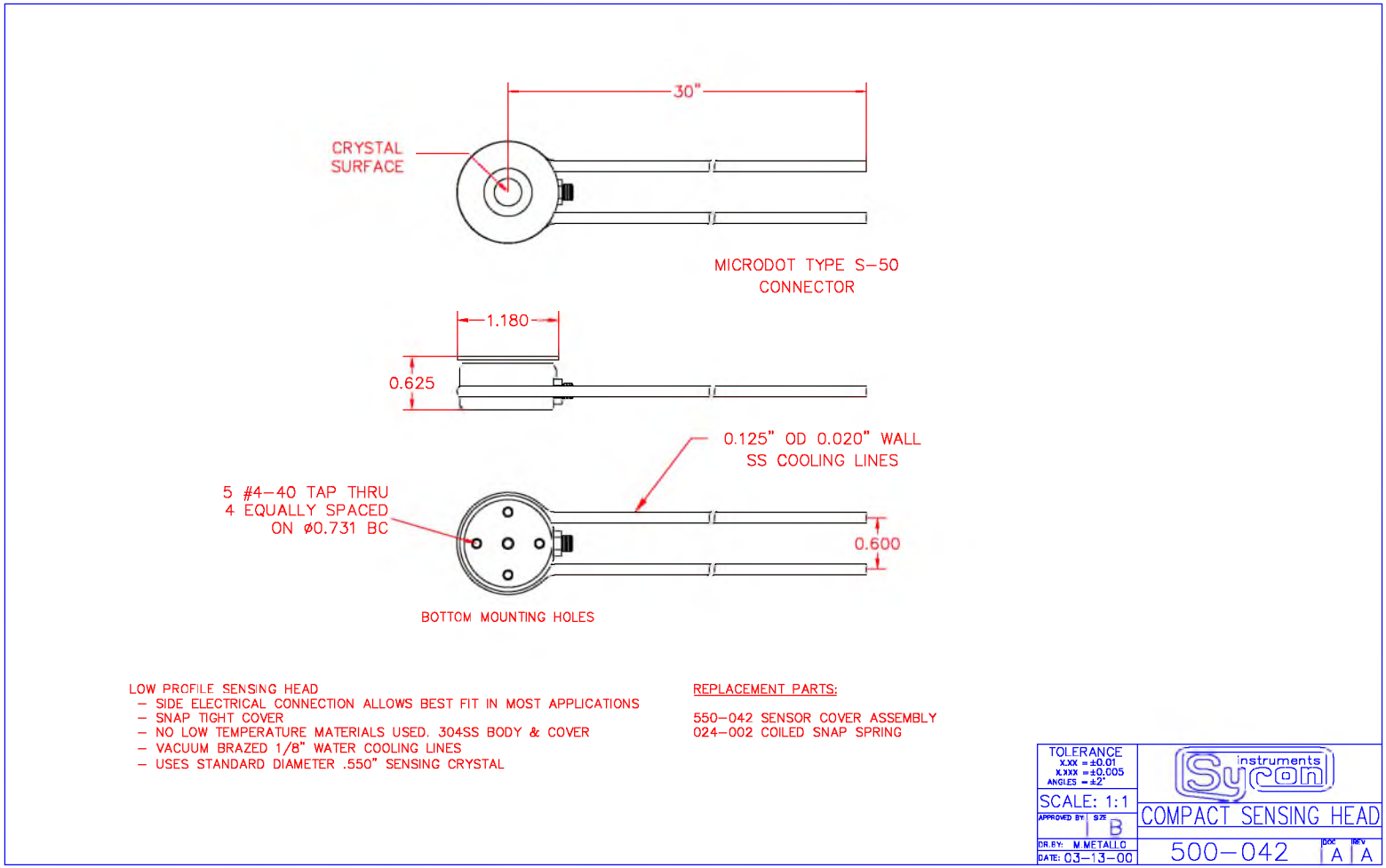

Figure C.3: 5MHz quartz crystal microbalance.

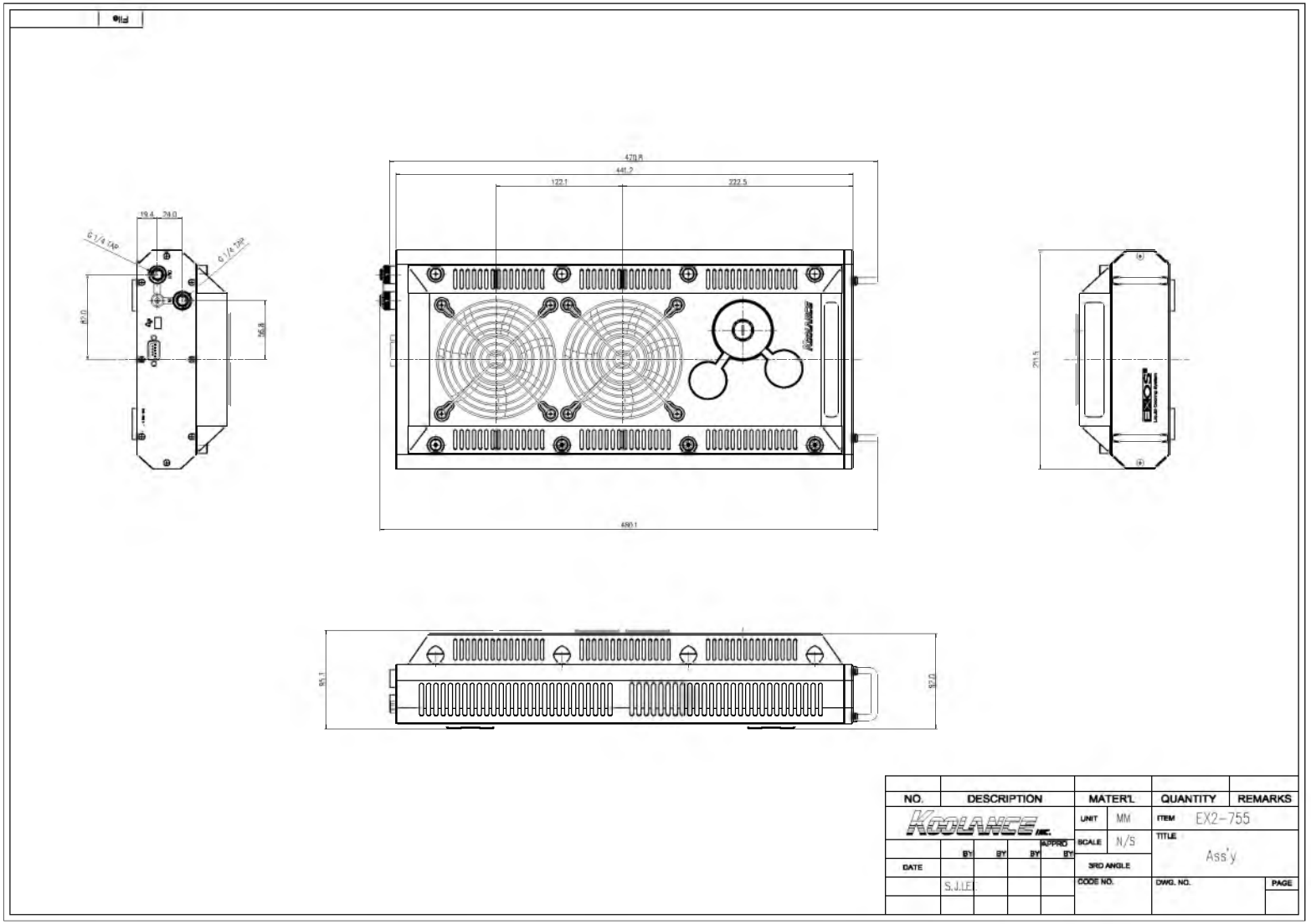

Figure C.4: Ambient liquid cooling system for QCM and turbopump.

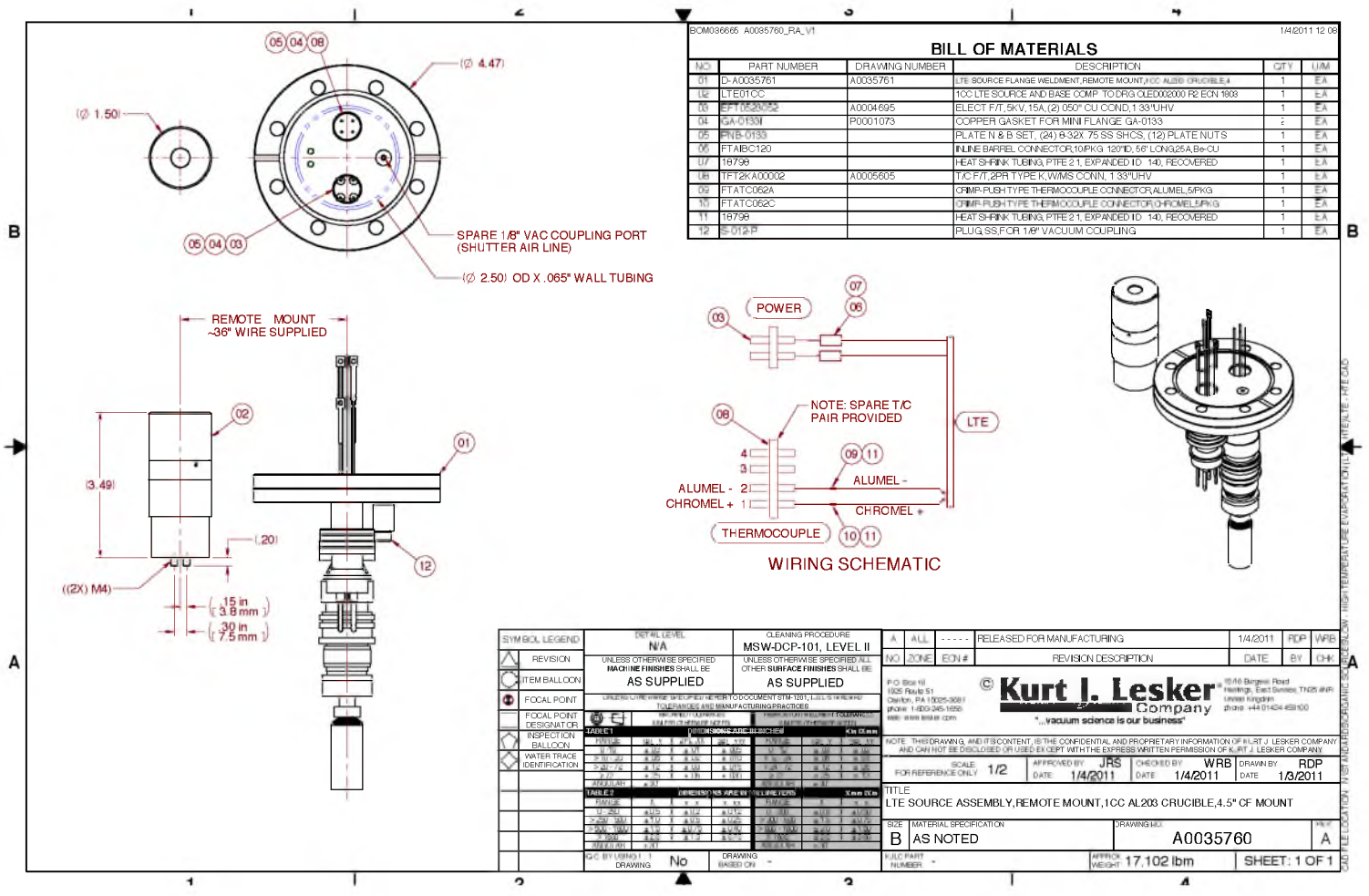

Figure C.5: LTE source assembly.

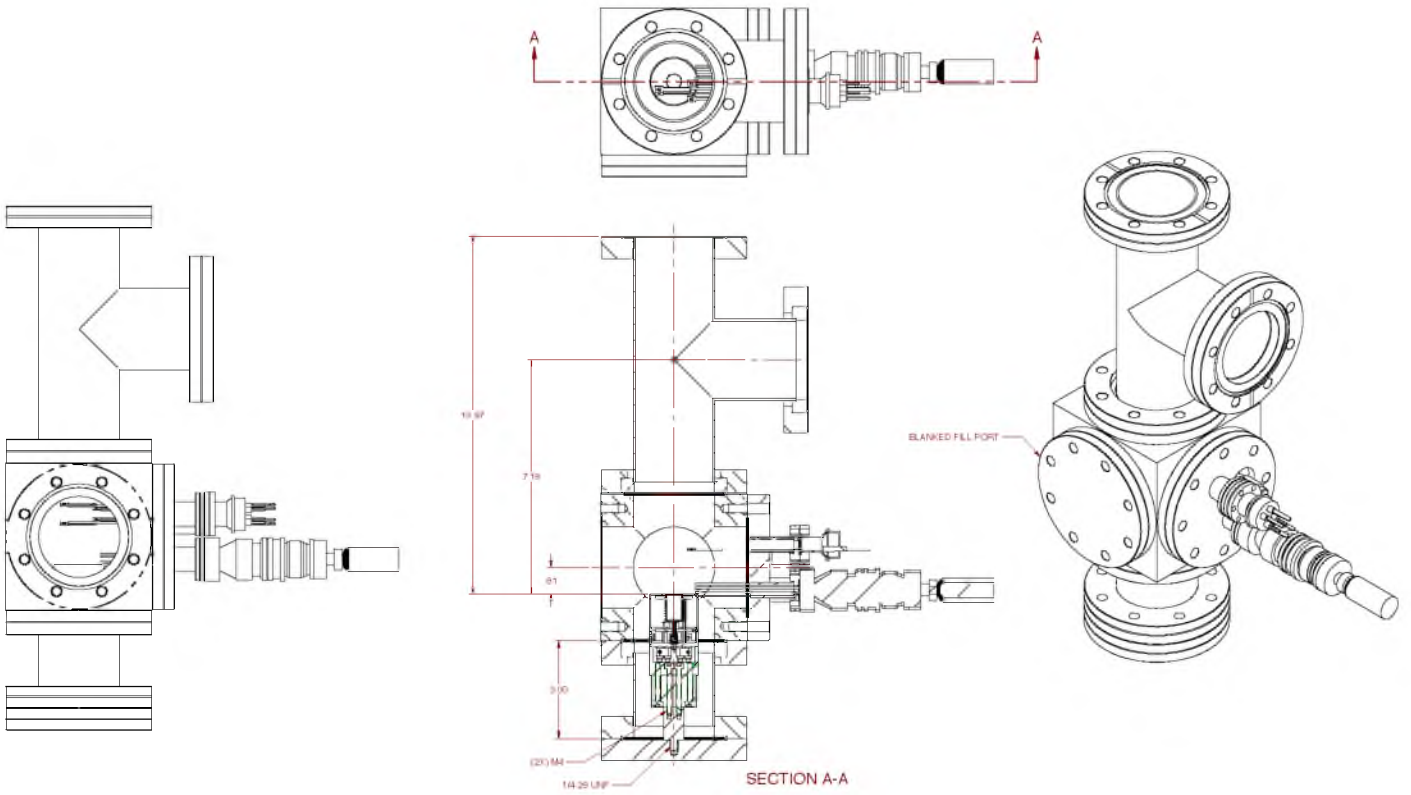

Figure C.6: Evaporator source test mount

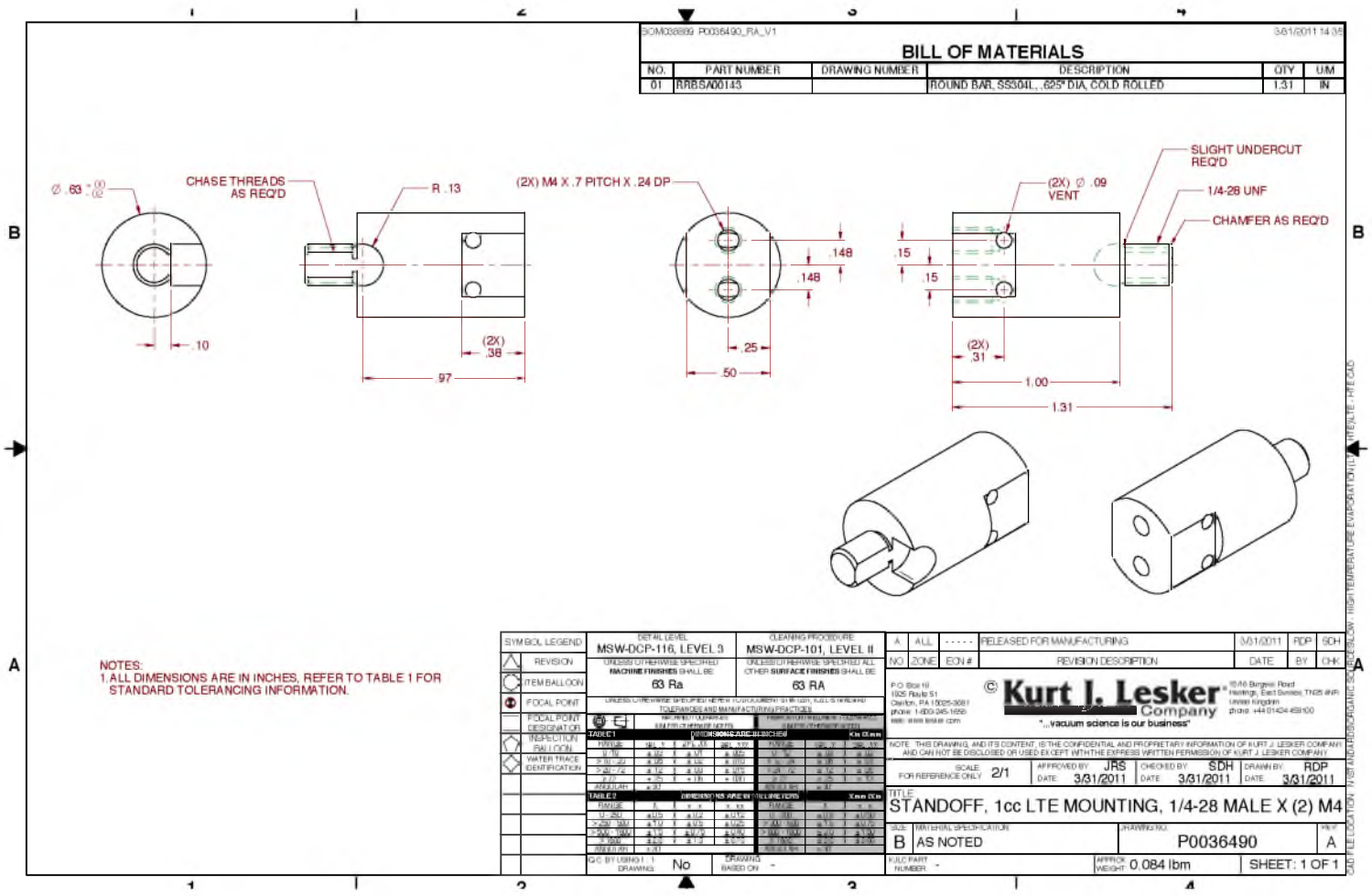

Figure C.7: Standoff for 1cc LTE mounting.

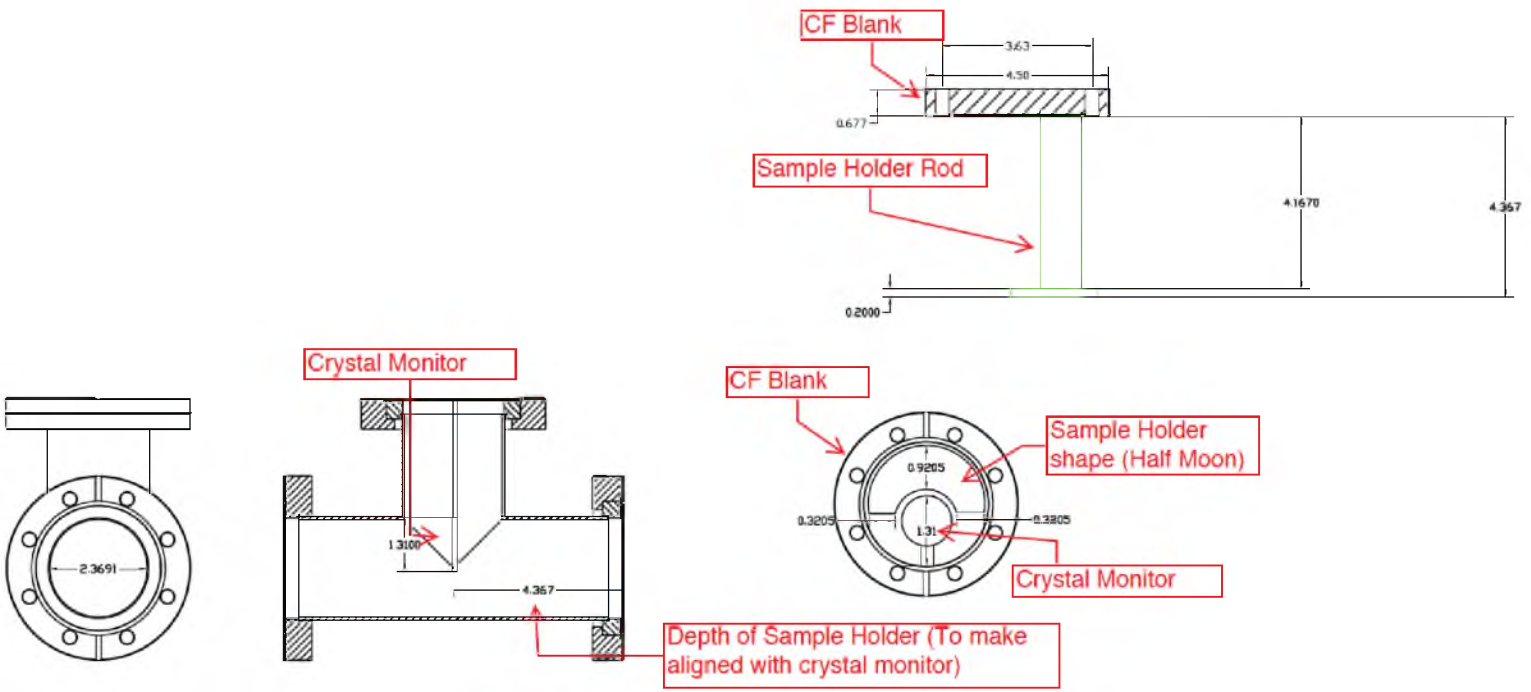

Figure C.8: Sample holder throw distance modification.